Online Trajectory Re-Planning and Anti-Jackknifing Control of a Two-Trailer System with a Car-like Tractor

Endrit Ziba

May 11, 2021

Die approbierte gedruckte Originalversion dieser Diplomarbeit ist an der TU Wien Bibliothek verfügbar
The approved original version of this thesis is available in print at TU Wien Bibliothek.

Contents

1 Introduction **4**

1.1 Motivation 4

1.2 Previous works 4

1.3 Present work 8

2 Methods **10**

2.1 Control problem 10

2.1.1 Kinematic model of the tractor with two trailers 10

2.1.2 I-O linearisation 14

2.2 Adopted control approach 19

2.2.1 Reference state trajectory 20

2.2.2 Corrective input and linear approximation 22

2.2.3 Change of coordinates and stability constraint 24

2.3 MPC Framework 26

2.3.1 Prediction model 27

2.3.2 Terminal constraint 28

2.3.3 State and input constraints 30

2.3.4 Optimal control problem (OCP) QP 32

2.4 Kalman filter 34

2.5 Obstacle avoidance 36

2.5.1 Free space 37

2.5.2 Collision check 38

2.5.3 Manipulation of the desired trajectory in order to avoid a collision 41

2.5.4 Initialisation of the evasive maneuver 41

2.6 Block diagram of the high-level control 43

3 Experimental platform **44**

3.1 Electronics 44

3.2 Actuating the DC motors 46

3.3 Numerical reconstruction of the current configuration 47

Die approbierte gedruckte Originalversion dieser Diplomarbeit ist an der TU Wien Bibliothek verfügbar
The approved original version of this thesis is available in print at TU Wien Bibliothek.
TU Bibliothek Your knowledge hub WIEN

4 Simulations **50**

5 Experiments **52**

5.1 One trailer - improvements 52

5.2 One trailer - obstacle avoidance 56

5.3 Two trailers 62

6 Conclusions and Future Work **68**

A System matrices after the linear approximation **72**

B Discrete stability condition **76**

Die approbierte gedruckte Originalversion dieser Diplomarbeit ist an der TU Wien Bibliothek verfügbar
The approved original version of this thesis is available in print at TU Wien Bibliothek.
TU Bibliothek Your knowledge hub WIEN

1 Introduction

1.1 Motivation

Vehicles with trailers have many applications in private life as well as in industry. In agriculture and logistics trailers help to increase the payload capacity and the maneuverability. Autonomous driving of such systems also needs to include the task of reversing the tractor. Truck-drivers or caravan owners will often experience during the reverse parking that the trailer folds easily on the driving vehicle, also at very low speed. The so-called hitch angle - which is the angle between the vehicle and the trailer - grows and finally becomes uncontrollable, and very often this ends up in many frustrating attempts of reversing the vehicle. The divergence of the hitch angle is referred to in literature as the *jackknife* effect. This task becomes even more complex when a second trailer and therefore a second degree of freedom is added, even for simple problems as reversing on a straight line. Backwards parking and the avoidance of possible obstacles that lie on the desired trajectory also entails the task of reversing on a circular trajectory and also on trajectories without constant curvature, such as on polynomial trajectories. The *jackknife* phenomenon also occurs in forward motion, but different to the backward motion, there it is related to slippage, which will not be considered in this work. However, even in controlled environments like harbors and airports, where automatised maneuvering of tractor-trailer systems is of big interest, unforeseen obstacles can appear on the pre-defined trajectory. Thus, for safety reasons and to avoid material damage, an online trajectory re-planning is neccesary in order to avoid the collision with obstacles.

1.2 Previous works

In [1] they address the path tracking problem for a general n-trailer system. Different to the trajectory tracking problem, in the path tracking problem there is no timing-law to be satisfied. Therefore, only the lateral dynamics is considered in this work. The use of Frenet frames allows them to decouple the longitudinal from the lateral dynamcis. The latter is specified by the sum of the error distances of the middle points of all the axles of the vehicle. By means of an input-output linearisation and a first-order high gain output feedback they try to stabilise the system around a path of constant curvature. This is done for the forward motion only as the

Die approbierte gedruckte Originalversion dieser Diplomarbeit ist an der TU Wien Bibliothek verfügbar
The approved original version of this thesis is available in print at TU Wien Bibliothek.
TU Bibliothek Your knowledge hub WIEN

zero dynamics in backward motion is (and also remains with the proposed approach) unstable.

Also in [2] they address the tracking problem of straight or circular paths, this time in forward and backward motion. The only control variable is the steering angle as the longitudinal and lateral dynamics is decoupled again and the timing law is of no concern in this work neither. There is only one guide point which is the mid point of tractor rear axle. For this the lateral offset and the orientation offset is defined which shall go to zero. They distinguish four cases (rectilinear or circular path in forward or backward motion) and for each of those a control law is proposed based on Lyaponov theory. Another approach based on non-linear control theory can be found in [3].

In [4] they suggest a hybrid control strategy that can switch between three tasks: backward driving along a rectilinear and a circular path, and forward driving along a line (to adjust an appropriate initial condition for the vehicle). In each task the system equations are linearised around a linear or circular path and a linear quadratic regulator is used to stabilise the system moving in backward direction.

A non-holonomic vehicle with two trailers is also considered in [5], where, proceeding from a feasible reference path, the angular error dynamics and the lateral error dynamics (related to the second trailer's rear-axle mid-point) is modelled using the Frenet frame. The obtained equations are linearised around the reference path yielding a locally controllable system. This is stabilised with a Linear Quadratic Regulator. To be able to take the physical limitations of the system into account they extended their work in [6], where a path-following controller based on a model predictive control (MPC) framework is suggested, instead of the LQ controller.

In [7] a vehicles representative point that is located aligned with the tractors steering angle, should track a cartesian reference trajectory. The x and y cartesian coordinates of this representative point correspond to the output vector. As in the previous approach, the non-holonomic constraints of the system are used to derive the kinematic model. A state feedback as described in [8] leads to an input-output (I-O) linear system and makes the representative point track the desired cartesian trajectory. However, the remaining angular states are unstable and can not be controlled by the tracking controller applied after the I-O linearisation. This is related to the non-minimum phase nature of the system in backward motion that gets inverted. It is like the case in which the zeros with positive real-part of a proper transfer function become

Die approbierte gedruckte Originalversion dieser Diplomarbeit ist an der TU Wien Bibliothek verfügbar
The approved original version of this thesis is available in print at TU Wien Bibliothek.
TU Bibliothek Your knowledge hub WIEN

the unstable poles of the inverted transfer function, as described by [9] for the inversion-based gait generation of humanoids having a non-minimum phase nature. To deal with this so-called unstable zero dynamics, a corrective action (input) is added to the just described tracking controller. It has the purpose to keep the forced zero dynamics bounded. In forward motion, the zero dynamics would remain bounded for the non-holonomic vehicle and no corrective action would be necessary. The corrective input is generated by a linear MPC, which is based on the linear approximation of the I-O linearised system around a feasible reference state trajectory. The feasible state trajectory contains a stable trajectory for the cartesian, as well as for the angular states. Further details are explained in [10], and [11] gives a more general overview about feeback-control of non-holonomic car-like robots. The advantage of the MPC framework is that it enables the inclusion of state and input constraints. Interestingly, the MPC framework in [7] has been developed previously for humanoid gait generation in [12].

The above mentioned controls are all based on a kinematically feasible trajectoy or path. A trajectory can be seen as a path with a timing law. A kinematically feasible and collision-free path can be computed offline if all the information about the workspace geometry is known a priori. This is not always the case, or just partially, and obstacles on the pre-computed path might appear. In this case the robot has to gradually discover the environment and perform the path planning online. In [13] those two approaches are combined. First a lattice-base path planner generates kinematically feasible motion primitives offline for an obstacle free environment, which are stored in a set. This requires a state space discretisation, i.e. the tracked point is constrained to a uniform grid, on which also the steering and hitch angels and their velocities are constrained to a discrete set of values. Then the motion primitives are obtained by solving optimal control problems (OCPs), where physical limitations of the vehicle and also the non-holonomic constraints are considered. The online planning then consists of a search over the set of the motion primitives. An ordered sequence of those primitives is chosen to assemble a collision free path. They assume that the workspace obstacles can be described analytically as circles, ellipsoids, polytopes etc.

A strategy that is suitable for online planning, is that of artificial potential field methods. This heuristic approach has been considered in [14] for a non-holonomic system. The initial (kinematically feasible) path is deformed incrementally, based on a potential function that

Die approbierte gedruckte Originalversion dieser Diplomarbeit ist an der TU Wien Bibliothek verfügbar
The approved original version of this thesis is available in print at TU Wien Bibliothek.
TU Bibliothek Your knowledge hub WIEN

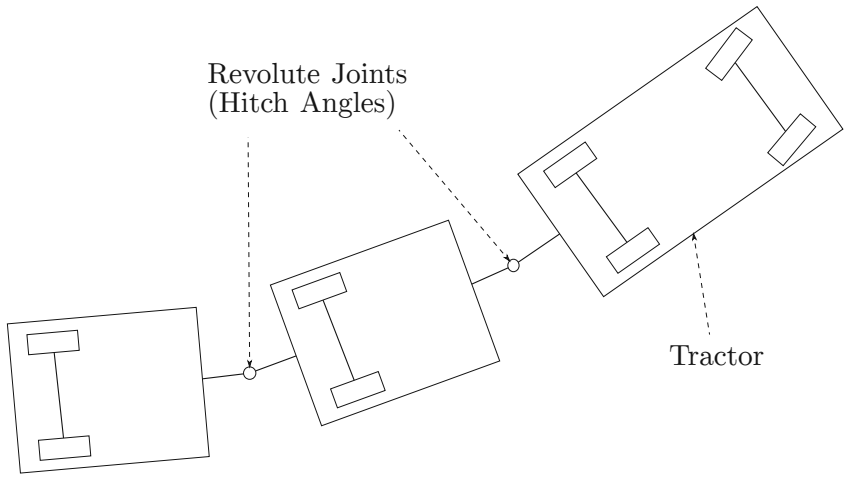

Figure 2: sketches the tractor with the two trailers. The angles between the tractor and the trailer, and between the two trailers are the so-called hitch angles.

increases with the length of the path and also when the path gets closer to an obstacle. The path deformation is based on minimising the potential function. Thus, by construction the force field originating from this potential pushes the path away from obstacles but also big path deformations are avoided. However, due to the path deformation the non-holonomic constraints get violated and at every step a correction of the non-holonomic deviation is necessary. A main shortcoming of this method is that it can be trapped in local minima and failing to deform the path.

In [15] and [16] workspace obstacle are considered at two levels. The first work describes a pursuit-evasion maneuver of two humanoid robots, and in the second this is extended and workspace obstacles are considered in an MPC framework. Each robot is equipped with a depth camera for determining the direction of the opposite robot. Based on the information of the sensing system, an evasive trajectory is obtained by controlling a unicycle to the desired position represented by the driving and steering velocity, v and ω, of the unicycle. A quadratic cost function is formulated that rewards the reproduction of v and ω, but also forces the robot to align its foot-steps with the tangent to the closest obstacle point. The obstacle avoidance is then again considered as an explicit constraint of the MPC. Thus, obstacles are considered in two levels, once when determining the evasive trajectory, and then as an MPC constraint. The first level has also the goal to maintain the linearity of the MPC.

Die approbierte gedruckte Originalversion dieser Diplomarbeit ist an der TU Wien Bibliothek verfügbar
The approved original version of this thesis is available in print at TU Wien Bibliothek.
TU Bibliothek WIEN Your knowledge hub

1.3 Present work

In the present work the output trajectory tracking of a tractor with two trailers will be presented as an extension of [7]. For this purpose not only the equations for the two-trailers system will be derived, but some further changes are realised, in order to successfully avoid the divergence of both hitch angles. The considered system is sketched in Fig. 2. The changes and other extensions are listed below

(i) a different approach for the numerical reconstruction of the states

(ii) changes in the odometry

(iii) the inclusion of a Kalman filter

(iv) a suggestion how to include input velocity-constraints

(v) a re-formulation of the quadratic problem (QP) in order to be able to use the faster and for MPC problems designed HPIPM solver [17]

The latter is necessary in order to not increase the sampling interval, which would be necessary for the two-trailers system, and especially if the task of avoiding obstacles shall be managed in real-time. For this purpose the stability constraint has to be re-written to a terminal constraint as motivated in [18]. Furthermore, the saturations of the input velocities, besides the state constraints, is discussed. The input constraints include future states that can be predicted by the prediction model. To overcome the problem that the current input sequence is not available, as it is the result of the QP that shall be computed, [19] suggests to take the input sequence computed at the last sampling time. References [20] and [21] were consulted for better understanding of MPC and the formulation of the QP with its constraints.

The second target of this work is the evasion of unexpected workspace obstacles in real-time. The vehicle is equipped with a depth camera to discover such obstacles. The proposed algorithmic framework to avoid obstacles takes the desired cartesian trajectory and the camera observations as inputs. The outcome is a collision free and kinematically feasible reference state trajectory, used in the MPC framework. At each sampling time the environment is scanned by the camera for workspace obstacles and determines the occupied and the free space. A collision check is then performed in a local coordinate system (fixed with the camera) based

Die approbierte gedruckte Originalversion dieser Diplomarbeit ist an der TU Wien Bibliothek verfügbar
The approved original version of this thesis is available in print at TU Wien Bibliothek.
TU Bibliothek WIEN Your knowledge hub

on the desired cartesian trajectory. If the desired cartesian trajectory does not lead to a collision free maneuver, it will be changed by adding a spline. The spline is chosen such that the deviation of the manipulated cartesian trajectory from the desired one is just as big as necessary to guarantee a collision free maneuver. Once such a cartesian trajectory is computed, a kinematically feasible reference state trajectory in backward motion can be generated from it. For this purpose the backward motion can be seen as a forward motion reverse in time with an appropriate retrograde initialisation. The state evolutions in forward motion can be easily obtained by pure tracking, as in this case the internal dynamics remains bounded, i.e. the hitch angles and the tractor heading and steering angle do not diverge. Summarising, the result is an online computed, collision free reference state trajectory for the backward motion that satisfies the non-holonomic contraints. The trajectory re-planning is done repetitively at each sampling time.

Die approbierte gedruckte Originalversion dieser Diplomarbeit ist an der TU Wien Bibliothek verfügbar
The approved original version of this thesis is available in print at TU Wien Bibliothek.
TU Bibliothek WIEN Your knowledge hub

2 Methods

This chapter is organised as follows. At the end of section 2.1 the control problem is stated, for which the approach in section 2.2 is suggested. The technical realisation of the proposed approach is described in 2.3. In section 2.4 the Kalman Filter is described which is used to reduce the deviation of the vehicle from the desired trajectory. A more precise tracking helps to avoid unforseen obstacles successfully or for the reverse parking of the vehicle. Finally, the obstacle avoidance is addressed in section 2.5.

2.1 Control problem

The behaviour of the tractor with its two trailers can be described by means of a kinematic model. The first step is to derive such a kinematic model for our system resulting in nonlinear system equations. The system output is defined by the cartesian coordinates of a chosen point on the tractor. The goal is to design a controller such that the chosen point tracks a desired cartesian trajectory - namely the reference output - while the vehicle moves in backward direction. For this purpose the system equations will be input-output (I-O) linearised through an input transformation. Based on the new inputs a state feedback control is implemented that makes the controlled output track the reference output. The I-O linearisation with the tracking controller yields a linear subsystem and a nonlinear, unstable internal dynamics that cannot be controlled by the just metioned feedback. From a control point of view the internal dynamics does not affect the output. However, the *jackknife* effect appears due to the instability of the internal dynamics which finally prevents a successful output tracking.

2.1.1 Kinematic model of the tractor with two trailers

The starting point is the kinematic model for the tractor with two trailers which will be derived in the following. For statical stability two wheels per axle are necessary, but for the kinematic model it is equivalent when two wheels on one axle are merged into one wheel on the mid axle, as shown in Fig. 3. An Ackermann steering mechanism on the real system makes sure that both zero motion lines of the front wheels coincide in the same instantaneous centre of rotation. In a first instance the generalised coordinates are chosen as $\tilde{q} = (\, x \quad y \quad \theta \quad \psi_1 \quad \psi_2 \quad \phi \,)^T$ (see

Die approbierte gedruckte Originalversion dieser Diplomarbeit ist an der TU Wien Bibliothek verfügbar
The approved original version of this thesis is available in print at TU Wien Bibliothek.
TU Bibliothek Your knowledge hub WIEN

the Fig.). We call ϕ the steering angle, θ the tractor heading and ψ_1, ψ_2 the hitch angles. The states $(x \quad y)$ correspond to the midpoint of the rear axle of the tractor.

For the derivation the 'pure rolling' constraint and the 'rigid body' constraint are considered. Pure rolling means that the instantaneous contact point of the wheel and the ground have the same velocity. Therefore, the velocity of the wheel midpoint $r \cdot \omega_{wheel}$ is aligned with the sagittal axis of the wheel. If the point $X = (x \quad y)$ is considered, the velocity can also be expressed in cartesian coordinates as $\dot{X} = (\dot{x} \quad \dot{y})$, which has the unit vector $n = (\cos\theta \quad \sin\theta)$. The unit vector $n_\perp = (\sin\theta \quad -\cos\theta)$ is orthogonal to n and therefore also to $\dot{X}$, and it is aligned with the zero motion line. Thus, the inner product of $\dot{X}$ and $n_\perp$ equals to zero. The same holds for the steering wheel and the wheels of the two trailers, which leads to

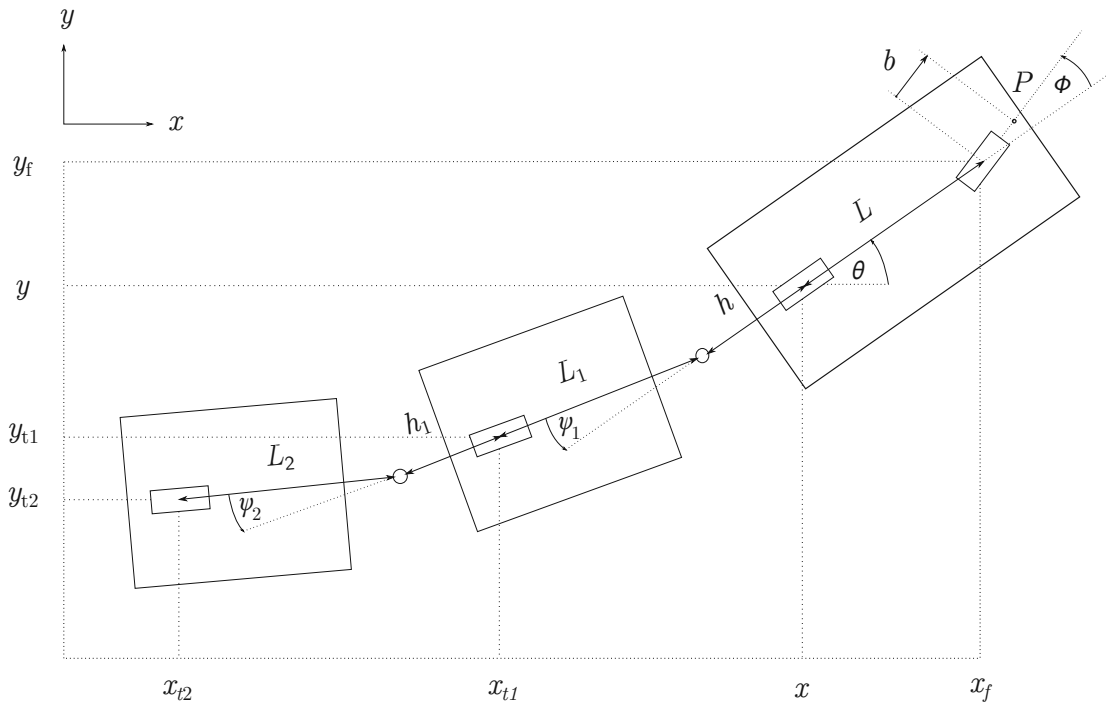

Figure 3: shows the model of the tractor with two trailers and the generalised coordinates. Note that the first and the second trailer's cartesian coordinates are denoted $(x_{t1} \quad y_{t1})$ and $(x_{t2} \quad y_{t2})$, respectively.

Die approbierte gedruckte Originalversion dieser Diplomarbeit ist an der TU Wien Bibliothek verfügbar
The approved original version of this thesis is available in print at TU Wien Bibliothek.
TU Bibliothek WIEN Your knowledge hub

$$
\begin{aligned}
0 &= \dot{x}_{t2}\,\sin(\theta+\psi_1+\psi_2) - \dot{y}_{t2}\,\cos(\theta+\psi_1+\psi_2) \\
0 &= \dot{x}_{t1}\sin(\theta+\psi_1) - \dot{y}_{t1}\cos(\theta+\psi_1) \\
0 &= \dot{x}\sin\theta - \dot{y}\cos\theta \\
0 &= \dot{x_f}\sin(\theta+\phi) - \dot{y_f}\cos(\theta+\phi).
\end{aligned}
$$

Here $(x_{t2} \quad y_{t2})$, $(x_{t1} \quad y_{t1})$, and $(x_f \quad y_f)$ are the cartesian coordinates of the second, the first trailer wheel and the front wheel of the tractor, respectively. We want to rewrite these coordinates as functions of $(x \quad y)$. For this the rigid body constraints are used

$$
\begin{aligned}
x_f &= x + L\,\cos\theta \\
y_f &= y + L\,\sin\theta \\
x_{t1} &= x - h\,\cos\theta - L_1\,\cos(\theta+\psi_1) \\
y_{t1} &= x - h\,\sin\theta - L_1\,\sin(\theta+\psi_1) \\
x_{t2} &= x - h\,\cos\theta - (L_1+h_1)\,\cos(\theta+\psi_1) - L_2\cos(\theta+\psi_1+\psi_2) \\
y_{t2} &= x - h\,\sin\theta - (L_1+h_1)\,\sin(\theta+\psi_1) - L_2\sin(\theta+\psi_1+\psi_2).
\end{aligned}
$$

For the lengths L, h, L_1, h_1, and L_2 see Fig. 3. With this equations the pure rolling constraints can be rewritten after some calculations as

$$
\begin{aligned}
0 = \;& \dot{x}\,\sin(\theta+\psi_1+\psi_2) - \dot{y}\,\cos(\theta+\psi_1+\psi_2) + (\dot{\theta}+\dot{\psi}_1+\dot{\psi}_2)L_2 + \cdots \\
& \cdots + (\dot{\theta}+\dot{\psi}_1)\,(L_1+h_1) + \dot{\theta}\,h\cos(\psi_1+\psi_2)
\end{aligned} \tag{1}
$$

$$0 = \dot{x}\,\sin(\theta+\psi_1) - \dot{y}\,\cos(\theta+\psi) + \dot{\theta}(h\cos\psi_1 + L_1) + \dot{\psi}_1 L_1 \tag{2}$$

$$0 = \dot{x}\,\sin\theta - \dot{y}\,\cos\theta \tag{3}$$

$$0 = \dot{x}\,\sin(\theta+\phi) - \dot{y}\cos(\theta+\phi) - \dot{\theta}L\cos\phi. \tag{4}$$

Die approbierte gedruckte Originalversion dieser Diplomarbeit ist an der TU Wien Bibliothek verfügbar
The approved original version of this thesis is available in print at TU Wien Bibliothek.
TU Bibliothek WIEN Your knowledge hub

Equations (1) to (4) are the non-holonomic constraints for the tractor-trailers system. They are in Pfaffian form, i.e. linear in the generalised velocities

$$A^T(\tilde{q}) \cdot \dot{\tilde{q}} = 0 \tag{5}$$

where the matrix $A(\tilde{q})$ is

$$A(\tilde{q}) = \begin{pmatrix} \sin\theta & \sin(\theta+\phi) & \sin(\theta+\psi_1) & \sin(\theta+\psi_1+\psi_2) \\ -\cos\theta & -\cos(\theta+\phi) & -\cos(\theta+\psi_1) & -\cos(\theta+\psi_1+\psi_2) \\ 0 & -L\,\cos\theta & h\,\cos\psi_1 + L_1 & h\,\cos(\psi_1+\psi_2) + L_1 + h_1 + L_2 \\ 0 & 0 & L_1 & L_1 + h_1 + L_2 \\ 0 & 0 & 0 & L_2 \\ 0 & 0 & 0 & 0 \end{pmatrix} \tag{6}$$

The generalised velocities $\dot{\tilde{q}}$ must be chosen according to equation (5) in order to satisfy the physical constraints on the system. Thus we have to determine the Nullspace of $A^T(\tilde{q})$. The matrix $A^T(\tilde{q})$ has $rank = 4 = k$ and therefore the Nullspace of $A^T(\tilde{q})$ has dimension $n - k = 6 - 4 = 2$. Hence, we have to look for two linearly independent vectors fields $\dot{\tilde{q}} = \tilde{g}_1(\tilde{q})$ and $\dot{\tilde{q}} = \tilde{g}_2(\tilde{q})$ that satisfy equation (5). Once two vector fields $\tilde{g}_1(\tilde{q})$ and $\tilde{g}_2(\tilde{q})$ are determined all admissible generalised velocities $\dot{\tilde{q}}$ can be expressed as a linear combination of those two

$$\dot{\tilde{q}} = \tilde{g}_1(\tilde{q}) \cdot v_1 + \tilde{g}_2(\tilde{q}) \cdot v_2, \tag{7}$$

where the two vectors $\tilde{g}_1(\tilde{q})$ and $\tilde{g}_2(\tilde{q})$ are

Die approbierte gedruckte Originalversion dieser Diplomarbeit ist an der TU Wien Bibliothek verfügbar
The approved original version of this thesis is available in print at TU Wien Bibliothek.
TU Bibliothek WIEN Your knowledge hub

$$\tilde{g}_1 = \begin{bmatrix} \cos\theta \\ \sin\theta \\ \frac{\tan\phi}{L} \\ -\frac{\tan\phi}{L}\left(\frac{h}{L_1}\cos\psi_1 + 1\right) - \frac{\sin\psi_1}{L_1} \\ \frac{h\tan\phi}{LL_2}\left(\frac{L_2\cos\psi_1}{L_1} + \frac{(L_1+h_1)\cos\psi_1\cos\psi_2}{L_1} - \cos(\psi_1+\psi_2)\right) + \frac{\sin\psi_1}{L_1}\left(1 + \frac{(L_1+h_1)\cos\psi_2}{L_2}\right) - \frac{\sin(\psi_1+\psi_2)}{L_2} \\ 0 \end{bmatrix}$$

and

$$\tilde{g}_2 = [0 \quad 0 \quad 0 \quad 0 \quad 0 \quad 1]^T.$$

The two coefficients v_1 and v_2 can be interpreted as the linear velocity of the rear tractor wheel $v_1 = v$ and the steering velocity $v_2 = \omega$. Equation (7) is called the kinematic model with $dim(q) = 6$ and two inputs v and ω. In fact, all admissible trajectories $\tilde{q}(t)$ are also constrained to the kinematic model as it is its time-integral.

2.1.2 I-O linearisation

To design a controller that tracks the output trajectory an input-output (I-O) linearisation is performed by means of an input transformation, corrsponding to a static state feedback. Thus, the problem consists of finding an output for which this I-O linearisation can be done.

An instinctive choice of the controlled output z for the tracking problem is the mid-point of the tractor's rear axle

$$z = \begin{pmatrix} x \\ y \end{pmatrix}$$

and for its time derivative one obtains directly from the kinematic model that

Die approbierte gedruckte Originalversion dieser Diplomarbeit ist an der TU Wien Bibliothek verfügbar
The approved original version of this thesis is available in print at TU Wien Bibliothek.
TU Bibliothek Your knowledge hub WIEN

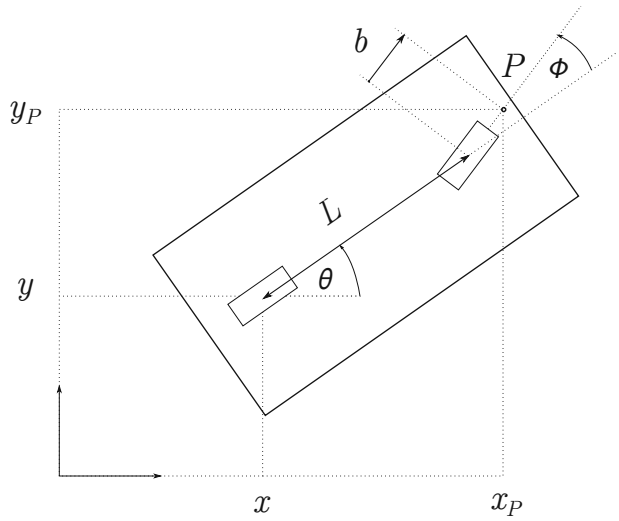

Figure 4: shows the tractor without the trailers and the controlled output P.

$$\begin{pmatrix} \dot{x} \\ \dot{y} \end{pmatrix} = \begin{pmatrix} \cos\theta & 0 \\ \sin\theta & 0 \end{pmatrix} \begin{pmatrix} v \\ \omega \end{pmatrix} = \tilde{D}(\theta) \begin{pmatrix} v \\ \omega \end{pmatrix}.$$

The static state feedback requires the inversion of the decoupling matrix $\tilde{D}(\theta)$. Since this matrix is singular the following work around is suggested. The controlled output will be changed and the point $P \to (x_P \quad y_P)$, which is a point on the tractor as well, will be tracked instead of $(x \quad y)$. Figure 4 shows point P, which, chosen as the new controlled ouput, will lead to a non singular decoupling matrix. The two points are in the following relation

$$\begin{aligned} x_P &= x + L\,\cos\theta + b\,\cos(\theta+\phi) \\ y_P &= y + L\,\sin\theta + b\,\sin(\theta+\phi). \end{aligned} \tag{8}$$

The state vector changes to $q = (\,x_P \quad y_P \quad \theta \quad \psi_1 \quad \psi_2 \quad \phi\,)^T$ and the kinematic model becomes

$$\dot{q} = g_1(q)\,v + g_2(q)\,\omega \tag{9}$$

where the vectors $g_1(q)$ and $g_2(q)$ are

Die approbierte gedruckte Originalversion dieser Diplomarbeit ist an der TU Wien Bibliothek verfügbar
The approved original version of this thesis is available in print at TU Wien Bibliothek.
TU Bibliothek WIEN Your knowledge hub

$$g_1 = \begin{bmatrix} \cos\theta - [L\,\sin\theta + b\,\sin(\theta+\phi)]\frac{\tan\phi}{L} \\ \sin\theta + [L\,\cos\theta + b\,\cos(\theta+\phi)]\frac{\tan\phi}{L} \\ \frac{\tan\phi}{L} \\ -\frac{\tan\phi}{L}\left(\frac{h}{L_1}\cos\psi_1 + 1\right) - \frac{\sin\psi_1}{L_1} \\ \frac{h\tan\phi}{LL_2}\left(\frac{L_2\cos\psi_1}{L_1} + \frac{(L_1+h_1)\cos\psi_1\cos\psi_2}{L_1} - \cos(\psi_1+\psi_2)\right) + \frac{\sin\psi_1}{L_1}\left(1 + \frac{(L_1+h_1)\cos\psi_2}{L_2}\right) - \frac{\sin(\psi_1+\psi_2)}{L_2} \\ 0 \end{bmatrix}$$

and

$$g_2 = [-b\,\sin(\theta+\phi) \quad b\,\cos(\theta+\phi) \quad 0 \quad 0 \quad 0 \quad 1]^T.$$

The time derivative of the output changes to

$$z = \begin{pmatrix} x_P \\ y_P \end{pmatrix} \qquad \Rightarrow \qquad \dot{z} = D(\theta,\phi)\begin{pmatrix} v \\ \omega \end{pmatrix}$$

$$\dot{z} \;=\; \begin{pmatrix} \cos\theta - [L\,\sin\theta + b\,\sin(\theta+\phi)]\frac{\tan\phi}{L} & -b\,\sin(\theta+\phi) \\ \sin\theta + [L\,\cos\theta + b\,\cos(\theta+\phi)]\frac{\tan\phi}{L} & b\,\cos(\theta+\phi) \end{pmatrix}\begin{pmatrix} v \\ \omega \end{pmatrix} \tag{10}$$

Equation (10) is obtained by differentiating (8). The determinant of the decoupling matrix is $det(D) = \frac{b}{\cos\phi}$. Thus, it is non-singular (i.e. invertible) if the parameter b is set to a non-zero value. The sign of the parameter b does not affect the singularity. However, its importance will be discussed later. The following input transformation

$$\begin{pmatrix} v \\ \omega \end{pmatrix} = D^{-1}(\theta,\phi)\begin{pmatrix} u_1 \\ u_2 \end{pmatrix} \tag{11}$$

Die approbierte gedruckte Originalversion dieser Diplomarbeit ist an der TU Wien Bibliothek verfügbar
The approved original version of this thesis is available in print at TU Wien Bibliothek.
TU Bibliothek WIEN Your knowledge hub

finally leads to the I-O linear system and the system equations become

$$\dot{x}_P = u_1$$

$$\dot{y}_P = u_2$$

$$\dot{\theta} = \frac{\sin\phi}{L}\left[\cos(\theta+\phi)u_1 + \sin(\theta+\phi)u_2\right]$$

$$\dot{\psi}_1 = -\frac{1}{L\,L_1}[L\,\cos\phi\,\sin\psi_1 + h\,\sin\phi\,\cos\psi_1 + L_1\sin(\phi)][\cos(\theta+\phi)u_1 + \sin(\theta+\phi)u_2] \tag{12}$$

$$\dot{\psi}_2 = \left[\tfrac{h\sin\phi}{LL_2}\left(\tfrac{L_2\cos\psi_1}{L_1} + \tfrac{(L_1+h_1)\cos\psi_1\cos\psi_2}{L_1}\cos(\psi_1+\psi_2)\right) + \tfrac{\cos\phi\sin\psi_1}{L_1}\left(1 + \tfrac{(L_1+h_1)\cos\psi_2}{L_2}\right) + \cdots \right.$$
$$\left. \cdots - \tfrac{\cos\phi\sin(\psi_1+\psi_2)}{L_2}\right](\cos(\theta+\phi)u_1 + \sin(\theta+\phi)u_2)$$

$$\dot{\phi} = -\left[\frac{\cos(\theta+\phi)\sin\phi}{L} + \frac{\sin(\theta+\phi)}{b}\right]u_1 - \left[\frac{\sin(\theta+\phi)\sin\phi}{L} + \frac{\cos(\theta+\phi)}{b}\right]u_2.$$

This system is I-O linear and it can be devided into a linear subsystem and the so-called zero dynamics as follows

$$\begin{pmatrix}\dot{x}_P\\ \dot{y}_P\end{pmatrix} = \begin{pmatrix}u_1\\ u_2\end{pmatrix} \quad : \quad \text{linear subsystem, two channels} \tag{13}$$

$$\dot{\eta} = P(\eta)u_1 + Q(\eta)u_2 = R(\eta)\begin{pmatrix}u_1\\ u_2\end{pmatrix} \quad : \quad \text{nonlinear zero dynamics.} \tag{14}$$

The linear subsystem consists of two decoupled equations, i.e. one integrator per channel. It has relative degree $r = 1$ and it is the only one responsible for the input-output behaviour. The nonlinear zero dynamics does not affect the output, which suggests that the zero dynamics does not have to be bounded for the tracking problem. The seperation into two subsystems is illustrated in Fig. 5. Practically, however, the divergence of the zero dynamics (more specifically if the two hitch angles ($\psi_{1,2}$) would diverge) is responsible for the *jackknife* effect and therefore for an unsuccessful output tracking. The zero dynamics plays the same role as the zeros of the transfer function. In the present case the instability of the zero dynamics appears due to the

Die approbierte gedruckte Originalversion dieser Diplomarbeit ist an der TU Wien Bibliothek verfügbar
The approved original version of this thesis is available in print at TU Wien Bibliothek.
TU Bibliothek WIEN Your knowledge hub

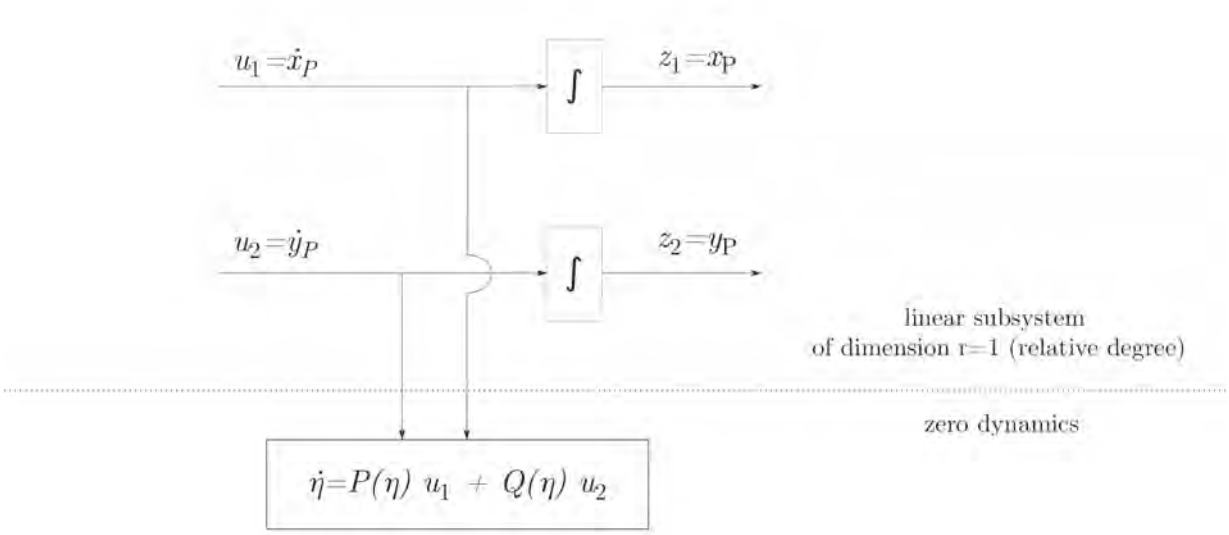

Figure 5: shows the linear subsystem as an integrator on each channel and the zero dynamics.

inversion of the system into an I-O linear system. The next step we want to do is to implement a state feedback controller in (12) that tracks the reference output $z_r(z) = (x_r(t) \quad y_r(t))^T$. The reference output for the representative point P will also be denoted as the cartesian reference trajectory. The cartesian reference velocities can be written as $\dot{z}_r(t) = (\,\dot{x}_r(t) \quad \dot{y}_r(t))^T$. A state feedback control of the following form

$$\begin{aligned} u_1 &= u_1^{track} = K_1\,(x_r - x_p) + \dot{x}_r \\ u_2 &= u_2^{track} = K_2\,(y_r - y_p) + \dot{y}_r, \end{aligned} \tag{15}$$

where $(K_1, K_2) > 0$, makes the two output variables $z = (x_P \quad y_P)^T$ converge exponentially to the reference output. To show this the resulting linear subsystem, where controller (15) is applied, will be shown in the following

$$\begin{aligned} \dot{x}_P &= K_1\,(x_r - x_p) + \dot{x}_r \quad (\Rightarrow\ \dot{\varepsilon_x} = -K_1\varepsilon_x) \\ \dot{y}_P &= K_2\,(y_r - y_p) + \dot{y}_r \quad (\Rightarrow\ \dot{\varepsilon_y} = -K_2\varepsilon_y)\,. \end{aligned}$$

The error dynamics in the paranthesis can be easily obtained knowing that the cartesian errors are defined as $\varepsilon_x = x_P - x_r$ and $\varepsilon_y = y_P - y_r$. The solution of the error dynamics makes the exponential convergence of the output to its reference clear. However, the tracking controller can not control the zero dynamics. It has already been mentioned, that, in backward direction,

Die approbierte gedruckte Originalversion dieser Diplomarbeit ist an der TU Wien Bibliothek verfügbar
The approved original version of this thesis is available in print at TU Wien Bibliothek.
TU Bibliothek Your knowledge hub WIEN

the zero dynamics does not affect the output, but in practice the divergence of the hitch angles will lead to the *jackknife* effect and thus failing the tracking problem. Later in the proposed approach a linear approximation around a bounded state trajectoy that gives time invariant linear dynamics will be introduced. For this system one can find that the zero dynamics is unobservable and the eigenvalues for the tractor heading θ and the two hitch angles $\psi_{1,2}$ have positive real part while the vehicle moves in backward direction. Hence they diverge.

Before the proposed approach to overcome the above described problem is presented in the next section, some further important comments are necessary. In foward direction the evolution of θ, ψ_1, and ψ_2 remains bounded. This will be important to generate a kinematic feasible cartesian reference trajectory. The steering angle ϕ is part of the zero dynamics, but has not been discussed yet. The evolution of ϕ remains bounded in both directions by choosing the sign of the parameter b appropriately. Remember, $b \neq 0$ for the I-O linearisation. To obtain a bounded evolution of the steering angle for the case in which the vehicle moves in backward direction b must be negative. On the contrary b must be positive to obtain a bounded evolution of ϕ when the vehicle moves in forward direction. If b takes the contrary sign then the steering angle would try to make a 180 degree rotation, which is, of course, only possible in a simulation as the experimental setup has its physical limitations. For a better understanding see the simulations in Fig. 6.

2.2 Adopted control approach

We have seen in the previous section that a state feedback controller applied on the I-O linearised system is not able to manoeuvre the vehicle in backward motion along a cartesian reference trajectory. This is due to the internal instability of the zero dynamics that appears due to the inversion. In this section the approach to obtain a stable inversion will be presented step by step. The basic idea, however, is to add a corrective term to the previously presented tracking controller. To model the corrective input the system equations will be linearised around a reference state trajectory q_r, which contains a reference for each state of the system, not only for x_P and y_P. A change of coordinates helps to split the system into a stable and an unstable subsystem. The solution of the linear unstable subsystem is composed by the forced evolution (driven by the corrective input) and by the free evolution, that contains the initial condition.

Die approbierte gedruckte Originalversion dieser Diplomarbeit ist an der TU Wien Bibliothek verfügbar
The approved original version of this thesis is available in print at TU Wien Bibliothek.
TU Bibliothek Your knowledge hub WIEN

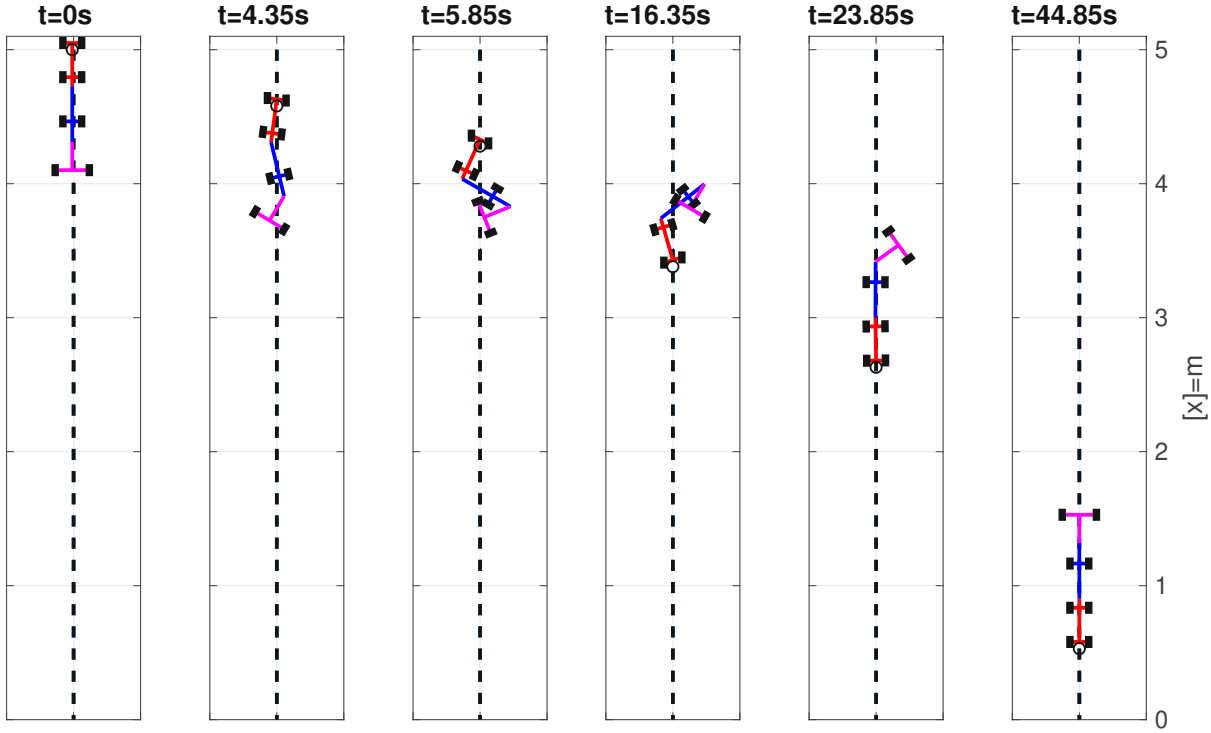

Figure 6: summarises the tracking problem by showing configuration plots at different t. The tractor is coloured in red, and the two trailers in the other two colours. The event shown in the figures happens if either (i) only the tracking controller is applied or (ii) $b > 0$ while the steering angle ϕ is not stabilised with the adopted approach. To fix (ii) one can simply change the sign of b. The unstable zero dynamics does not affect the output tracking, however, the *jackknife* effect occurs, and the front wheels perform a π rad rotation in the simulation. The last configuration corresponds to the one in which the reference output is tracked in forward direction with $b > 0$.

In order to make the evolution of the unstable states bounded the initial condition is chosen such that the free evolution cancels the forced evolution. This is done repetitively at every sampling time. The inital state for later sampling times results from the vehicle moving, that's why the condition on the initial state is shifted to a condition on the corrective input.

2.2.1 Reference state trajectory

The feasible reference state trajectory is denoted with $q_r = (x_r \quad y_r \quad \theta_r \quad \psi_{1,r} \quad \psi_{2,r} \quad \phi_r)^T$, and can be also written as

Die approbierte gedruckte Originalversion dieser Diplomarbeit ist an der TU Wien Bibliothek verfügbar
The approved original version of this thesis is available in print at TU Wien Bibliothek.
TU Bibliothek Your knowledge hub WIEN

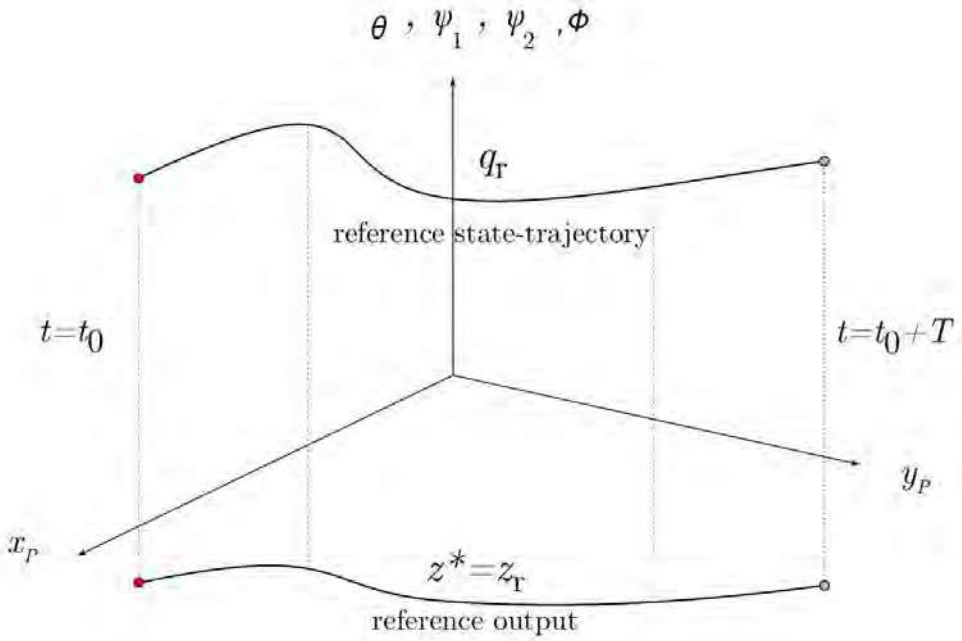

Figure 7: shows the reference state trajectory and its projection on the x_P, y_P plane, i.e. the reference output. The forward maneuver starts at the initial time $t = t_0$ (red configuration) and stops at $t = t_0 + T$ (grey configuration). This evolution seen reverse in time yields the reference state trajectory for the backward maneuver q_r.

$$q_r = \begin{pmatrix} z_r \\ \eta_r \end{pmatrix}. \tag{16}$$

We need to find an 'internally stable' reference state trajectory that is kinematically feasible. In forward motion the zero dynamics is stable. Therefore, using the kinematic model and the tracking controller presented previously a forward maneuver is computed. For this computation the initial configuration at t_0 is one, in which the tractor and the trailers are in one line. This finally gives a kinematically feasible reference state trajectory in forward motion as illustrated in Fig. 7. Remember, during the forward motion b has to be non-zero and positive. The forward maneuver reverse in time can be considered as the backward maneuver (with b non-zero and negative this time). From now onwards the parameter b is non-zero and positive in forward motion, and non-zero and negative in backward motion, if not stated explicitely. The

Die approbierte gedruckte Originalversion dieser Diplomarbeit ist an der TU Wien Bibliothek verfügbar
The approved original version of this thesis is available in print at TU Wien Bibliothek.
TU Bibliothek Your knowledge hub WIEN

algorithm will be described in the following.

(i) $z^*(t) = (x_P^*(t) \quad y_P^*(t))$: is a desired cartesian trajectory in backward motion and shall be given.

(ii) $z_{fw}^* = (x_{P,fw}^*(t) \quad y_{P,fw}^*(t))$: contains the same path as z^*, but in forward motion. This can be also understood as z^* reverse in time, and vice versa. In the code this is done by simply flipping the vectors over.

(iii) To track $z_{fw}^*(t)$ the kinematic model is integrated using the Matlab ode15s solver and the following state feedback control (tracking controller)

$$u_1^{track} = K_1 \left(x_{P,fw}^* - x_{P,fw}\right) + \dot{x}_{P,fw}$$

$$u_2^{track} = K_2 \left(y_{P,fw}^* - y_{P,fw}\right) + \dot{y}_{P,fw},$$

obtaining a feasible state trajectory in forward motion

$$q_{fw}(t) = (x_{P,fw} \quad y_{P,fw} \quad \theta_{fw} \quad \psi_{1,fw} \quad \psi_{2,fw} \quad \phi_{fw})^T,$$

which we can take as the reference state trajectory in forward motion

$$q_{r,fw} = q_{fw}.$$

(iv) Finally $q_r(t)$ is obtained by considering $q_{r,fw}(t)$ reverse in time.

Note that $q_r(t)$ can be computed a priori if the trajectory remains the same for all times. If an obstacle shall be avoided by changing the trajectory, $q_r(t)$ has to be computed or manipulated online and therefore the whole algorithm has to run in real-time.

2.2.2 Corrective input and linear approximation

Now the corrective term u^{corr} is added to the tracking controller (15) in order to deal with the instability occuring in the zero dynamics

$$\begin{aligned} u_1 &= K_1 \left(x_r - x_p\right) + \dot{x}_r + u_1^{corr} = u_1^{track} + u_1^{corr} \\ u_2 &= K_2 \left(y_r - y_p\right) + \dot{y}_r + u_2^{corr} = u_2^{track} + u_2^{corr}. \end{aligned} \tag{17}$$

Die approbierte gedruckte Originalversion dieser Diplomarbeit ist an der TU Wien Bibliothek verfügbar
The approved original version of this thesis is available in print at TU Wien Bibliothek.
TU Bibliothek Your knowledge hub WIEN

This is applied on the I-O linearised system (12), which leads to a nonlinear system of following form

$$\dot{q}(t) = f(q, u^{corr}, t), \tag{18}$$

$$q = (x_P \quad y_P \quad \theta \quad \psi_1 \quad \psi_2 \quad \phi)^T, \qquad u^{corr} = (u_1^{corr} \quad u_2^{corr})^T.$$

The corrective term will be designed based on a linear approximation of (18) around the reference state trajectory $q_r(t)$ and $u^{corr} = (0 \quad 0)^T$. Furthermore, it is more comfortable and expedient to work with the error dynamics of (18). The error and its velocity can be expressed as

$$\varepsilon(t) = q(t) - q_r(t) \tag{19}$$

$$\dot{\varepsilon}(t) = \dot{q}(t) - \dot{q}_r(t) = F(\varepsilon, u^{corr}, t). \tag{20}$$

If the error becomes zero, then $q(t) = q_r(t)$. Note that

$$\varepsilon(t) = (\varepsilon_1(t) \quad \varepsilon_2(t) \quad \varepsilon_3(t) \quad \varepsilon_4(t) \quad \varepsilon_5(t) \quad \varepsilon_6(t))^T.$$

In these new coordinates the point around which the linear approximation is performed becomes $(\varepsilon \quad u^{corr})^T = (\mathbf{0} \quad \mathbf{0})^T$

$$\dot{\varepsilon}(t) \simeq F(\mathbf{0}, \mathbf{0}, t) + \left.\frac{\partial F}{\partial \varepsilon}\right|_{(\mathbf{0}\ \mathbf{0})^T} (\varepsilon - \mathbf{0}) + \left.\frac{\partial F}{\partial u^{corr}}\right|_{(\mathbf{0}\ \mathbf{0})^T} (u^{corr} - \mathbf{0})$$

with

$$A(t) = \left.\frac{\partial F}{\partial \varepsilon}\right|_{(\mathbf{0}\ \mathbf{0})^T} \qquad B(t) = \left.\frac{\partial F}{\partial u^{corr}}\right|_{(\mathbf{0}\ \mathbf{0})^T} \qquad F(\mathbf{0}, \mathbf{0}, t) = 0$$

Die approbierte gedruckte Originalversion dieser Diplomarbeit ist an der TU Wien Bibliothek verfügbar
The approved original version of this thesis is available in print at TU Wien Bibliothek.
TU Bibliothek WIEN Your knowledge hub

$$\dot{\varepsilon}(t) = A(t)\,\varepsilon(t) + B(t)\,u^{corr}(t). \tag{21}$$

The matrices $A(t)$ and $B(t)$ are not shown here to keep the text compact. The reader can find them in the Appendix A. Note that system (21) is linear time variant.

2.2.3 Change of coordinates and stability constraint

The stability constraint shall be formulated for the unstable states only, which includes the states $\theta(t)$, $\psi_1(t)$, and $\psi_2(t)$. Therefore $\varepsilon_3(t)$, $\varepsilon_4(t)$, and $\varepsilon_5(t)$ are the diverging components. The goal would be to write a change of coordinates in the following form

$$\begin{pmatrix} \varepsilon_s(t) \\ \varepsilon_u(t) \end{pmatrix} = T\varepsilon(t) \qquad \text{where} \qquad T = U^{-1}\text{ , the eigenvectors of } A(t) \text{ in (21).}$$

The difficulty is that the considered system (21) is linear time variant (LTV). To deal with this problem some results from the next section will be anticipated. There, an MPC problem on the sampled system will be formulated which determines the corrective input u^{corr} iteratively at each sampling time. The MPC framework consists of two approximations. The first one is that the LTV system (21) is assumed to be time invariant during each sampling interval, i.e. a piecewise time invariant system. However, after this approximation the transformation matrix T would not be the same for all sampling intervals. The second approximation consists of assuming that at the current sampling time t_k the transformation matrix is constant also for future time instants that are considered at $t = t_k$, i.e. $T_j = T_k$ for $j = k, k+1, \cdots$.

Before the above mentioned is done the stability constraint is derived for a generic linear time invariant system (LTI)

$$\dot{\varepsilon}(t) = A\,\varepsilon(t) + B\,u^{corr}(t)$$

in order to create an understanding for the stability constraint. If the considered system has no eigenvalues with zero real part, then, in general, there exists a change of coordinates

Die approbierte gedruckte Originalversion dieser Diplomarbeit ist an der TU Wien Bibliothek verfügbar
The approved original version of this thesis is available in print at TU Wien Bibliothek.
TU Bibliothek WIEN Your knowledge hub

$$\begin{pmatrix} \varepsilon_s(t) \\ \varepsilon_u(t) \end{pmatrix} = T \cdot \varepsilon(t)$$

such that

$$\begin{pmatrix} \dot{\varepsilon}_s(t) \\ \dot{\varepsilon}_u(t) \end{pmatrix} = \begin{pmatrix} \Lambda_s & 0 \\ 0 & \Lambda_u \end{pmatrix} \begin{pmatrix} \varepsilon_s(t) \\ \varepsilon_u(t) \end{pmatrix} + \begin{pmatrix} G_s \\ G_u \end{pmatrix} u^{corr}(t) \tag{22}$$

$$\Lambda = TAT^{-1} \qquad \& \qquad G = TB \qquad \& \qquad T = U^{-1},$$

where U contains the right eigenvectors of the system and $\Lambda = diag(\Lambda_s, \Lambda_u)$ the eigenvalues. Λ_s and Λ_u have negative and positive real parts, respectively, and both are in diagonal form. The evolution of the diverging states can be written as

$$\begin{aligned} \varepsilon_u(t) &= e^{\Lambda_u(t-t_0)}\varepsilon(t_0) + \int_{t_0}^{t} e^{\Lambda_u(t-\tau)} G_u u^{corr}(\tau) d\tau \\ &= e^{\Lambda_u(t-t_0)} \left[\varepsilon(t_0) + \int_{t_0}^{t} e^{\Lambda_u(t_0-\tau)} G_u u^{corr}(\tau) d\tau \right]. \end{aligned}$$

A special initial condition $\varepsilon_u^\star$ is chosen such that the free evolution cancels the forced evolution, and therefore making the error zero

$$\varepsilon_u(t_0) = \varepsilon_u^\star(t_0) \quad = \quad -\int_{t_0}^{\infty} e^{\Lambda_u(t_0-\tau)} G_u u^{corr}(\tau) d\tau. \tag{23}$$

Then one obtains

$$\begin{aligned} \varepsilon_u^\star(t) &= e^{\Lambda_u(t-t_0)} \left[-\int_{t_0}^{\infty} e^{\Lambda_u(t_0-\tau)} G_u u^{corr}(\tau) d\tau + \int_{t_0}^{t} e^{\Lambda_u(t_0-\tau)} G_u u^{corr}(\tau) d\tau \right] \\ &= -e^{\Lambda_u(t-t_0)} \int_{t}^{\infty} e^{\Lambda_u(t-\tau)} G_u u^{corr}(\tau) d\tau. \end{aligned}$$

Die approbierte gedruckte Originalversion dieser Diplomarbeit ist an der TU Wien Bibliothek verfügbar
The approved original version of this thesis is available in print at TU Wien Bibliothek.
TU Bibliothek WIEN Your knowledge hub

And finally

$$\varepsilon_u^\star(t) \quad = \quad -\int_t^\infty e^{-\Lambda_u(\tau-t)} G_u u^{corr}(\tau) d\tau. \tag{24}$$

The stability constraint (23) is a special initial condition of the unstable states, which makes their evolutions (24) bounded. Note that the two constraints (23) and (24) are equivalent. The left hand side in (23) cannot be chosen by will, whereas the corrective input on the right hand side can be. Therefore, eq. (24) can be used to design the corrective input by zeroing the error evolution of the unstable states. The real-time algorithm will go through this designing process at every sampling interval of duration δ to counteract the diverging character of ε_u. At each sampling time $t = t_k$ eq. (24) depends on the future history of the control action. Moreover, it is valid for the LTI system and will be modified in the next section in order to take the time dependency of the matrices A and B into account. More precisely they will be considered to be piecewise constant and therefore also the matrices Λ_u and G_u. However, to derive the latter matrices, the transformation matrix T is kept constant for the whole future history during one designing process.

2.3 MPC Framework

This section provides a framework to technically realise the design of the corrective input u^{corr}. The basic idea is to set at each sampling time a quadratic problem (QP) in which the decision variable is the corrective input. The cost function is subject to a discrete stability constraint that will be derived in a similar manner as (24), thus to a 'bounded' state evolution of the zero dynamics. As the stability constraint is an improper integral depending on the future history of the control action some requirements such as e.g. the prediction of the future states will be necessary. Furthermore, a discretisation of the equations will be presented.

Die approbierte gedruckte Originalversion dieser Diplomarbeit ist an der TU Wien Bibliothek verfügbar
The approved original version of this thesis is available in print at TU Wien Bibliothek.
TU Bibliothek Your knowledge hub WIEN

2.3.1 Prediction model

The prediction model, as the name suggests, is used to compute the state vector q at future time instants. To this end the time variant error dynamics (21) of the system will be discretised first. The system matrices and the corrective input will be considered piecewise time invariant over a time intervall of $\delta = t_{k+1} - t_k$

$$\dot{\varepsilon}(t) = A_k \cdot \varepsilon(t) + B_k \cdot u_k^{corr} \qquad t_k \leq t \leq t_{k+1}. \tag{25}$$

Secondly, the prediction model is obtained by solving the time invariant system (25) for the next sampling time

$$\begin{aligned} \varepsilon_{k+1} &= e^{A_k(t_{k+1}-t_k)}\varepsilon_k + \int_{t_k}^{t_{k+1}} e^{A_k(t_{k+1}-\tau)} B_k u_k^{corr} d\tau \\ &= \left[e^{A_k\delta}\right]\varepsilon_k + \left[\left(\int_{t_k}^{t_{k+1}} e^{A_k(t_{k+1}-\tau)} d\tau\right) B_k\right] u_k^{corr} \end{aligned}$$

leading to

$$\varepsilon_{k+1} = \left[e^{A_k\delta}\right]\varepsilon_k + \left[A_k^{-1}\left(e^{A_k\delta} - I\right) B_k\right]\ u^{corr}. \tag{26}$$

where the two terms in the squared brackets are abbreviated with A_k^D and B_k^D, yielding the prediction model

$$\varepsilon_{k+1} = A_k^D \varepsilon_k + B_k^D u_k^{corr}. \tag{27}$$

where

$$\varepsilon_{k+1} = \begin{pmatrix} \varepsilon_{1,k+1} & \varepsilon_{2,k+1} & \varepsilon_{3,k+1} & \varepsilon_{4,k+1} & \varepsilon_{5,k+1} & \varepsilon_{6,k+1} \end{pmatrix}^T.$$

Note that the whole state vector can be predicted. A part of the prediction model will be used by the HPIPM solver. There only the unstable states need to be predicted as the QP is set for the unstable subsystem only. The prediction of stable states is also used as for example by the Kalman filter, that will be discussed later. Furthermore, also stable states, such as the steering angle ϕ, can be included in the QP in order to set a state constraint. For these reasons the full prediction model has been presented in this section.

Die approbierte gedruckte Originalversion dieser Diplomarbeit ist an der TU Wien Bibliothek verfügbar
The approved original version of this thesis is available in print at TU Wien Bibliothek.
TU Bibliothek WIEN Your knowledge hub

2.3.2 Terminal constraint

The two step approximation for the stability constraint (24) has already been mentioned. It consists of assuming piecewise constant system matrices Λ_u and G_u in eq. (24) while for each QP the transformation matrix T in eq. (22) is kept constant for all future time instants. This leads to a sum with an infinite upper limit of summation. The result of it is the discrete stability condition shown in the Appendix B. In the Appendix there are also two strategies discussed in more detail of how to deal with the infinite upper limit occuring in the stability condition. They will be shortly mentioned here as well (for further details refer to the Appendix B). To this end a finite control horizon $T_C = C \cdot \delta$ is defined, where C is the number of time steps to reach $t_{k+C} = t_k + T_C$ from the current time instant t_k.

1. The first strategy is that of the 'truncated' tail, in which the corrective input u^{corr} will be set to zero for $t > t_k + T_C$, and only control actions within the control horizon are considered.

2. The second is that of the 'periodic' tail, where the tail is assumed to be a finite replication of the first C corrective control actions.

In the current work the first strategy (truncated tail) is used for reasons that will become successively clear. The HPIPM solver does not allow the implementation of the discrete version of the stability constraint (24). Therefore, it is necessary to rewrite the stability constraint (24) into a terminal constraint that acts at the end of the control horizon. For this purpose the unstable subsystem of (22) will be integrated up to t_{k+C}

$$\varepsilon_u(t_{k+C}) = e^{\Lambda_u(t_{k+C}-t_k)}\varepsilon_u(t_k) + \int_{t_k}^{t_{k+C}} e^{\Lambda_u(t_{k+C}-\tau)} G_u u^{corr}(\tau) d\tau \tag{28}$$

and using the stability constraint (24) at the instant t_k as initial condition yields

Die approbierte gedruckte Originalversion dieser Diplomarbeit ist an der TU Wien Bibliothek verfügbar
The approved original version of this thesis is available in print at TU Wien Bibliothek.
TU Bibliothek WIEN Your knowledge hub

$$
\begin{aligned}
\varepsilon_u^\star(t_{k+C}) &= -e^{\Lambda_u(t_{k+C}-t_k)} \int_{t_k}^{\infty} e^{\Lambda_u(t_k-\tau)} G_u u^{corr}(\tau) d\tau + \int_{t_k}^{t_{k+C}} e^{\Lambda_u(t_{k+C}-\tau)} G_u u^{corr}(\tau) d\tau = \\
&= e^{\Lambda_u(t_{k+C}-t_k)} \left[-\int_{t_k}^{\infty} e^{\Lambda_u(t_k-\tau)} G_u u^{corr}(\tau) d\tau + \int_{t_k}^{t_{k+C}} e^{\Lambda_u(t_k-\tau)} G_u u^{corr}(\tau) d\tau \right] = \\
&= -e^{\Lambda_u(t_{k+C}-t_k)} \int_{t_{k+C}}^{\infty} e^{\Lambda_u(t_k-\tau)} G_u u^{corr}(\tau) d\tau.
\end{aligned}
$$

Therefore the terminal stability-constraint becomes

$$
\varepsilon_u^\star(t_{k+C}) = -\int_{t_{k+C}}^{\infty} e^{\Lambda_u(t_{k+C}-\tau)} G_u u^{corr}(\tau) d\tau. \tag{29}
$$

It will be referred to this equation as the 'terminal' constraint, knowing that it is equivalent to the stability constraint. The system matrices Λ_u and G_u in (29) arise from the change of coordinates (section 2.2.3) of the LTI system into a stable and an unstable subsystem. But only for the change of coordinates an LTI system shall be assumed. The time dependency of the system matrices will be approximated as already done by the piecewise time invariant system (25)(there A_k, B_k, and u_k^{corr} are piecewise constant). The time t also runs through a discrete set of equidistant values $t_{j+1} = t_j + \delta$. Finally, the system matrices in (29) are modified as follows

$$
\Lambda_{u,j} = T_{u,k} A_{u,j} T_{u,k}^{-1} \quad \& \quad G_{u,j} = T_{u,k} B_{u,j} \quad \& \quad T_{u,k} = U_{u,k}^{-1} \quad \forall \quad j = k, k+1, \cdots \infty.
$$

Note that the transformation matrix stays constant $T_j = T_k$. We apply this discretisation on (29) yielding

$$
\begin{aligned}
\varepsilon_u^\star(t_{k+C}) &\cong -\sum_{j=k+C}^{\infty} \left[\int_{t_j}^{t_{j+1}} e^{-\Lambda_{u,j}(-t_{k+C}+\tau)} d\tau \right] G_{u,j} u_j^{corr} = \\
&= \sum_{j=k+C}^{\infty} \left[\Lambda_{u,j}^{-1} e^{-\Lambda_{u,j}(-t_{k+C}+\tau)} \right]_{t_j}^{t_{j+1}} G_{u,j} u_j^{corr} = \\
&= \sum_{j=k+C}^{\infty} \Lambda_{u,j}^{-1} \left[e^{-\Lambda_{u,j}(-t_{k+C}+t_j+\delta)} - e^{-\Lambda_{u,j}(-t_{k+C}+t_j)} \right] G_{u,j} u_j^{corr},
\end{aligned}
$$

Die approbierte gedruckte Originalversion dieser Diplomarbeit ist an der TU Wien Bibliothek verfügbar
The approved original version of this thesis is available in print at TU Wien Bibliothek.
TU Bibliothek WIEN Your knowledge hub

and thus the terminal constraint becomes

$$\varepsilon_u^\star(t_{k+C}) = \sum_{j=k+C}^{\infty} \Lambda_{u,j}^{-1} e^{-\Lambda_{u,j}(-t_{k+C}+t_j)} \left[e^{-\Lambda_{u,j}\delta} - I\right] G_{u,j} u_j^{corr}. \tag{30}$$

The terminal constraint (30) acts only on the tail that gets truncated yielding a very simple expression for the terminal constraint in which no transformation matrix occurs.

$$\varepsilon_u^\star(t_{k+C}) = 0. \tag{31}$$

2.3.3 State and input constraints

The physical limitations of the system can be considered as constraints of the QP. There are limitations for the traction and steering velocity v and ω, as well as for some states. In this section the index j is always a non-negative integer $j = k, ..., k + C$. The integer will appear, but for convenience its range will not be written explicitly every time.

State constraints

The HPIPM solver enables to set a state constraint individually for each time instant within the control horizon. More precisely, a lower and upper bound can be set for every state at every time instant. If the lower and uper bound are chosen identical, then an equality constraint is enforced. However, often in an MPC framework a state constraint is set for the first few time instants within the control horizon. In particular the steering angle ϕ and the two hitch angles $\psi_{1,2}$ cannot exceed certain values for any time instant j

$$\begin{bmatrix} -\psi_{1,max} \\ -\psi_{2,max} \\ -\phi_{max} \end{bmatrix} \leq \begin{bmatrix} J_{b,\psi_1,j} \cdot \psi_{1,j} \\ J_{b,\psi_2,j} \cdot \psi_{2,j} \\ J_{b,\phi,j} \cdot \phi_j \end{bmatrix} \leq \begin{bmatrix} \psi_{1,max} \\ \psi_{2,max} \\ \phi_{max} \end{bmatrix}$$

where the matrices $J_{b,q,j}$ allow further transformation and correspond to the identity matrix $J_{b,q,j} = I$, the identity matrix, in the present problem. Now we can substract $\psi_{1,r,j}$, $\psi_{2,r,j}$, and

Die approbierte gedruckte Originalversion dieser Diplomarbeit ist an der TU Wien Bibliothek verfügbar
The approved original version of this thesis is available in print at TU Wien Bibliothek.
TU Bibliothek WIEN Your knowledge hub

$\phi_{r,j}$ from the first, second, and third row, respectively, and obtain:

$$\begin{bmatrix} -\psi_{1,max} - \psi_{1,r,j} \\ -\psi_{2,max} - \psi_{2,r,j} \\ -\phi_{max} - \phi_{r,j} \end{bmatrix} \leq \begin{bmatrix} I \cdot \varepsilon_{4,j} \\ I \cdot \varepsilon_{5,j} \\ I \cdot \varepsilon_{6,j} \end{bmatrix} \leq \begin{bmatrix} \psi_{1,max} - \psi_{1,r,j} \\ \psi_{2,max} - \psi_{2,r,j} \\ \phi_{max} - \phi_{r,j} \end{bmatrix} \tag{32}$$

Input constraints

The input constraints can be set in similar manner. Again, the solver offers a box constraint individually for each time instant in the control horizon in the form of:

$$\underline{u}_j \leq J_{b,u,j} \cdot u_j^{corr} \leq \overline{u}_j.$$

This time we have to think more of how to choose the matrix $J_{b,u,j}$. The inputs v and ω cannot exceed certain values at any time instant j

$$\begin{bmatrix} v_{min} \\ \omega_{min} \end{bmatrix} \leq \begin{bmatrix} v_j \\ \omega_j \end{bmatrix} \leq \begin{bmatrix} v_{max} \\ \omega_{max} \end{bmatrix}$$

Now the tranformation (11) can be used to obtain:

$$\begin{bmatrix} v_{min} \\ \omega_{min} \end{bmatrix} \leq D^{-1}(\theta_j, \phi_j) \begin{bmatrix} u_{1,j}^{track} + u_{1,j}^{corr} \\ u_{2,j}^{track} + u_{2,j}^{corr} \end{bmatrix} \leq \begin{bmatrix} v_{max} \\ \omega_{max} \end{bmatrix}.$$

And finally one obtains

$$\begin{bmatrix} v_{min} \\ \omega_{min} \end{bmatrix} - D_j^{-1} \cdot u_j^{track} \leq D^{-1} \cdot u_j^{corr} \leq \begin{bmatrix} v_{max} \\ \omega_{max} \end{bmatrix} - D_j^{-1} \cdot u_j^{track}, \tag{33}$$

where the lower bound, the upper bound and the matrix $J_{b,u,j}$ can be identified as

Die approbierte gedruckte Originalversion dieser Diplomarbeit ist an der TU Wien Bibliothek verfügbar
The approved original version of this thesis is available in print at TU Wien Bibliothek.
TU Bibliothek Your knowledge hub WIEN

$$
\begin{aligned}
J_{b,u,j} &= D^{-1}(\theta_j, \phi_j) = D_j \\
\underline{u} &= \begin{bmatrix} v_{min} \\ \omega_{min} \end{bmatrix} - D_j^{-1} \cdot u_j^{track} \\
\overline{u} &= \begin{bmatrix} v_{max} \\ \omega_{max} \end{bmatrix} - D_j^{-1} \cdot u_j^{track}.
\end{aligned}
$$

2.3.4 Optimal control problem (OCP) QP

The HPIPM solver uses the interior point method for optimisation and offers different QPs types: dense QPs (like Matlab quadprog solver) and optimal control problem (OCP) QPs. The OCP QP brings some advantages and better performance in the real system that are discussed later. The cost function to minimise is the following.

$$
\min_{u^{corr}} J = \min_{u^{corr}} \frac{1}{2} \sum_{j=k}^{k+C} \left(u_j^{corr}\right)^2 \tag{34}
$$

Die approbierte gedruckte Originalversion dieser Diplomarbeit ist an der TU Wien Bibliothek verfügbar
The approved original version of this thesis is available in print at TU Wien Bibliothek.
TU Bibliothek Your knowledge hub WIEN

subject to:

(i) Prediction Model (see also (27)) :

$$\varepsilon_{\eta,j+1} = A^D_{\eta,j}\varepsilon_j + B^D_{\eta,j}u^{corr}_j \qquad j = k, \ldots, k+C-1$$

(ii) Terminal Stability-Constraint (31):

$$\begin{bmatrix} 0 \\ 0 \\ 0 \end{bmatrix} \leq \begin{bmatrix} \varepsilon_{3,j} \\ \varepsilon_{4,j} \\ \varepsilon_{5,j} \end{bmatrix} \leq \begin{bmatrix} 0 \\ 0 \\ 0 \end{bmatrix} \qquad j = k+C$$

(iii) State Constraint (32):

$$\begin{bmatrix} -\psi_{1,max} - \psi_{1,r,j} \\ -\psi_{2,max} - \psi_{2,r,j} \\ -\phi_{max} - \phi_{r,j} \end{bmatrix} \leq \begin{bmatrix} \varepsilon_{4,j} \\ \varepsilon_{5,j} \\ \varepsilon_{6,j} \end{bmatrix} \leq \begin{bmatrix} \psi_{1,max} - \psi_{1,r,j} \\ \psi_{2,max} - \psi_{2,r,j} \\ \phi_{max} - \phi_{r,j} \end{bmatrix} \qquad j = k+1, \ldots, k+10$$

(iv) Input Constraint (33):

$$\begin{bmatrix} v_{min} \\ \omega_{min} \end{bmatrix} - D_j^{-1} \cdot u_j^{track} \leq D_j^{-1} \cdot u_j^{corr} \leq \begin{bmatrix} v_{max} \\ \omega_{max} \end{bmatrix} - D_j^{-1} \cdot u_j^{track} \qquad j = k+1, \ldots, k+10$$

(v) Initial Condition for the QP:

$$\begin{bmatrix} \varepsilon_{3,odo} \\ \varepsilon_{4,odo} \\ \varepsilon_{5,odo} \\ \varepsilon_{6,odo} \end{bmatrix} \leq \begin{bmatrix} \varepsilon_{3,j} \\ \varepsilon_{4,j} \\ \varepsilon_{5,j} \\ \varepsilon_{6,j} \end{bmatrix} \leq \begin{bmatrix} \varepsilon_{3,odo} \\ \varepsilon_{4,odo} \\ \varepsilon_{5,odo} \\ \varepsilon_{6,odo} \end{bmatrix} \qquad j = k$$

Die approbierte gedruckte Originalversion dieser Diplomarbeit ist an der TU Wien Bibliothek verfügbar
The approved original version of this thesis is available in print at TU Wien Bibliothek.
TU Bibliothek Your knowledge hub WIEN

where

$$\varepsilon_\eta = (\varepsilon_3 \qquad \varepsilon_4 \qquad \varepsilon_5 \qquad \varepsilon_6)$$

is the error vector that consists of the states of the zero dynamics, in which the first three correspond to the unstable states and the last one corresponds to the steering angle ϕ.

In the initial Condition (v) the bounds are set equal to the current states that are partly obtained directly from the odometry and partly reconstructed numerically from the odometry. In particular $\varepsilon_{4,odo}$, $\varepsilon_{6,odo}$, and $\varepsilon_{6,odo}$ - corresponding to the states ψ_1, ψ_2, and ϕ - are obtained directly by the odometry. All the other states are reconstructed from the odometry. However, the odometry data is not taken directly, but passes a Kalman filter described later. The initial condition (v) is the feedback part of the MPC, and as the initial condition cannot be changed by will, the corrective input u^{corr} is designed such that the stability condition is fulfilled.

The state and the input constraints are not used for some of the final experiments (two-trailers system, or one-trailer system with obstacle avoidance) as the capacity of the computer where this framework is implemented would otherwise not suffice to run the code in real-time. That's why the inclusion of the state and input constraints, i.e. points (iii) and (iv) remain as suggestions. The state and the input constraints are often implemented for the first few prediction steps only, as common in MPC. Note that the matrix D_j^{-1} includes future states that can be predicted by the prediction model. For this, the input sequence of the last sampling time can be used, as suggested by [19], as the current sequence is yet not available. As usual in MPC only the control input u^{corr} at the current time instant is implemented and not all C inputs. A new QP problem is set repetitively at every sampling time.

2.4 Kalman filter

The system with one trailer showed in early experiments a deviation from the desired trajectory in the direction of the tangent to z^* as well as normal to the tangent. The two-trailers system even includes one more measurement. A Kalman filter is used to correct these measurements in order to reduce the deviations. Avoiding this so-called dead reckoning enables precise reverse parking in a slot, even if the trajectory is long.

The Kalman filter considers process and measurement noise. The noise is added to the

Die approbierte gedruckte Originalversion dieser Diplomarbeit ist an der TU Wien Bibliothek verfügbar
The approved original version of this thesis is available in print at TU Wien Bibliothek.
TU Bibliothek WIEN Your knowledge hub

linearised equation (27) in the following way

$$q_{k+1} = q_{r,k+1} + A_k^D \varepsilon_k + B_k^D u_k^{corr} + v_k \tag{35}$$

$$y_k = C_k q_k + w_k, \tag{36}$$

where v_k is the process and w_k is the measurement noise. Both are Gaussian noises with zero mean and covariance matrices V_k and W_k. The matrix $C_k = \text{diag}(0,\ 0,\ 0,\ 1,\ 1,\ 1)$ returns the two hitch angles and the steering angle, which are the measured states and correspond to the system output y_k. The filter then works in two steps.

(i) Prediction: As this is a random process both the state q_{k+1} and the associated covariance P_{k+1} have to be estimated at the current time t_k. In the following equations this is indicated by the bar in the indices and the hat on the variable. The state is predicted using the knowledge of the process dynamics (prediction model) and the fact that the noises have zero mean. Also, the covariance has to be predicted and grows, therefore the uncertainty grows, as the following equation shows.

$$\hat{q}_{k+1|k} = q_{r,k+1} + A_k^D \hat{\varepsilon}_k + B_k^D u_k^{corr} \tag{37}$$

$$\hat{P}_{k+1|k} = A_k^{D^T} \hat{P}_k A_K^D + V_k \tag{38}$$

(ii) Correction: The predictions shall be corrected using the actual sensor readings y_{k+1}. More precisely it is corrected based on the difference between predicted and the measured output, the so-called innovation $\mu_{k+1} = y_{k+1} - C_{k+1} \cdot \hat{q}_{k+1|k}$. The corrected state and covariance matrix result in

$$\hat{q}_{k+1} = \hat{q}_{k+1|k} + R_{k+1}\mu_{k+1} \tag{39}$$

$$\hat{P}_{k+1} = \hat{P}_{k+1|k} - R_{k+1} C_{k+1} \hat{P}_{k+1|k} \tag{40}$$

where

$$R_{k+1} = \hat{P}_{k+1|k} C_{k+1}^T \left(C_{k+1} \hat{P}_{k+1|k} C_{k+1}^T + W_{k+1} \right) \tag{41}$$

Die approbierte gedruckte Originalversion dieser Diplomarbeit ist an der TU Wien Bibliothek verfügbar
The approved original version of this thesis is available in print at TU Wien Bibliothek.
TU Bibliothek WIEN Your knowledge hub

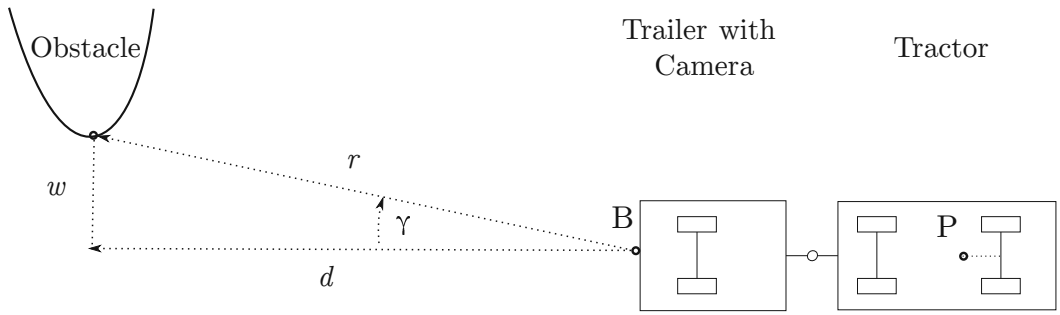

Figure 8: shows the range of the camera which is located in point B. The first trailer carries the camera and the second one is not shown for simplicity. The camera provides the normal distance d in every pixel. To each pixel an angle γ has been assigned experimentally.

is the Kalman gain matrix. It weights the accuracy of the prediction against that of the measurement. A large R matrix suggests that the measurements are more reliable. A small R suggests that the prediction is more reliable. The initial values for the covariances V_k and W_k are set by trial and error

$$\begin{aligned} V_k &= \mathrm{diag}(0,0,0,1,1,1) \\ W_k &= \mathrm{diag}(0.01,0.01,0.01). \end{aligned}$$

2.5 Obstacle avoidance

A feasible reference state trajectory $q_r(t_0 < t < T)$ can be precomputed offline for a given desired trajectory $z^*(t_0 < t < T)$, as described in section 2.2.1. However, if necessary a manipulation of the trajectory z^* shall be possible at every sampling time in order to avoid unexpected obstacles. The desired trajectory is changed by adding a spline, as described later in more detail. This requires that the feasible reference state trajectory $q_r(t)$ has to be computed online at each sampling time. In particular, the online computation of $q_r(t)$ needs only to be done for the control horizon, i.e. $t_k < t < t_k + T_C$, where t_k is the current time, and not until the end of the trajectory $t_k < t < T$. This saves computation time.

In the presence of an obstacle the goal is to perform the smallest deviation from the original trajectory necessary to avoid collision. In order to explore the environment the ASUS Prime-

Die approbierte gedruckte Originalversion dieser Diplomarbeit ist an der TU Wien Bibliothek verfügbar
The approved original version of this thesis is available in print at TU Wien Bibliothek.
TU Bibliothek WIEN Your knowledge hub

1	2	3	4	5	6	7	8	9	10	11	12	13	14	15	16	17
O	O	O	O					O	O	O						

Table 1: shows 17 width-pixels (i.e. they are aligned with w in Fig. 8) to illustrate the occupancy grid. Note that values are also obtained for the height-pixels but they are not shown here for simplicity. If a pixel is denoted with 'O' it is occupied, otherwise it is free. Keep in mind that the value of the distance (object to camera) is available in every occupied pixel.

Sense depth camera is used, where the access to the camera data is realised via the ROS (robot operating system) middleware. The camera is located on the end of the first trailer, aligned with the sagittal axis of the trailer. Let's consider the one-trailer system for simplicity. The camera has a resolution of 480 (height) x 640 (width) pixels. For each pixel a depth value denoted with d (normal distance to the camera, i.e. parallel to the sagittal axis) and an RGB (red green blue) value is obtained. For better understanding, see Fig. 8 as an example. To each d, an angle γ can be assigned and therefore also the range r and the width w from the sagittal axis can be computed.

2.5.1 Free space

At each sampling time the camera scans the area up to $2.5m$ in front of the trailer and returns the depth value d for each pixel, only if there is an obstacle. A free space is defined where there is no obstacle, i.e. each pixel with no value returned. All adjacent neighbours which return a depth value are interpreted as an occupied space (see in table 1 spaces 1 to 4 and 9 to 11), whereas the adjacent neighbours (pixels) that return no value are connected and interpreted as the free space. In table 1 this corresponds to the two spaces 5 to 8 and 12 to 17. Everything outside the range of the camera (let's say the fictitious pixels 18 and higher) can be only considered as occupied.

Therefore we could also say that the two free spaces in this example are between the pixels 4 & 9 and between 11 & 18 (see the table). This is done because only the free spaces shall be considered from now on and we do not want to lose the knowledge of how far away the obstacle is, which shall be avoided. In this way also each free space that exists is confined by

Die approbierte gedruckte Originalversion dieser Diplomarbeit ist an der TU Wien Bibliothek verfügbar
The approved original version of this thesis is available in print at TU Wien Bibliothek.
TU Bibliothek WIEN Your knowledge hub

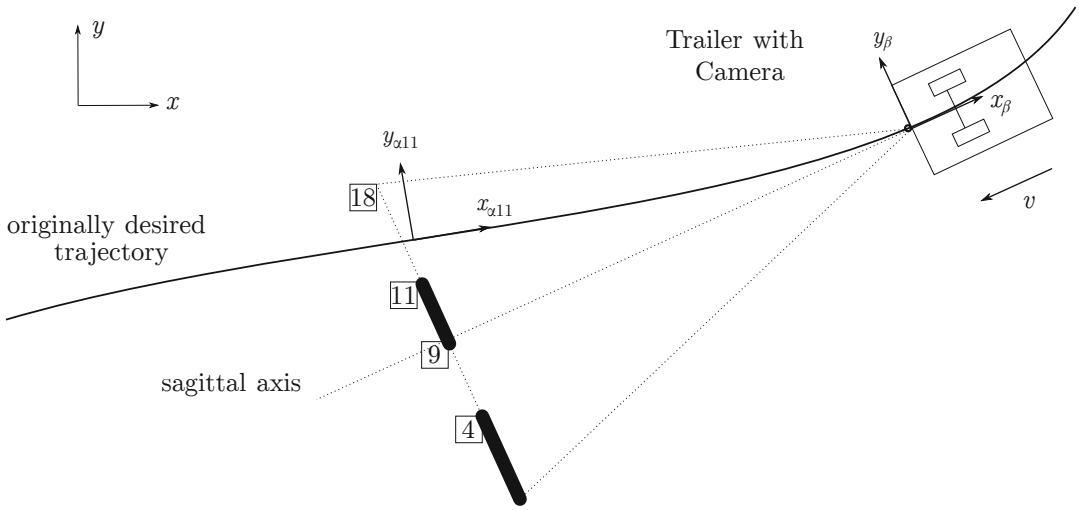

Figure 9: shows the trailer without the tractor and the view of the camera (triangle). Note that some pixels of table 1 are indicated by the numbers in the figure. Therefore the bold lines correspond to the occupied space and the rest is considered to be a free space. Also note that the obstacles (bold) in the figure are all depicted at the same normal distance d to the camera. This is done to simplify the illustration, hence d can vary for each point. Moreover the trailer lies perfectly on the desired trajectory to simplify the figure. In the experiments the actual position is considered.

two obstacles. In case that the whole visible range is free the free space is confined only by the invisible range. This would be pixel "0" and lower, and pixel "18" and higher.

2.5.2 Collision check

Clearly, if the originally desired trajectory lies within the free space and the free space is on both sides (i.e. to the left and to the right of the desired trajectory) wide enough, then no avoidance manoeuvre needs to be initialised. Therefore a collision check is necessary.

As already discussed above, each free space is confined by two points. This confinement points (4 & 9, and 11 & 18) derived from table 1 are depicted in Fig. 9. In a first step the normal distance to the desired trajectory z^* is computed for each of these points. This is discussed as an example for point 11. See Fig. 10 for this purpose.

Die approbierte gedruckte Originalversion dieser Diplomarbeit ist an der TU Wien Bibliothek verfügbar
The approved original version of this thesis is available in print at TU Wien Bibliothek.
TU Bibliothek Your knowledge hub WIEN

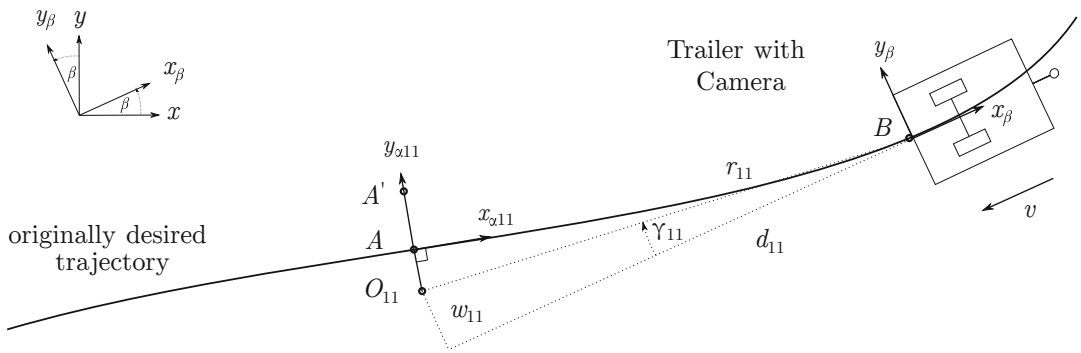

Figure 10: shows the trailer without the tractor and how the minimal distance from the edge of an obstacle (O_{11}) w.r.t. the desired trajectory is determined. For this purpose point A is determined. Furthermore it shows in which direction the point of the trajectory $A \rightarrow A'$ has to be moved in order to avoid the obstacle that is confined by Point O_{11}.

(i) The values d_{11}, r_{11}, γ_{11}, and $w_{11} = d_{11} \cdot \tan(\gamma_{11})$ are obtained by the camera. All correspond to point 11. The current angle β is known because the whole state has been numerically reconstructed. It is used for a coordinate transformation of point O_{11} between the two systems $(x_\beta,\ y_\beta)\ \rightarrow\ (x,\ y)$. Remember, O_{11} is obtained by the camera and therefore in the β system.

(ii) The desired trajectory z^* is a given list of $(x_i,\ y_i)$ values. Each pair has an index i. The point O_{11} has coordinates $(x_O,\ y_O)$. In order to compute the minimal distance of O_{11} w.r.t. z^*, the point A has to be determined. Point A is a point in the list z^* with index i_A and coordinates $(x_A,\ y_A)$ and can be determined in the following way

$$(x_A,\ y_A) = \min_i \left((x_i - x_O)^2 + (y_i - y_O)^2\right). \tag{42}$$

The index i_A allows to determine α_{11} as the whole originally desired trajectory is computed offline a priori. Therefore, the coordinate system in point A is defined, which is rotated by the angle α_{11}. In this way every point on the right of A has a positive $y_{\alpha 11}$ value and every point on the left of it has a negative value. This is useful for determining the direction of the evasion. Furthermore, the $y_{\alpha 11}$ component of the point O_{11} gives directly the normal distance $\overline{AO}_{11}$ with sign. The sign tells that O_{11} is to the left of A.

This is done for both confining points of each free space detected. In a second step, the length of each free space (e.g. 11-18) is projected on the $x_{\alpha 11} = 0$ plane, to check if the free

Die approbierte gedruckte Originalversion dieser Diplomarbeit ist an der TU Wien Bibliothek verfügbar
The approved original version of this thesis is available in print at TU Wien Bibliothek.
TU Bibliothek WIEN Your knowledge hub

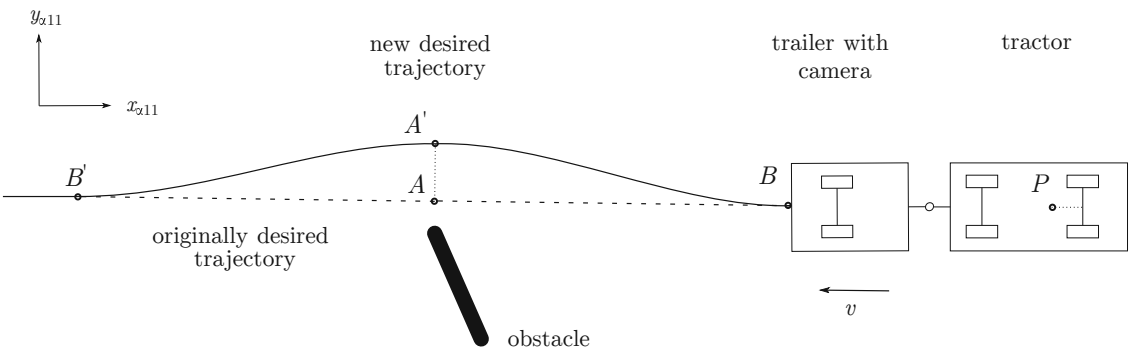

Figure 11: shows how the desired trajectory z^* is changed. Note that z^* does not have to be linear. Here z^* is linear to save space and to simplify the illustration.

space would be wide enough such that the vehicle could pass collision free. All too narrow free spaces will be sorted out. The third step consists of choosing the free space closest to z^* as we want to stay 'as close as possible' to it. Now only one free space remains with its left and right confining point. Finally, the collision check is performed. For this purpose, it is necessary and easy to understand that the right point of the free space has to be avoided to the left and vice versa. The points O_{11} & O_{18} remain (see Fig. 9). One of them has to be avoided to the left or right and the point which is closer to z^* is chosen:

$$\overline{AO} = min\left(\left|\overline{AO}_{11}\right|, \left|\overline{AO}_{18}\right|\right), \tag{43}$$

where $\overline{AO}$ keeps the sign of the chosen one. Now the collision check is performed:

$$\pm\overline{AO} > |\text{threshold}| \quad \Rightarrow \quad \text{no obstacle avoidance initialised}, \tag{44}$$

where the sign in equation (44) depends whether the right (-) or the left (+) confining point of the free space is considered. The threshold is determined by the geometry of the vehicle. If $O = O_{11}$, then $\overline{AO}_{11}$ would have a negative sign. As O_{11} is the left confining point the negative sign in equation (44) is used, and therefore $-\overline{AO}_{11} > 0$ would be used for the collision check. In case of $O = O_{18}$ then $+\overline{AO}_{18} > 0$ would be used for the collision check. However, if the point O has to be avoided, then the originally desired trajectory will be manipulated.

Die approbierte gedruckte Originalversion dieser Diplomarbeit ist an der TU Wien Bibliothek verfügbar
The approved original version of this thesis is available in print at TU Wien Bibliothek.
TU Bibliothek Your knowledge hub WIEN

2.5.3 Manipulation of the desired trajectory in order to avoid a collision

Let's assume the point $O = O_{11}$ in Fig. 10 has to be bypassed by manipulating the originally desired trajectory z^*. By adding a spline to z^* the point A can be moved along the $y_{\alpha 11}$ axis. How much and in which direction A has to be moved is already determined by the previous considerations. In the following equation w_y has vector properties. It tells the direction and the minimum amount (with some tolerance) that A has to be moved along $y_{\alpha 11}$, in order to avoid a collision. In particular it shifts $A \rightarrow A'$ as illustrated in Fig. 10.

$$w_y = \overline{AO} \mp w_T, \tag{45}$$

where w_T is the trailer axle length and the sign depends again whether the right (+) or the left (-) confining point of the free space is considered.

Now we know that our new desired trajectory $z^{*\prime}$ should go through A'. We also demand that the vehicle manoeuvres back to z^* after the obstacle. This is considered in Fig. 11 by laying a spline through the points A', B, and B'. Up to point B and after point B' the original and the new trajectory are identical and the time to travel from both points to A' is the same. Note that z^* is depicted as a straight line to make the illustration simplier.

The new desired trajectory $z^{*\prime}$ is then defined for the entire time domain $t_0 < t < T$, and a feasible reference state trajectory q_r is computed online for the control horizon based on $z^{*\prime}$. If later another obstacle occurs, z'^* can be manipulated again at any time.

2.5.4 Initialisation of the evasive maneuver

One last question remains to be answered, which is when the evasive menuver should be initialised. As already mentioned, the area is scanned for obstacles 2.5m in advance. Furthermore the camera in point B - see Fig. 11 - is around 60cm far away from point P. One strategy is to start the evasive maneuver when a fixed distance to the obstacle is reached. In other words the spline to maipulate the trajectory is generated if the distance $|\overline{AB}|$ deceeds a certain threshold

$$|\overline{AB}| \leq 1.5\text{m}.$$

This can be done independently of how the desired trajectory looks like. In the code it is achieved by simply comparing the indices of the two points A and B w.r.t. the desired trajectory.

Die approbierte gedruckte Originalversion dieser Diplomarbeit ist an der TU Wien Bibliothek verfügbar
The approved original version of this thesis is available in print at TU Wien Bibliothek.
TU Bibliothek Your knowledge hub WIEN

It seems reasonable, however, to choose the initial time instant of the evasive menauver depending on the amount $|w_y|$ of the deviation to the original z^*. In other words, smaller evasions could start later then bigger ones. An approach for a condition to choose the initialisation instant of the evasion in case of the linear trajectory is shown here. For this purpose some preceding experiments have been performed. These consists of letting the one-trailer system track circular trajectories in backward motion. The radius of these trajectories has been successively reduced. In this way the minimum radius $R_{min} = 2\text{m}$ has been determined that could still successfully be tracked. However, it is not the circle that the vehicle is capable tracking in forward direction, when the steering angle is set to its saturation value (this case yields $R_{min} = 1\text{m}$). This is due to the corrective steering that is necessary to avoid the *jackknife* effect. Thus, a circular trajectory with $1\text{m} < R < 2\text{m}$ would in theory still be kinematically feasible, but the necessary corrective steering in backward motion would not allow it. For the linear trajectory it is very easy to compute the curvature radius that the evasive path will have in every point. We could then construct the evasive path such that the minimal curvature radius that will appear on this path will equal $R_{min} = 2\text{m}$, plus some tolerance. In this way we make sure that the trajectory is kinematically feasible and that the curvature of the trajectory always allows a corrective steering. In this case the evasive path is chosen to be a cubic polynomial $y(x)$, and the curvature radius ρ can be computed and then approximated as follows.

$$\rho = \frac{(1 + y'(x))^{\frac{3}{2}}}{y''(x)} \geq \frac{1}{|y''(x)|}, \tag{46}$$

where $y'(x)$ is the derivative of y w.r.t. x. The cubic polynomial has to go through point A' in Fig. 11, which has a height of $|w_y|$. The minimal curvature radius of the cubic polynomial is obtained in point A', which is the same as in point B. The second derivative in that point can be found as

$$|y''(A')| = \frac{6|w_y|}{\overline{AB}^2}. \tag{47}$$

Recall, the condition that has to be fulfilled is

$$\rho \geq R_{min} = 2\text{m}. \tag{48}$$

Die approbierte gedruckte Originalversion dieser Diplomarbeit ist an der TU Wien Bibliothek verfügbar
The approved original version of this thesis is available in print at TU Wien Bibliothek.
TU Bibliothek WIEN Your knowledge hub

Therefore, the following condition can be used to choose the length $|\overline{AB}|$, and thus to choose the time instant at which the evasive maneuver shall be initialised

$$\frac{6w_y}{\overline{AB}^2} = \frac{1}{R_{min}} \quad \Rightarrow \quad |\overline{AB}| = \sqrt{6w_y R_{min}}. \tag{49}$$

2.6 Block diagram of the high-level control

An overview of the whole high-level control is given in figure 12. The low level control - indicated in the bottom of the figure - and the high-level control communicate every $\delta = 0.15$s.

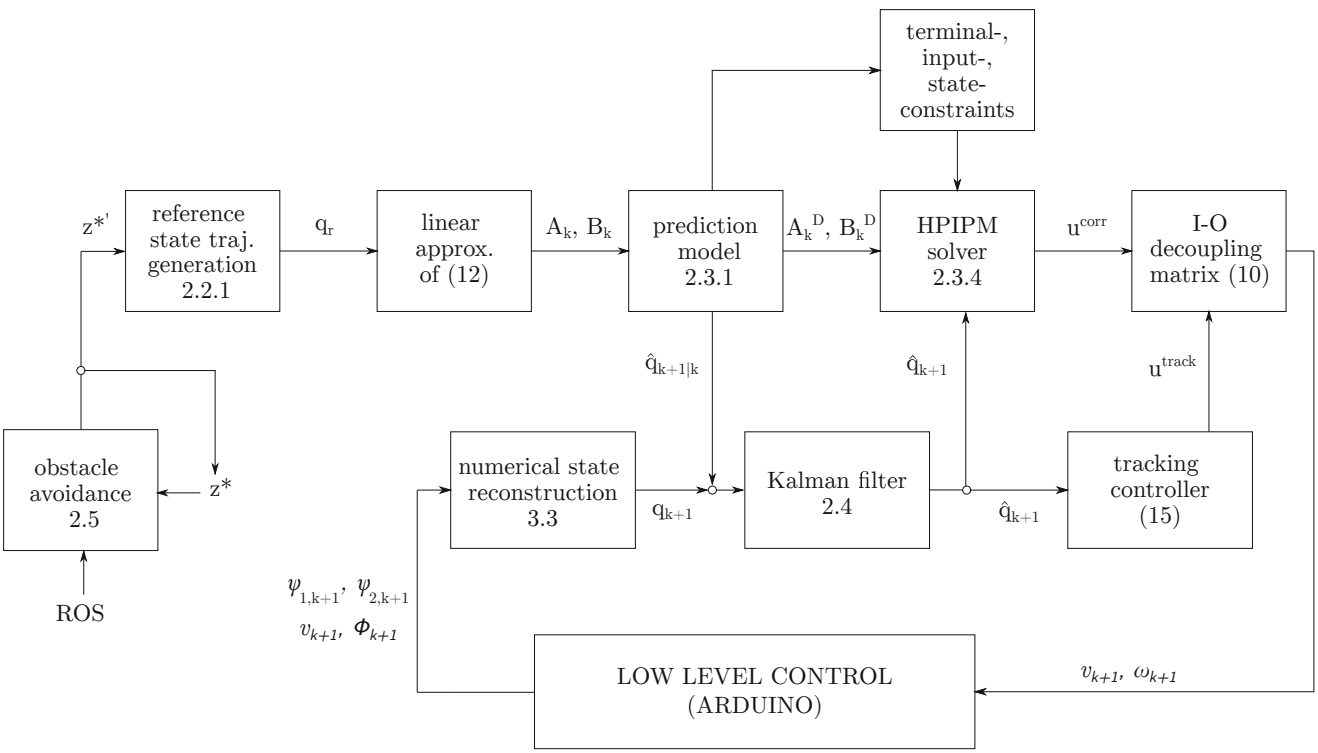

Figure 12: shows the block diagram of the high-level control.

Die approbierte gedruckte Originalversion dieser Diplomarbeit ist an der TU Wien Bibliothek verfügbar
The approved original version of this thesis is available in print at TU Wien Bibliothek.
TU Bibliothek Your knowledge hub WIEN

3 Experimental platform

This chapter is organised as follows. Components and specifications of the experimental platform are described in section 3.1. The control inputs computed at the high-level control at each sampling time are seen as reference values to be achieved by the experimental platform. This corresponds to the low-level control, which will be described in section 3.2. The MPC framework and the tracking controller (high-level control) require the feedback of the whole state vector. Section 3.3 shows how the states that are not measured by the odometry are numerically reconstructed by the odometry.

3.1 Electronics

The platform used for the experiments is a radio controlled (RC) vehicle, in which the electronics are modified and equipped with additional components in order to perform the control. The Carson Unimog U300 is chosen for this purpose with the following dimensions (manufacturer specification):

- tractor width of 0.175m
- total length (tractor with both trailers) between the two tips of the two chassis of about $1.2\,m$ (measured)
- wheel radius $r = 0.45$m
- axle length of all axles $w_T = 0.14$m
- Furthermore the lengths used in the equations are the following: $L = 0.255$m, $h = 0.068$m, $L_1 = 0.262$m, $h_1 = 0.153$m, $L_2 = 0.211$m, and $b = -0.05$m (partly measured)

The original electronic board of the RC vehicle is substituted with an Arduino Uno microcontroller to actuate the electronics mentioned in the following paragraph. This Arduino will be referred to as the Slave Arduino. See Fig. 13 to understand better how the low level control works.

On the rear axle of the tractor acts a DC motor to set the linear velocity v of the tractor, while another DC motor acts on a mechanism mimicking the Ackermann steering on the front

Die approbierte gedruckte Originalversion dieser Diplomarbeit ist an der TU Wien Bibliothek verfügbar
The approved original version of this thesis is available in print at TU Wien Bibliothek.
TU Bibliothek WIEN Your knowledge hub

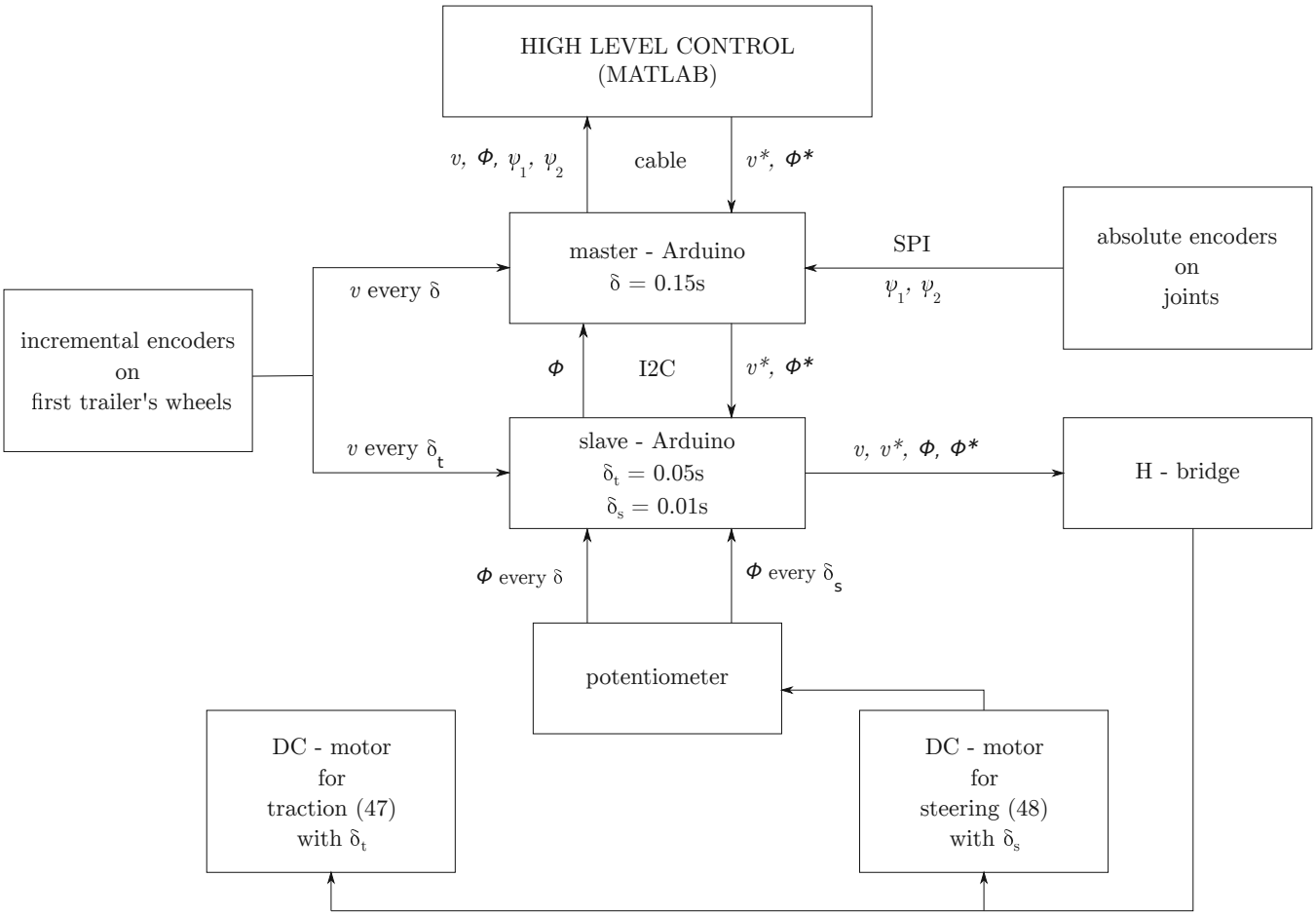

Figure 13: shows the block diagram of the low-level control. The different δs in the diagram indicate the sampling time with which a component runs.

axle of the tractor to set the steering angle ϕ. The latter also consists of a Potentiometer which is used to read the current steering angle ϕ. To drive the two DC motors the dual H-bridge motor driver L298N is used that allows to control two DC motors simultaneously.

The Slave Arduino communicates via I2C protocol with the Master Arduino. The Master Arduino performs the real-time communication with the High Level Control (computer) through a serial port (cable). It also actuates the electronics in the following paragraph.

The absolute encoders AMT 203 V (SPI protocol) are mounted on the joints between the tractor and the first trailer, and between the two trailers to read the current hitch angles ψ_1 and ψ_2. Furthermore, two incremental encoders of the type CUI INC AMT102 are mounted, of which one is on the left and the other on the right wheel of the trailer to read the current linear velocity v_T of the trailer.

Die approbierte gedruckte Originalversion dieser Diplomarbeit ist an der TU Wien Bibliothek verfügbar
The approved original version of this thesis is available in print at TU Wien Bibliothek.
TU Bibliothek WIEN Your knowledge hub

The data sheets and the specifications can easily be found online, and will not be shown here. Furthermore, it shall be just mentioned that the ASUS depth camera is in use. It has already been discussed before.

3.2 Actuating the DC motors

The high level control in the MPC framework computes the optimal control inputs $(v\,,\,\omega)$, which act as reference values $(v^*\,,\,,\omega^*)$ for the low level control (Arduino). In fact the values $(v^*\,,\,\phi^*)$ (hence not the angular velocity, but the angle) are sent every δ seconds to the Arduino. There local PI controllers run to achieve these values:

$$u_v(k) \;=\; k_{pv}(v_k^* - v_k) + k_{iv}\sum_{j=1}^{k} T_v \cdot j \cdot (v_j^* - v_j) + v_k^* \tag{50}$$

$$u_\phi(k) \;=\; k_{p\phi}(\phi_k^* - \phi_k) + k_{i\phi}\sum_{j=1}^{k} T_\phi \cdot j \cdot (\phi_j^* - \phi_j). \tag{51}$$

Equation (51) is subject to the condition which sets the sum equal to zero (the summation starts once the vehicle starts moving) if $\phi_k^* = 0$. This means that summation is started again from zero after this particular instant and continues adding the values until the next $\phi^* = 0$ occurs. This is expressed as follows

$$u_\phi(k) = 0 \quad \& \quad \text{reset}\left(\sum_{j=1}^{k} T_\phi \cdot j \cdot (\phi_j^* - \phi_j)\right) \qquad \text{if } \phi^* = 0. \tag{52}$$

This is necessary as the sum in equation (51) is not necessarily zero if $\phi_k^* - \phi_k = 0$, which would lead to a non zero u_ϕ and move the steering away from the position it is supposed to be. The values for the coefficients k_{pv}, k_{iv}, $k_{p\phi}$, and $k_{i\phi}$, and the time constants $T_v = 0.05s$ and $T_\phi = 0.01s$ are set empirically (by trial and error).

The DC motor takes integers in the range of $u_{DC}\ \epsilon\ [-255, 255]$, driving the motor in forward and backward direction. In general, to drive the vehicle at a desired speed in $[v] = \frac{m}{s}$ one has to find the corresponding value u_{DC} which actually actuates the DC motor. In our case, in the presence of the PI controller the desired v doesn't have to correspond to the actual

Die approbierte gedruckte Originalversion dieser Diplomarbeit ist an der TU Wien Bibliothek verfügbar
The approved original version of this thesis is available in print at TU Wien Bibliothek.
TU Bibliothek Your knowledge hub WIEN

u_{DC} as the (offset-) error will be cancelled by the integral part of the PI controller. For our experiments we choose $v = const. = -0.1\frac{m}{s}$. In fact, the corresponding u_{DC} would be so low that the (in the initialisation inactive) vehicle would not start moving unless it gets a little push. Thus, we will not map it correctly. The value u_{DC} is during a time step δ not a constant value (the low level reference v is). So, it can move in the beginning of δ faster and towards the end slower. However, the experiments described in the next paragraph suggest that correctly

$$u_{DC} = -90 \quad \sim \quad v = -0.3\frac{m}{s},$$

whereas in use is

$$u_{DC} = -110 \quad \sim \quad v = -0.3\frac{m}{s}.$$

On the other hand we do request that an incremental increase of Δv shall lead to the corresponding incremental increase of Δu_{DC}. The approach to do this is simple. We let the vehicle drive in forward direction (as it is stable there) for $20s$ at a specific u_{DC} and compute the corresponding v, by measuring the distance the vehicle makes. This is done for several u_{DC}, then the differences are taken. For each experimental run, a fully charged battery was taken, and it could be observed that a second run with the same battery would already lead to non-reliable data. The result suggests to take a linear map with

$$\Delta u_{DC} = 1 \quad \longleftrightarrow \quad \Delta v = 0.01\frac{m}{s}.$$

Another parameter that has been changed was the radius of the wheels. After measuring it again, it has been determined to $r = 0.046m$.

3.3 Numerical reconstruction of the current configuration

Each of the two incremental encoders perform 250 pulses during a 360 degree rotation. The number of pulses of the right (left) wheel is denoted as N_R (N_L). Assuming pure rolling, the current velocity of the trailer $v_{T,k}$ and tractor v_k is computed in Matlab as follows

Die approbierte gedruckte Originalversion dieser Diplomarbeit ist an der TU Wien Bibliothek verfügbar
The approved original version of this thesis is available in print at TU Wien Bibliothek.
TU Bibliothek Your knowledge hub WIEN

$$v_{T,k} = r \cdot \frac{(N_R + N_L)}{2\delta} \tag{53}$$

$$v_k = \frac{v_{T,k}}{\left(\cos(\psi_k) - \frac{L_1}{L}(\cos(\psi_k)\sin(\psi_k)\tan(\phi_k) - \tan(\phi_k)\right)^{0.5}} \tag{54}$$

where the current angles ϕ_k, $\psi_{1,k}$. and $\psi_{2,k}$ can directly be read from the potentiometer and the absolute encoder, respectively. For the missing states x_{Pk}, y_{Pk}, and θ_k, and the angular velocity $\dot{\phi}_k = \omega_k$ finite differences are used to compute the values with the following approach. An explicit expression is chosen, as only the previous values are available. We want to express the derivative in the following way (finite differences)

$$\dot{\theta}_k = a\theta_{k-2} + b\theta_{k-1} + c\theta_k. \tag{55}$$

The current and the two previous state values are taken into account. A higher number of points taken into account will generally lead to a smaller truncation error. The Tailor series is written around the current point θ_k

$$\dot{\theta}_k = a\left(\theta_k - \frac{2\delta}{1!}\frac{d\theta_k}{dt} + \frac{(2\delta)^2}{2!}\frac{d^2\theta_k}{dt^2} - \frac{(2\delta)^3}{3!}\frac{d^3\theta_k}{dt^3} + \frac{(2\delta)^4}{4!}\frac{d^4\theta_k}{dt^4} - + \cdots\right) + \cdots$$
$$\cdots + b\left(\theta_k - \frac{\delta}{1!}\frac{d\theta_k}{dt} + \frac{(\delta)^2}{2!}\frac{d^2\theta_k}{dt^2} - \frac{(\delta)^3}{3!}\frac{d^3\theta_k}{dt^3} + \frac{(\delta)^4}{4!}\frac{d^4\theta_k}{dt^4} - + \cdots\right) + c\theta_k$$

Now the coefficients a,b, and c can be chosen such that only the first derivative on the right hand side remains. This leads to the following conditions

$$\begin{aligned} a + b + c &= 0 \\ -a2\delta - b\delta &= 1 \\ a\frac{(2\delta)^2}{2} + b\frac{\delta^2}{2} &= 0 \end{aligned}$$

Die approbierte gedruckte Originalversion dieser Diplomarbeit ist an der TU Wien Bibliothek verfügbar
The approved original version of this thesis is available in print at TU Wien Bibliothek.
TU Bibliothek WIEN Your knowledge hub

Remember that $t_k - t_{k-2} = 2\delta$. The coefficients result in

$$a = \frac{1}{2\delta}, \qquad b = \frac{-4}{2\delta}, \qquad c = \frac{3}{2\delta}.$$

For this choice one obtains for the third derivative (plug the values of a,b, and c in the taylor series)

$$-a\frac{(3\delta)^3}{3!} - b\frac{\delta^3}{3!} = -\frac{1}{2\delta}\frac{(3\delta)^3}{6} + \frac{4}{2\delta}\frac{\delta^3}{6} \neq 0$$

and therefore a truncation error of $O(\delta^3)$. The kinematic model then yields

$$\dot{\theta}_k \simeq \frac{\theta_{k-2} - 4\theta_{k-1} + 3\theta_k}{2\delta} = \frac{v_k \tan(\phi_k)}{L}$$

$$\theta_k = \frac{2\delta v_k \tan(\phi_k)}{3L} + \frac{4}{3}\theta_{k-1} - \frac{1}{3}\theta_{k-2}.$$

This discretisation is convergent (i.e. with $\delta \to 0$, the numerical solution $\to$ analytical solution) for this differential equation. For initialisation, where the configuration is available at only one previous time step, a discretisation of the type of $\theta_k = a\theta_{k-1} + b\theta_k$ is used ($O(\delta^2)$). The same approach has been used for x_{Pk}, y_{Pk}, and ω_k. In the Matlab simulations, the 'ode15s' solver for stiff problems is used to computed the states at the next time instant.

Die approbierte gedruckte Originalversion dieser Diplomarbeit ist an der TU Wien Bibliothek verfügbar
The approved original version of this thesis is available in print at TU Wien Bibliothek.
TU Bibliothek Your knowledge hub WIEN

4 Simulations

In this chapter Matlab simulations of the two-trailers system will be presented. In particular a linear, a circular, and a cubic trajectory are used as reference trajectories. In a later section, the exact same trajectories will be taken as a reference for the experimental platform. The evolution of the cartesian errors and the inputs as well as the simulation of the configuration can be observed for the three trajectories in figures 14, 15, and 16, respectively. Note that the simulations are performed using the Matlab build-in solver Quadprog with the stability constraint as described in the Appendix B as well as with the HPIPM solver using the terminal constraint as described in section 2.3.2. The configuration plots though refer only to the simulations using the HPIPM solver. The same parameters as already described for the experimental platform are also taken for the simulations. However, for each simulation an y-cartesian error of 0.01m has been set as the initial condition. In general all three figures show that the proposed controller using both, the HPIPM and Quadprog solver, guarantees successful trajectory tracking in backwards motion. For the linar trajectory the two solvers even show the exact same evolutions for the cartesian errors and inputs, as seen in Fig. 14. However, for the circular trajectory, see Fig. 15, the two solvers show a very small difference in the error evolution and for the steering velocity. The difference is in the order of 10^{-3}. The solvers show the biggest discrepancy for the cubic trajectory in Fig. 16. But also here, the differences are too small to be able to say that one or the other would give better performance in the real experiments. During the experiments it became obvious that the HPIPM solver performs better. Adding a second trailer and also the obstacle avoidance algorithm require significantly more computation power, and compared to the Quadprog solver the HPIPM solver is twice as fast. The higher speed is especially noticeable if state and input constraints are considered. All simulations were run on a Acer Aspire 5 with a 1.8 GHz Intel Core i7 processor acquired in 2017.

Die approbierte gedruckte Originalversion dieser Diplomarbeit ist an der TU Wien Bibliothek verfügbar
The approved original version of this thesis is available in print at TU Wien Bibliothek.
TU Bibliothek Your knowledge hub WIEN

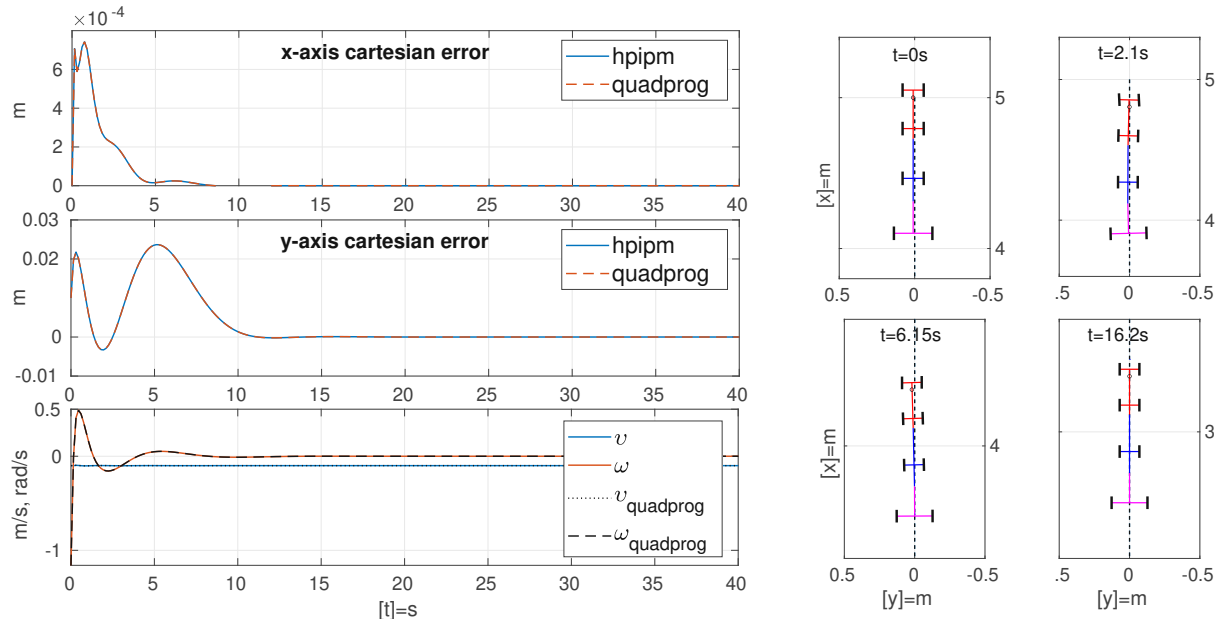

(a) evolution of cartesian errors and inputs

(b) configuration plots at different t

Figure 14: the simulation in which the tractor with two trailers tracks a *linear trajectory* in backward motion. A y-cartesian error of 0.01m has been set as initial condition.

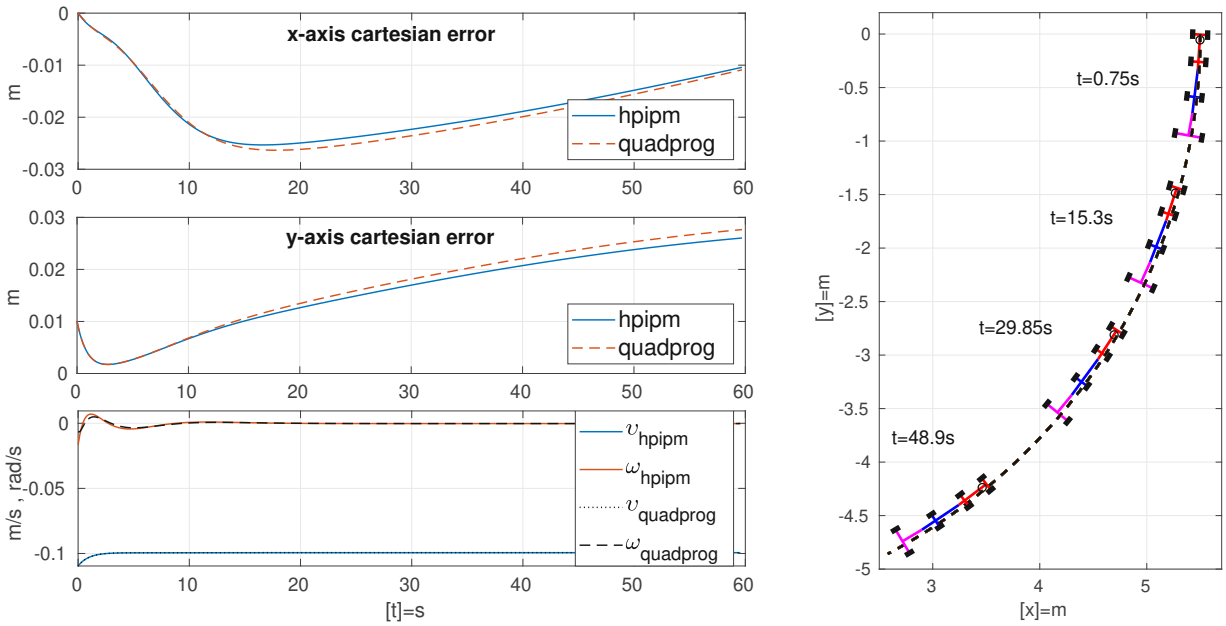

(a) evolution of cartesian errors and inputs

(b) configuration plots at different t

Figure 15: the simulation in which the tractor with two trailers tracks a *circular trajectory* in backward motion. A y-cartesian error of 0.01m has been set as initial condition.

Die approbierte gedruckte Originalversion dieser Diplomarbeit ist an der TU Wien Bibliothek verfügbar
The approved original version of this thesis is available in print at TU Wien Bibliothek.
TU Bibliothek Your knowledge hub WIEN

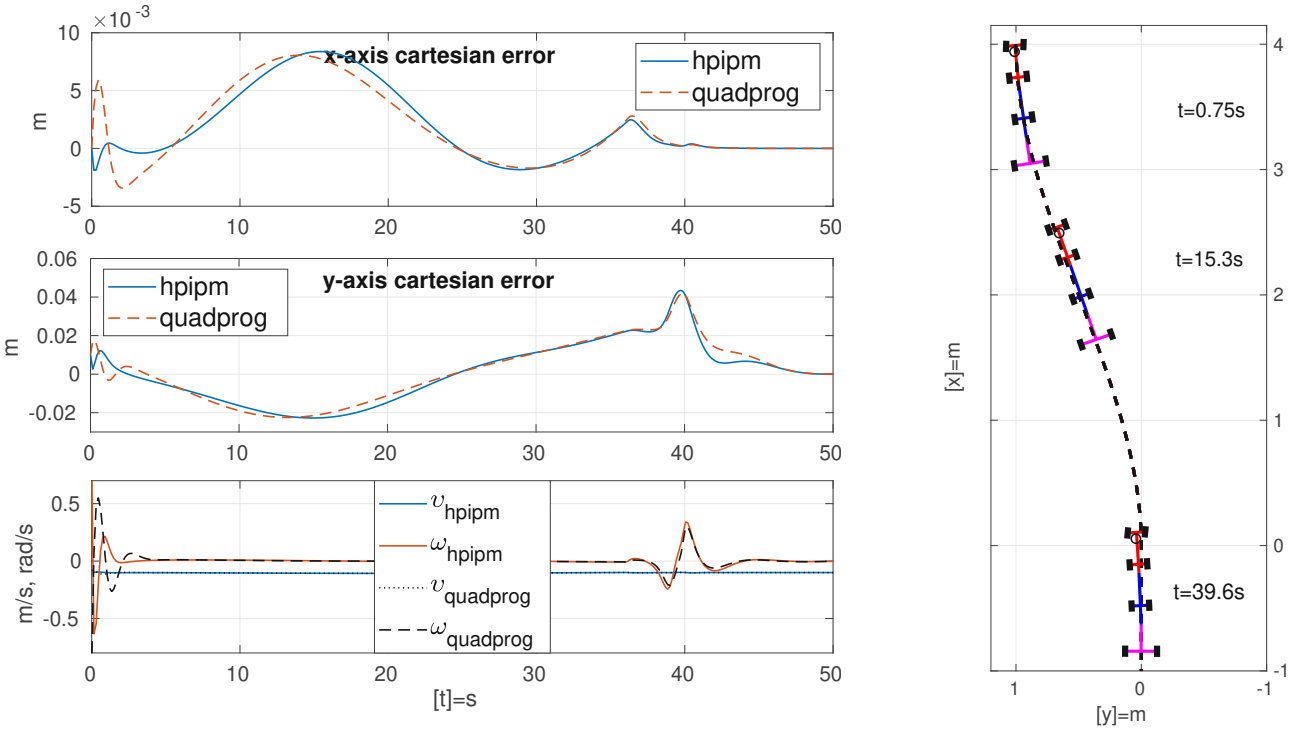

(a) evolution of cartesian errors and inputs **(b)** configuration plots at different t

Figure 16: the simulation in which the tractor with two trailers tracks a *cubic trajectory* in backward motion. A y-cartesian error of 0.01m has been set as initial condition.

5 Experiments

All the experiments discussed in this chapter have been filmed and most of those video files are attached to the folder where this document can be found as well. The experiments will be enumerated with letters in the text as well as the video files in the folder.

5.1 One trailer - improvements

In this section the improvement due to the modifications shown in sections 3.2 and 3.3 shall be discussed first. To show this, some experiments are performed before and after the modification. A linear trajectory should be followed first for $T_{fin} = 20$s then for $T_{fin} = 30$s with a constant velocity $v = -0.1$m/s. Therefore, the travelled distance should be 2m and 3m, respectively. Table 2 shows these results. Note that 'Fail' in the tables means that the *jackknife* effect occurred before T_{fin} was reached. On a 3 m long trajectory the vehicle, after the modifications,

Die approbierte gedruckte Originalversion dieser Diplomarbeit ist an der TU Wien Bibliothek verfügbar
The approved original version of this thesis is available in print at TU Wien Bibliothek.
TU Bibliothek Your knowledge hub WIEN

T_{fin} = 20s	[try 1]=cm	[try 2]=cm	[try 3]=cm	[try 4]=cm	[try 5]=cm	[try 6]=cm
before	207	211	209	210	210	210
modified	201	201	201	202	200	202
T_{fin} = 30s	[try 1]=cm	[try 2]=cm	[try 3]=cm	[try 4]=cm	[try 5]=cm	[try 6]=cm
before	FAIL	313	312	FAIL	312	312
modified	302	302	306	302	303	302

Table 2: shows the travelled distance of the vehicle in backward motion before and after the modification for a travelling time of T_{fin} = 20s and T_{fin} = 30s. Note that an experiment is considered as 'fail' if the *jackknife* effect occured.

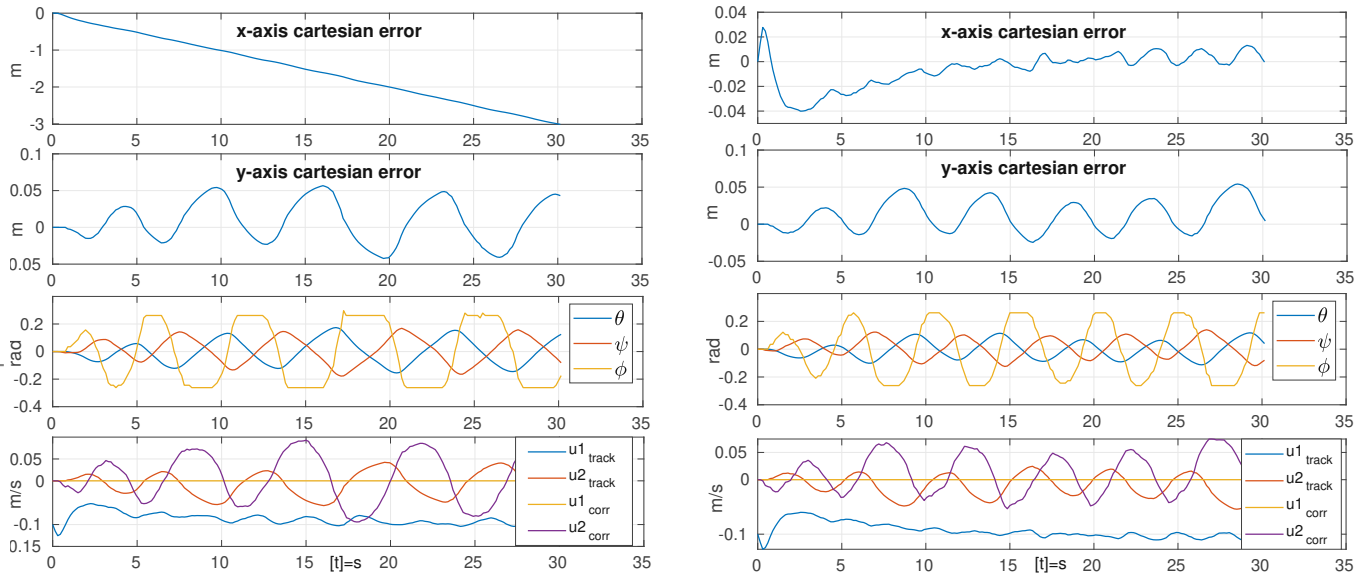

(a) Before modification.

(b) After modification.

Figure 17: Typical evolution of the x & y error, of the angles, and the inputs. $T_{fin} = 30sec$. Note that the two ordinates of the x-cartesian error plots 17a and 17b have different scales.

moves in general around 3 cm too far. This is for such kind of electronics very acceptable. Figure 17 shows typical error and state evoultions for the experiments mentioned above. The first plot of Fig. 17a shows the x-cartesian error, thus $x_P(t) - x_r(t)$. The error in the plot is negative, hence the $\dot{x}_P$ reconstructed from the odometry is smaller than the actual $\dot{x}_P$. The vehicle is actually moving too fast in this direction. Also note that the error grows continuously. After the modification the x-cartesian error tends to zero which can be observed in the first

Die approbierte gedruckte Originalversion dieser Diplomarbeit ist an der TU Wien Bibliothek verfügbar
The approved original version of this thesis is available in print at TU Wien Bibliothek.
TU Bibliothek WIEN Your knowledge hub

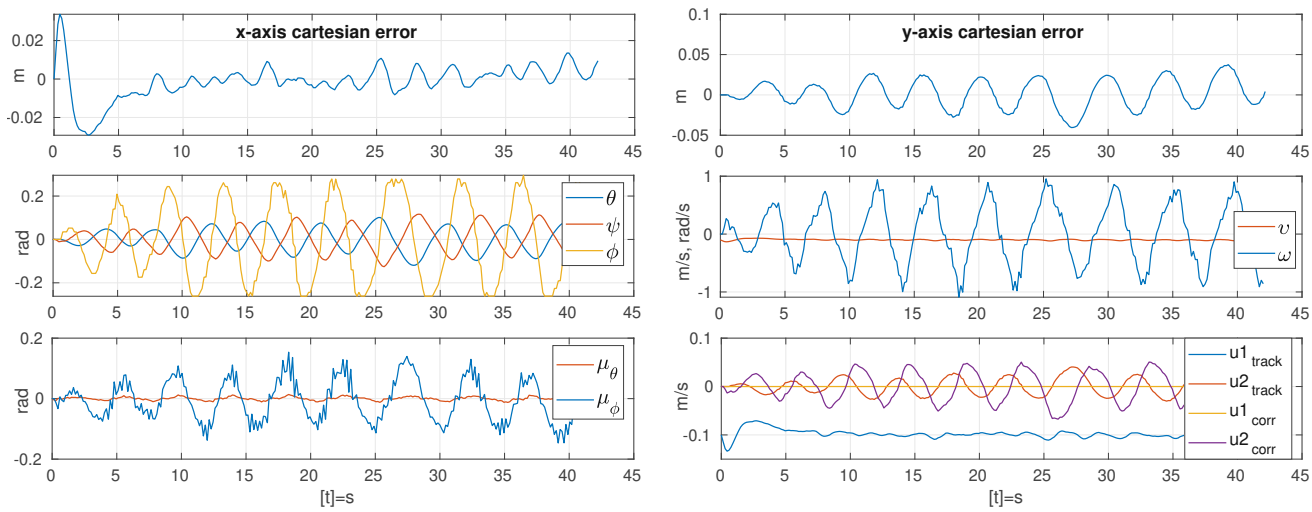

Figure 18: shows the evolution of the states, errors, inputs, and the innovation using all the methods described in sections 2 und 3. The vehicle moves on a linear trajectory of more than 4 meters and the deviation in both cartesian coordinates remains small. Note that indices of the innovation μ in the bottom left figure declares the state to which it refers. The plots correspond to experiment (**A**).

plot of Fig. 17b. In general, the plots for the system after the modification seem to be less amplified. Another interesting time evolution is that of the steering angle ϕ (third plots in 17, yellow lines). The steering angle is constraint to $[-0.2618rad\ ,\ 0.2618rad]$ (15 degree), and the plot shows that ϕ often gets saturated. This often comes along with a growing y-cartesian error. In Fig. 17b the saturated periods seem to be shorter. Since the vehicle in Fig. 17a travels at a higher velocity, it seems that it has to steer earlier at the maximum angle to avoid the growing y-error. Then the y-error grows in the other direction and the steering angle has to change its sign. Furthermore, in all these experiments (except of 2) there was a deviation normal to the tangent of the trajectory of about 4 to 6 cm as well.

The HPIPM solver is used and the Kalman filter is now added as well. The previous experiments have been repeated and typical state and error evolutions are shown in Fig. 18. Moreover, experiment (**A**) shows the vehicle moving very accurately along the line on the pavement, such as the cartesian errors in Fig. 18 suggest. The figure also shows that the steering angle does not remain for a long time saturated (mid-left subfigure), and that the innovation for the steering angle is of the same order of magnitude as the state itself (bottom-left). Figure

Die approbierte gedruckte Originalversion dieser Diplomarbeit ist an der TU Wien Bibliothek verfügbar
The approved original version of this thesis is available in print at TU Wien Bibliothek.
TU Bibliothek WIEN Your knowledge hub

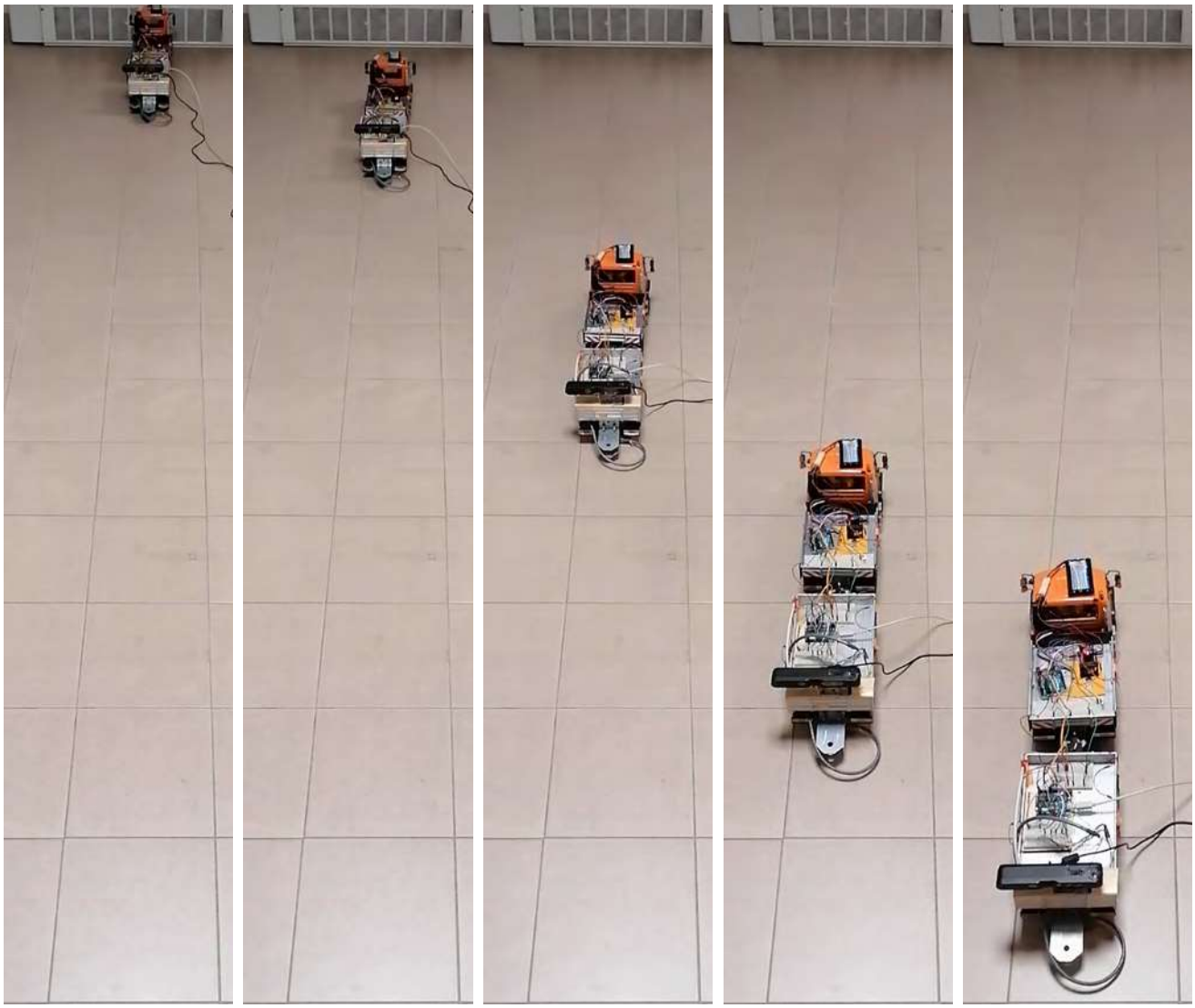

(a) $t = 0$s **(b)** $t = 5$s **(c)** $t = 22$s **(d)** $t = 31$s **(e)** $t = 36$s

Figure 19: shows experiment (**A**).

19 shows snapshots of the experiment and confirms the error evolution mentioned before. It shall be mentioned that setting the vehicle in the correct initial condition is still crucial for a successful experiment, i.e. avoiding the *jackknife* effect while tracking the trajectory with minimum deviation. The vehicle is set by hand into its initial condition and therefore this remains as a source for errors.

Die approbierte gedruckte Originalversion dieser Diplomarbeit ist an der TU Wien Bibliothek verfügbar
The approved original version of this thesis is available in print at TU Wien Bibliothek.
TU Bibliothek WIEN Your knowledge hub

5.2 One trailer - obstacle avoidance

In the experiments shown in this section an obstacle lies on the trajectory that has to be avoided. In experiments (**B**) and (**C**) the originally linear trajectory has to be avoided, first less (**B**) and then more (**C**). After the obstacle is passed, the vehicle starts to turn back to the original task. One can observe that the vehicle starts the evasion earlier in the case of the bigger evasion (experiment (**C**)). To illustrate this the actually tracked path is plotted in Fig. 20, in red for the smaller evasion and in yellow for the bigger evasion. It seems reasonable to start a bigger evasion earlier than a smaller evasion. However, the evasion starts generally around 1.5 m before the trailer would collide with the obstacle. The state and error evolutions in figures 22 and 23, respectively, correspond to these two experiments. Also snapshots of the experiments are shown there. Remember, the error evolutions stay very close to zero as the original linear reference output has been changed, maintaining the linearity of the MPC.

The circular trajectory tracked in experiment (**D**) contains an obstacle in experiment (**E**). Note that in the video file, the original task, which is to follow a circular trajectory, is depicted as a dashed line. The two tracked paths are shown in Fig. 21, where for the red one there was no obstacle to avoid. Figure 24a and 24b show the evolutions of the errors and the states of these experiments. The tractor heading θ in Fig. 24b oscillates from $t = 15$s up to $t = 35$s around a constant value of approximately 0.5 radiants. There it more or less follows a linear trajectory and short cuts the circle for collision avoidance. The corresponding snapshots of these two experiments are provided in Fig. 25 and 26.

Die approbierte gedruckte Originalversion dieser Diplomarbeit ist an der TU Wien Bibliothek verfügbar
The approved original version of this thesis is available in print at TU Wien Bibliothek.
TU Bibliothek WIEN Your knowledge hub

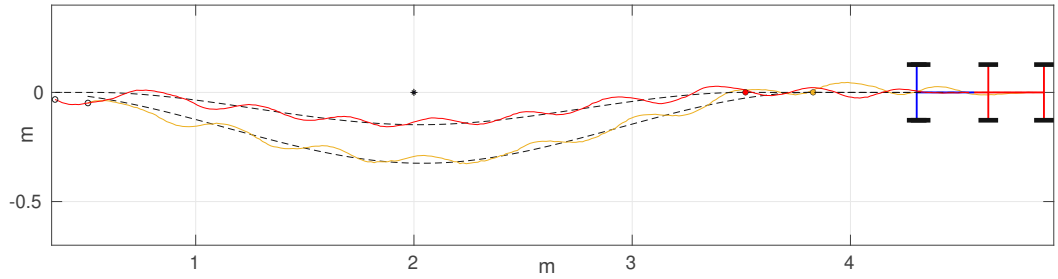

Figure 20: shows the actually tracked path by the vehicle (experiments (**B**) and (**C**)), where the original task was to follow a linear trajectory. The smaller evasion is shown in red and the circular red marker indicates its initialisation. The bigger evasion is shown in similar manner in yellow.

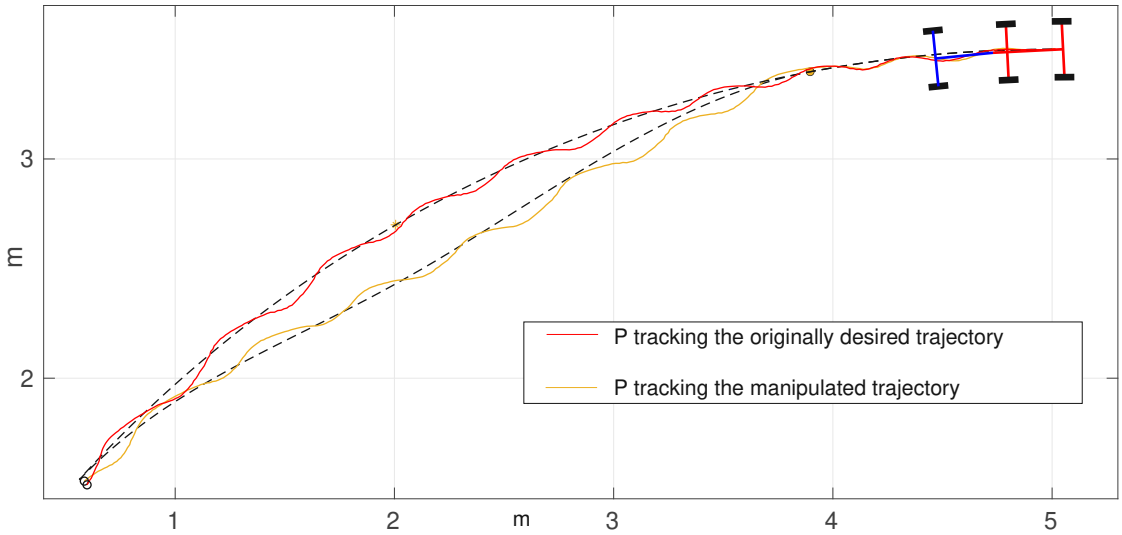

Figure 21: shows the actually tracked path by the vehicle in red when there is no obstacle, and in yellow in order to avoid an obstacle, as shown in experiments (**D**) and (**E**). The original task is a circular trajectory.

Die approbierte gedruckte Originalversion dieser Diplomarbeit ist an der TU Wien Bibliothek verfügbar
The approved original version of this thesis is available in print at TU Wien Bibliothek.
TU Bibliothek Your knowledge hub WIEN

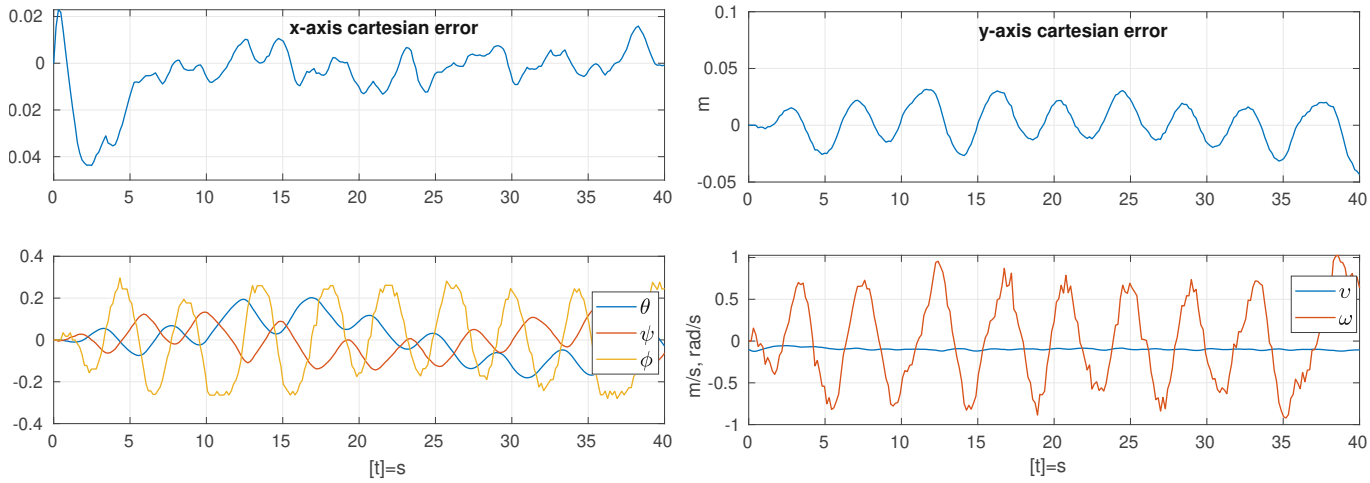

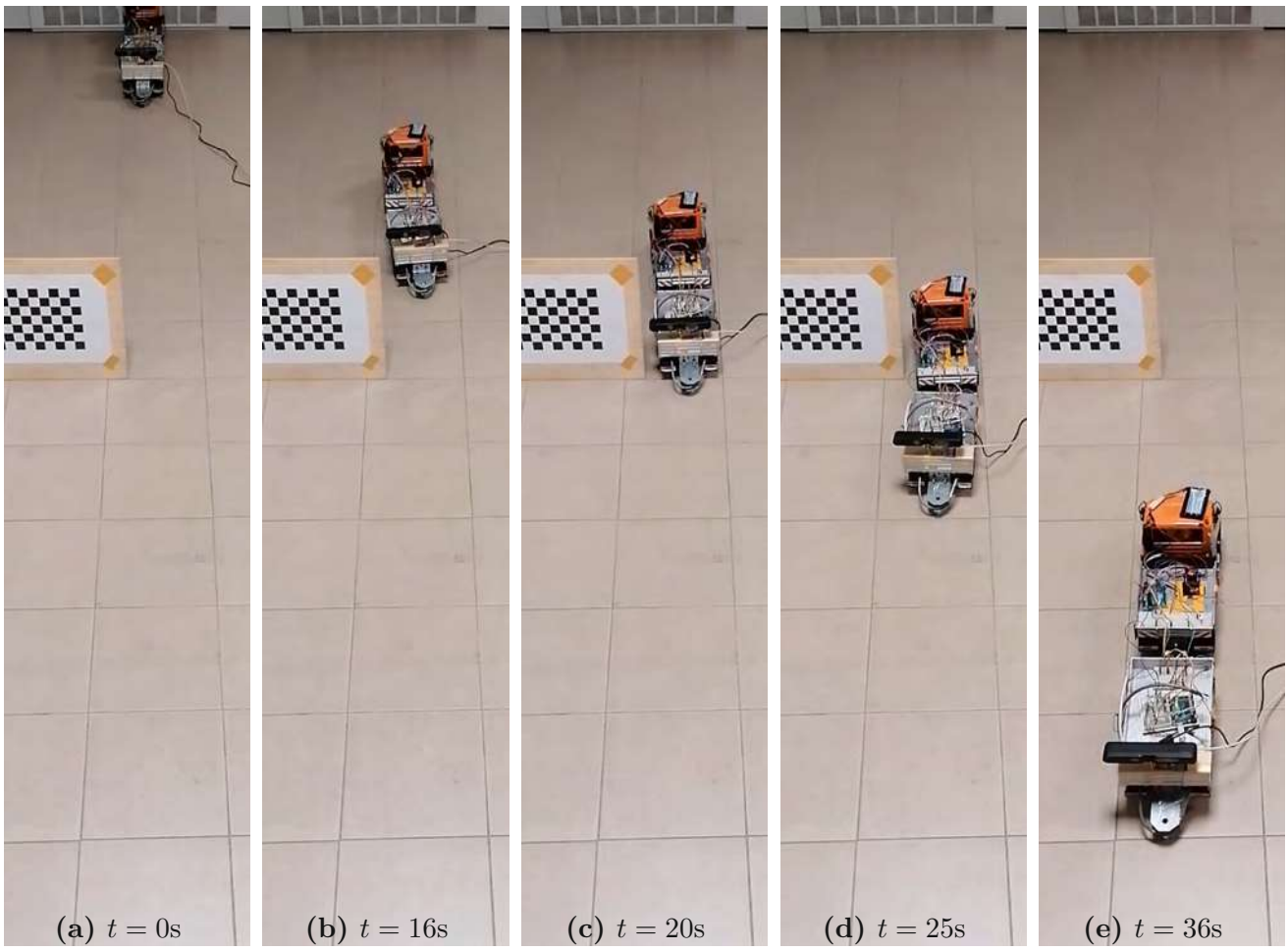

(a) $t = 0$s (b) $t = 16$s (c) $t = 20$s (d) $t = 25$s (e) $t = 36$s

Figure 22: shows experiment (**B**) and its evolution of the errors, states, and inputs. The deviation from the original trajectory is $w_y = -0.148$m.

Die approbierte gedruckte Originalversion dieser Diplomarbeit ist an der TU Wien Bibliothek verfügbar
The approved original version of this thesis is available in print at TU Wien Bibliothek.

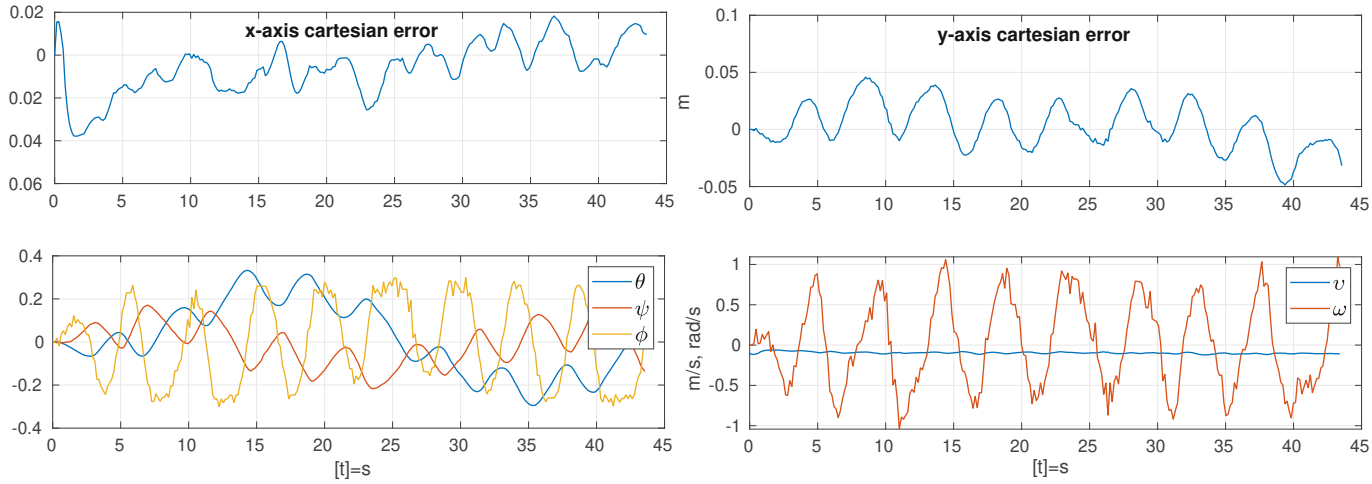

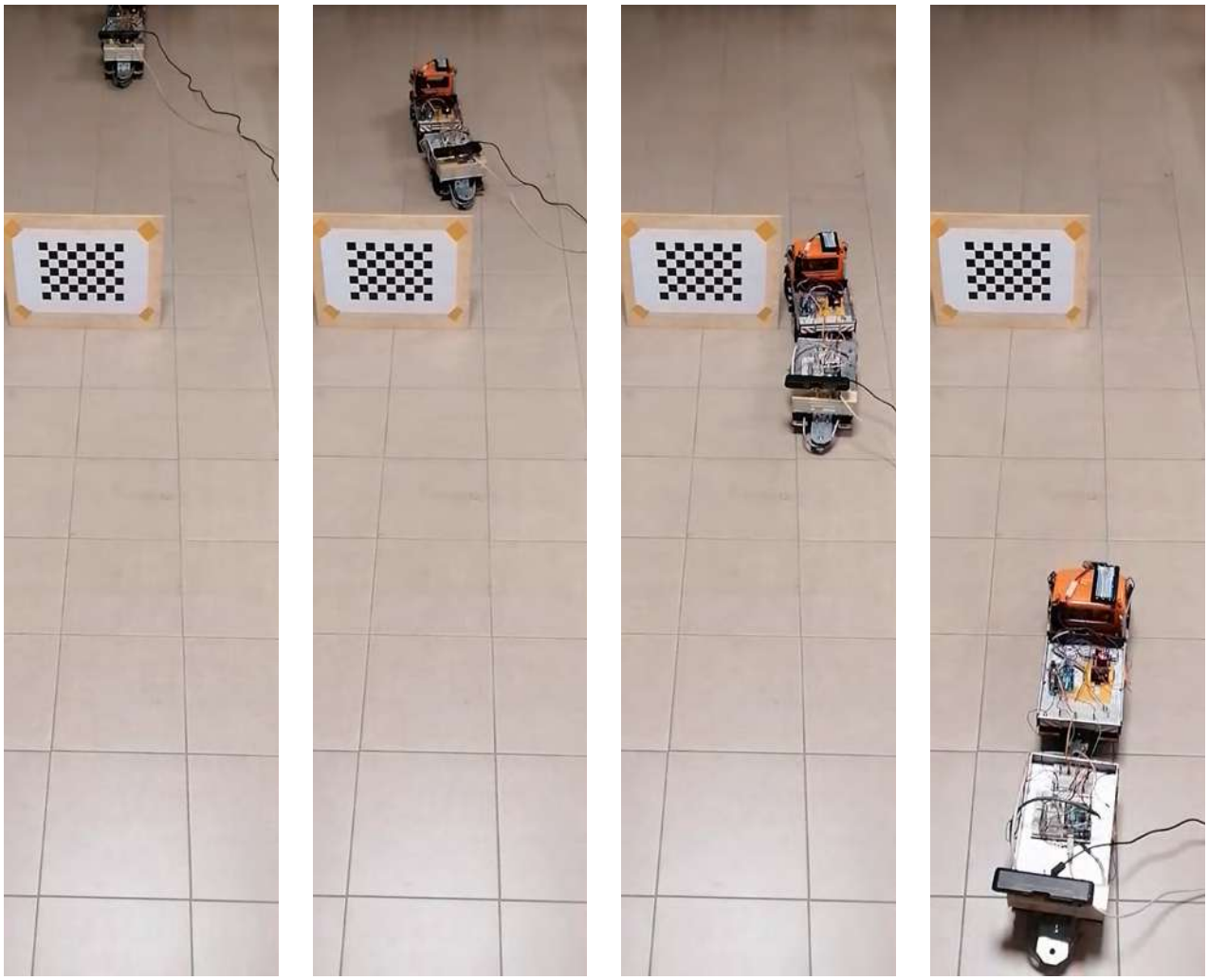

(a) $t = 1$s **(b)** $t = 12$s **(c)** $t = 26$s **(d)** $t = 39$s

Figure 23: shows experiment (**C**) and its evolution of the errors, states, and inputs. The deviation from the original trajectory is $w_y = -0.324m$

Die approbierte gedruckte Originalversion dieser Diplomarbeit ist an der TU Wien Bibliothek verfügbar
The approved original version of this thesis is available in print at TU Wien Bibliothek.
TU Bibliothek Your knowledge hub WIEN

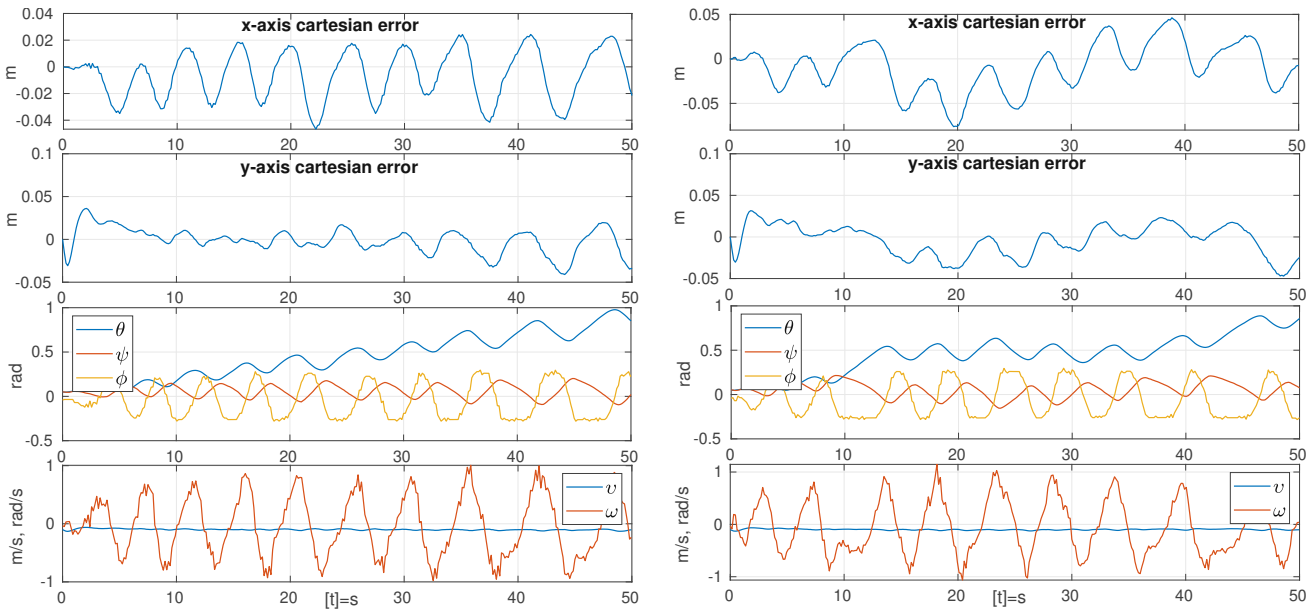

(a) experiment (**D**), no evasion

(b) experiment (**E**), evasion $w_y = -0.255m$

Figure 24: shows the evolution of the cartesian errors and the states of the vehicle, once when there is no obstacle 24a, and once when an obstacle has to be avoided 24b. The original task is a circular trajectory.

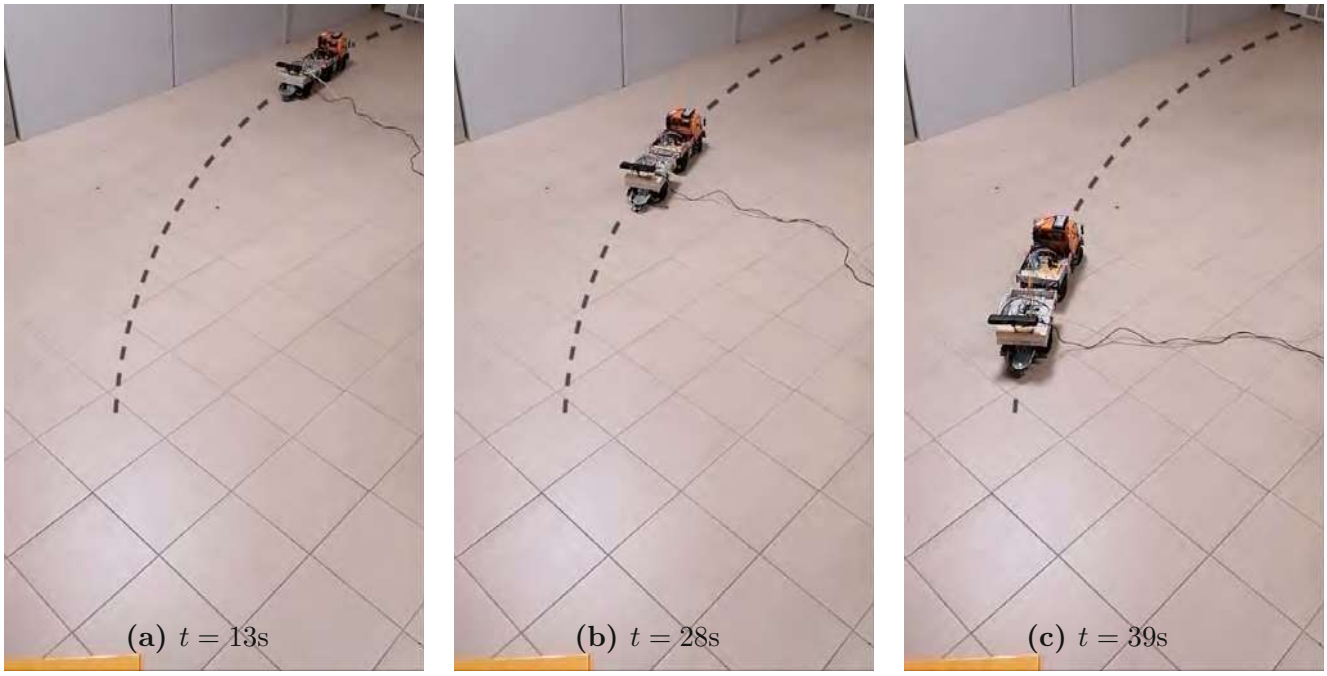

(a) $t = 13$s **(b)** $t = 28$s **(c)** $t = 39$s

Figure 25: shows experiment (**D**).

Die approbierte gedruckte Originalversion dieser Diplomarbeit ist an der TU Wien Bibliothek verfügbar
The approved original version of this thesis is available in print at TU Wien Bibliothek.
TU Bibliothek Your knowledge hub WIEN

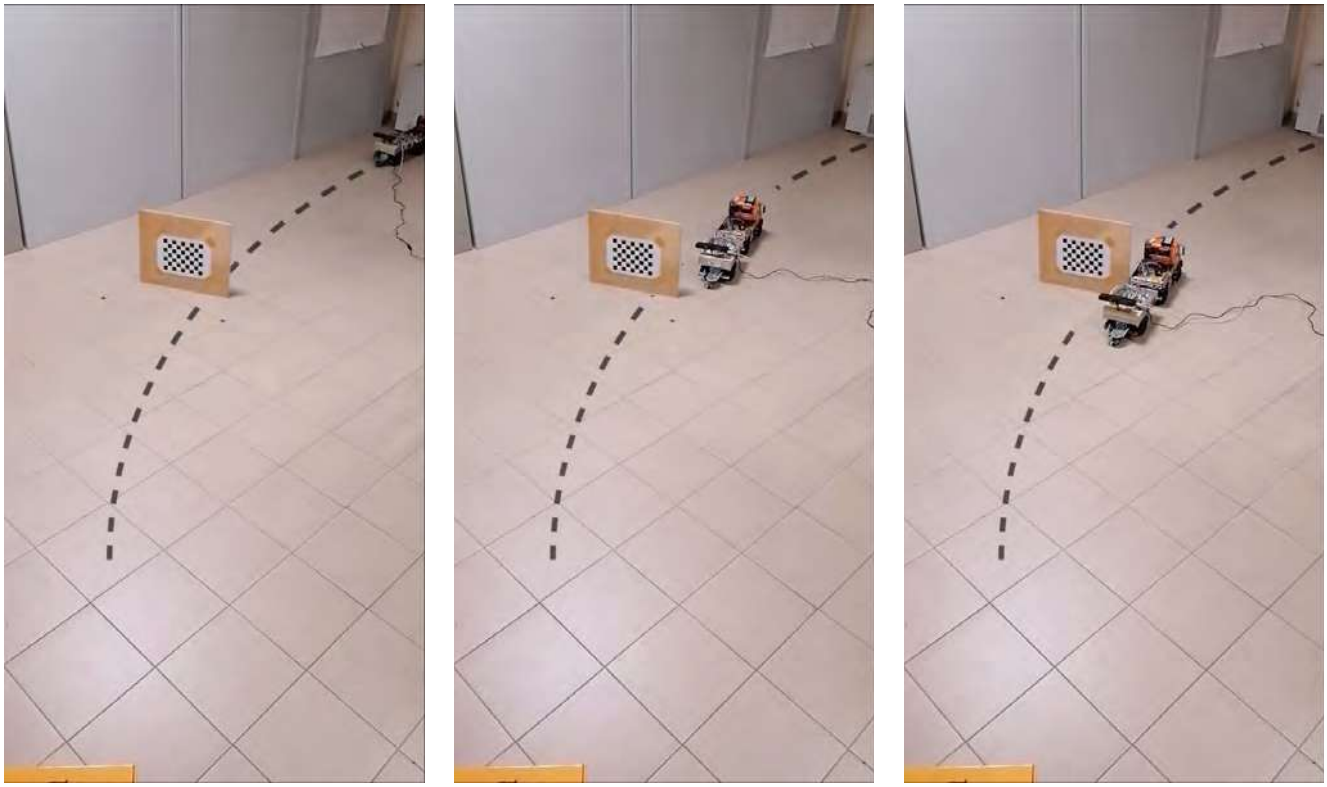

(a) $t = 1\text{s}$ **(b)** $t = 23\text{s}$ **(c)** $t = 28\text{s}$

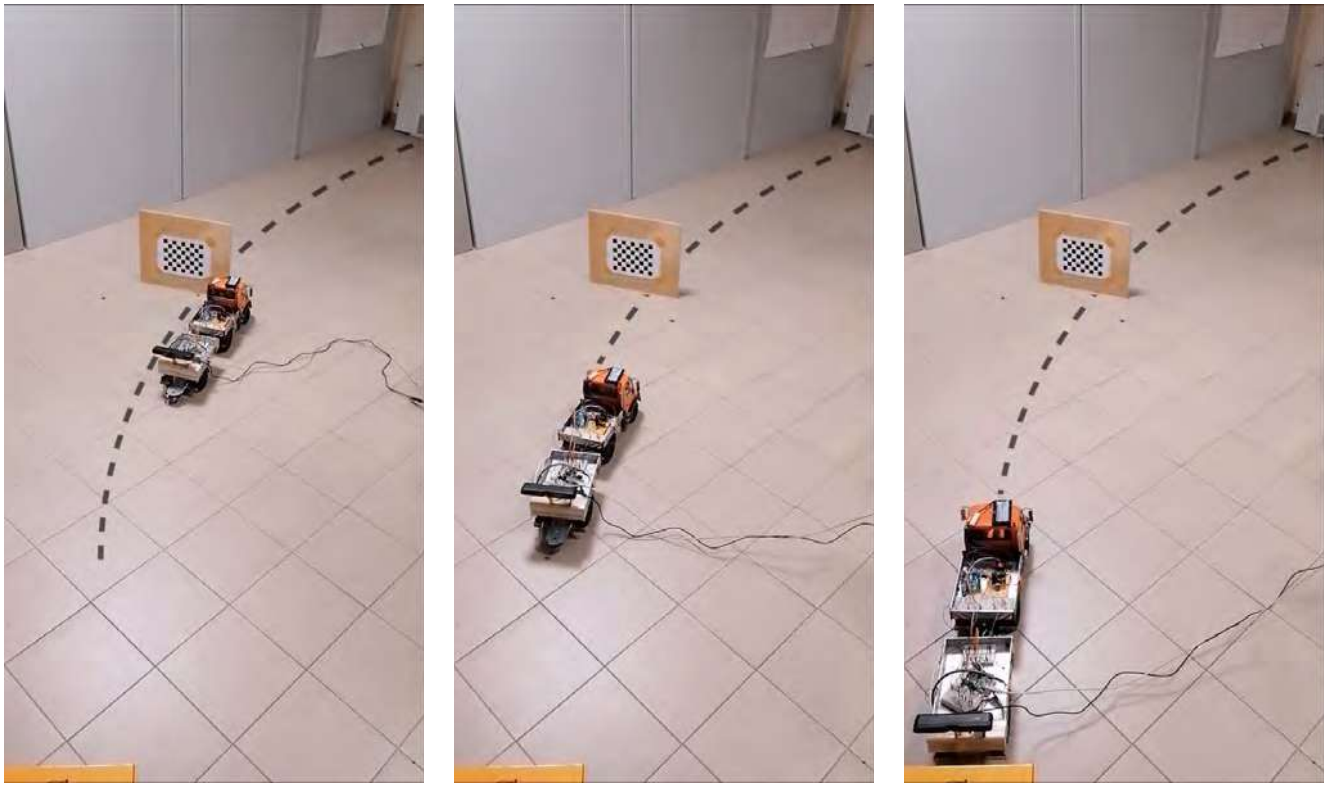

(d) $t = 33\text{s}$ **(e)** $t = 43\text{s}$ **(f)** $t = 51\text{s}$

Figure 26: shows experiment (**E**).

Die approbierte gedruckte Originalversion dieser Diplomarbeit ist an der TU Wien Bibliothek verfügbar
The approved original version of this thesis is available in print at TU Wien Bibliothek.
TU Bibliothek Your knowledge hub WIEN

5.3 Two trailers

The experiments (**F**),(**G**), and (**H**) address the two-trailers system having the task to follow a linear, circular, and cubic trajectory, respectively. Note that the desired trajectory is depicted in the experiments as a dashed line. The evolution of the cartesian errors, states, and the inputs is shown in figures 27, 29, and 30, respectively. It can be observed that in all three experiments the cartesian errors oscillate with small amplitudes around zero, i.e. the vehicle tracks the trajectory quite accurately. In experiment (**H**) a short linear segment is added to the cubic trajectory, such that the vehicle and the trailers would stop straightened. The corresponding snapshots are available in Fig. 28, 31, and 32.

Figures 34 and 33 shows the one-trailer and the two-trailers system maneuvered in backward direction when the tracking controller is implemented only, without the corrective input. The *jackknife* effect occurs after 9 sec. for the one-trailer system and even after 4 sec. for the two-trailers system.

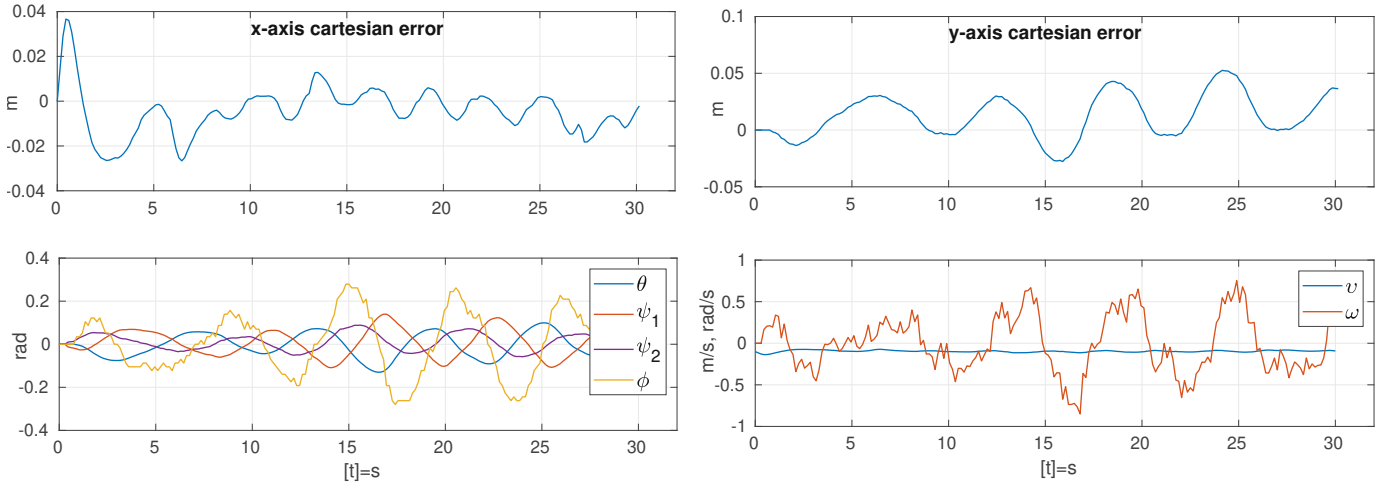

Figure 27: shows the evolution of the cartesian errors, states, and the inputs of the two-trailers system. The task is to follow a linear trajectory. It corresponds to experiment (**F**)

Die approbierte gedruckte Originalversion dieser Diplomarbeit ist an der TU Wien Bibliothek verfügbar
The approved original version of this thesis is available in print at TU Wien Bibliothek.
TU Bibliothek Your knowledge hub WIEN

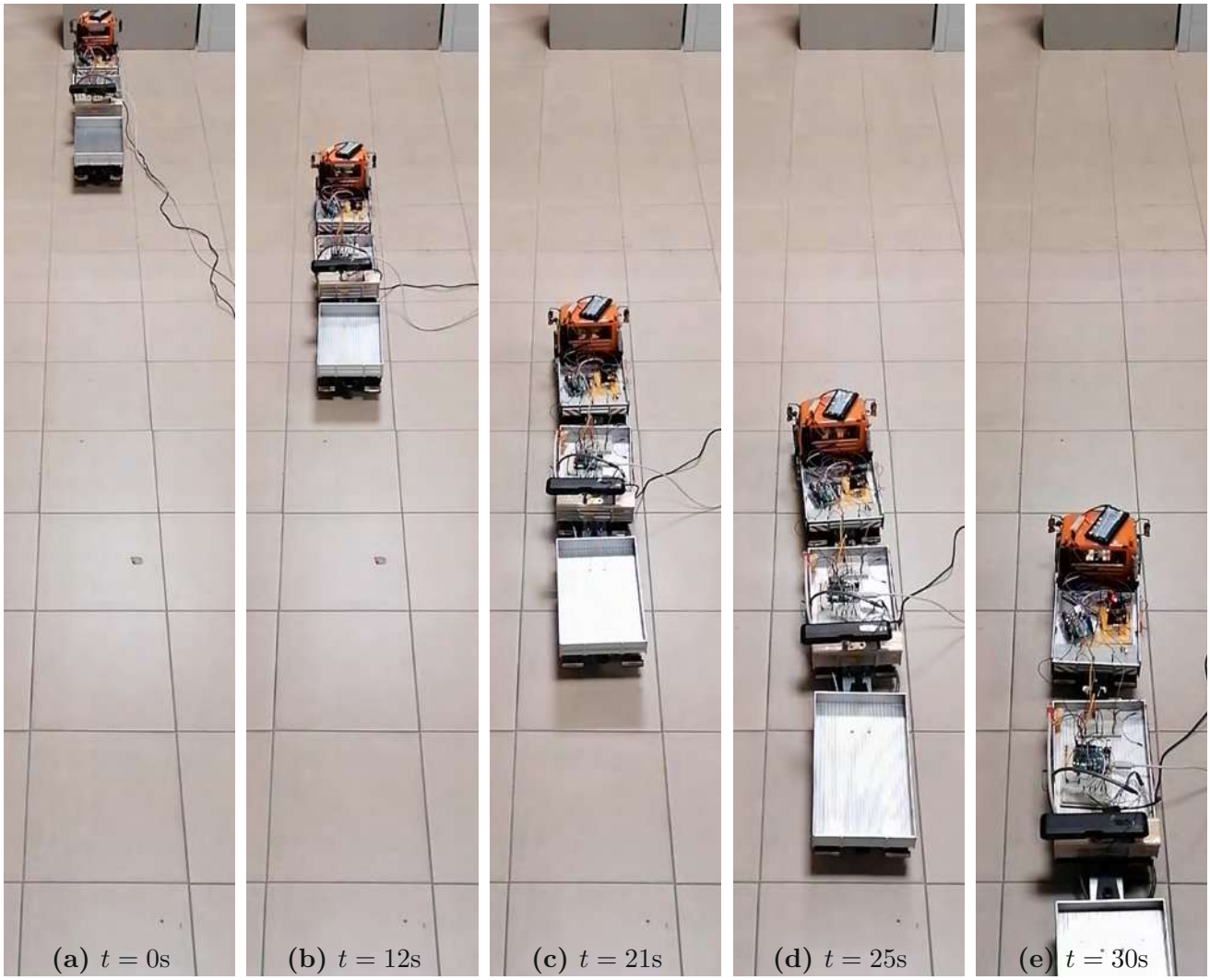

Figure 28: shows experiment (**F**).

Die approbierte gedruckte Originalversion dieser Diplomarbeit ist an der TU Wien Bibliothek verfügbar
The approved original version of this thesis is available in print at TU Wien Bibliothek.
TU Bibliothek Your knowledge hub WIEN

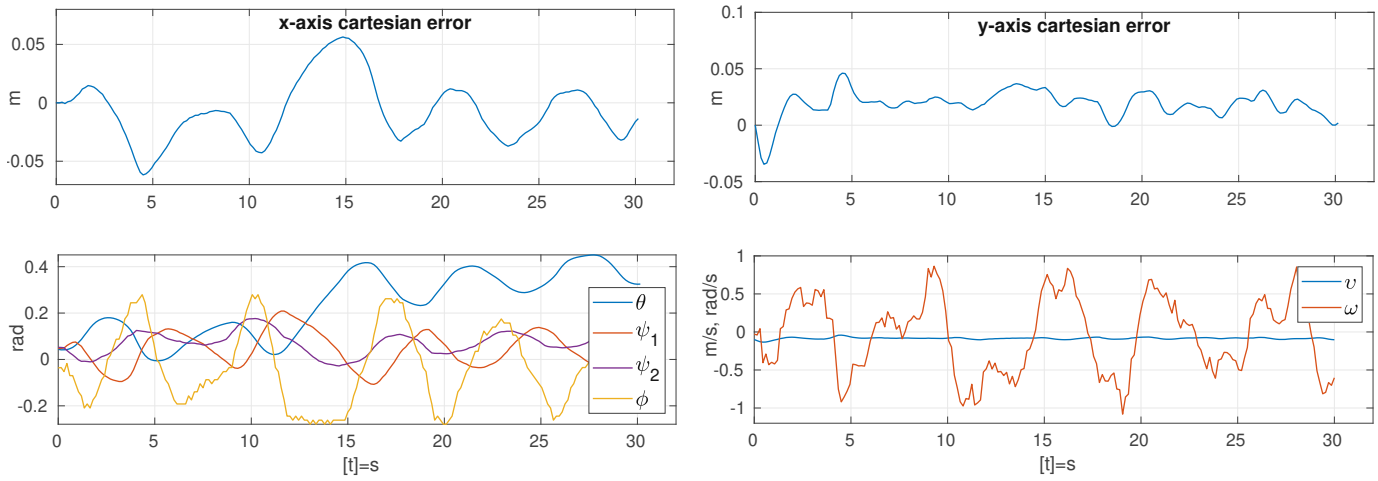

Figure 29: shows the evolution of the cartesian errors, states, and the inputs of the two-trailers system. The task is to follow a circular trajectory. The task is to follow a linear trajectory. It corresponds to experiment (**G**)

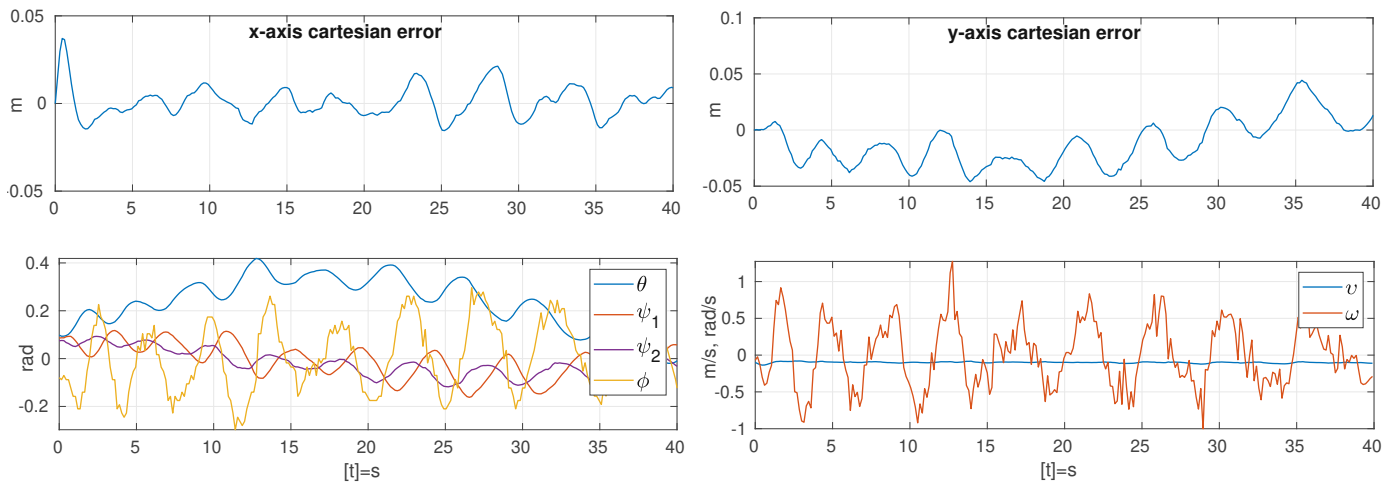

Figure 30: shows the evolution of the cartesian errors, states, and the inputs of the two-trailers system. The task is to follow a cubic trajectory, to which a linear segment is added at the end. The task is to follow a linear trajectory. It corresponds to experiment (**H**)

Die approbierte gedruckte Originalversion dieser Diplomarbeit ist an der TU Wien Bibliothek verfügbar
The approved original version of this thesis is available in print at TU Wien Bibliothek.
TU Bibliothek Your knowledge hub WIEN

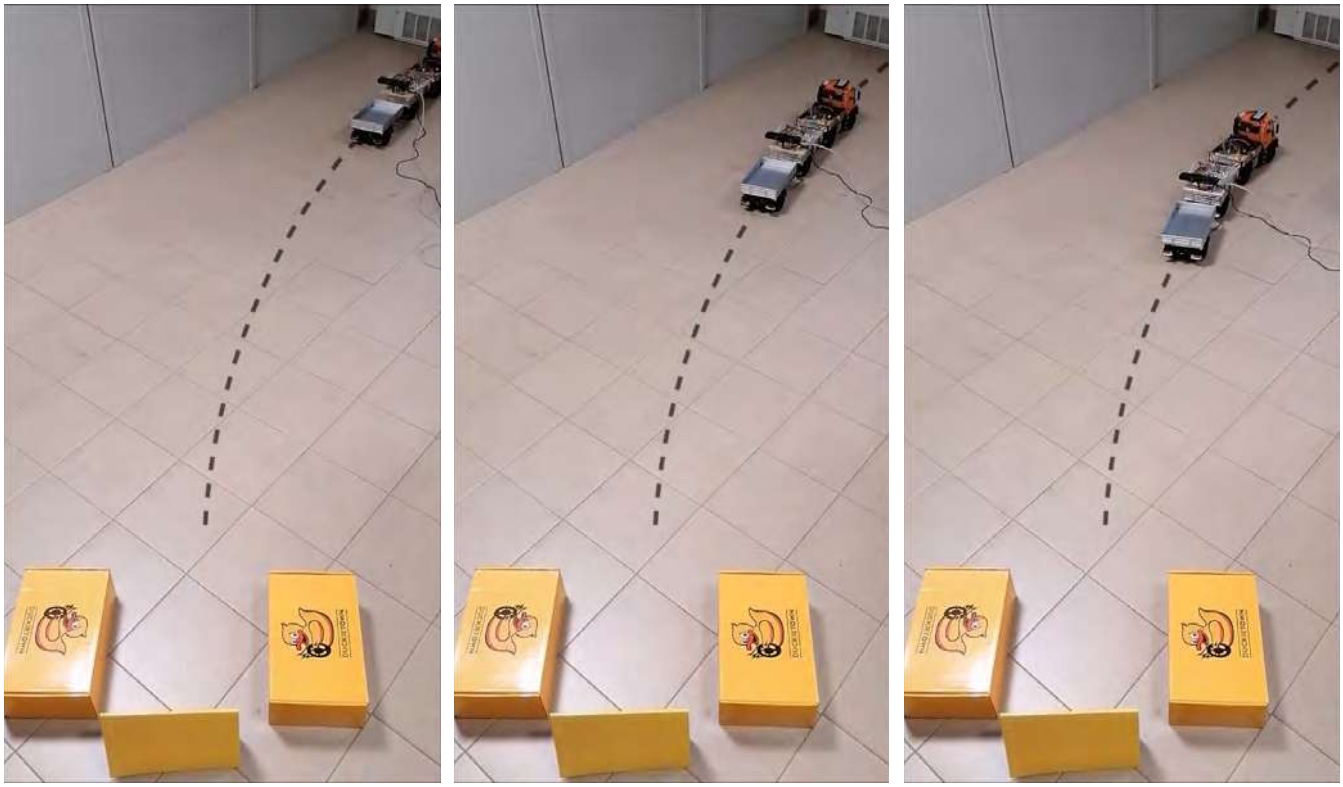

(a) $t = 0$s (b) $t = 9$s (c) $t = 14$s

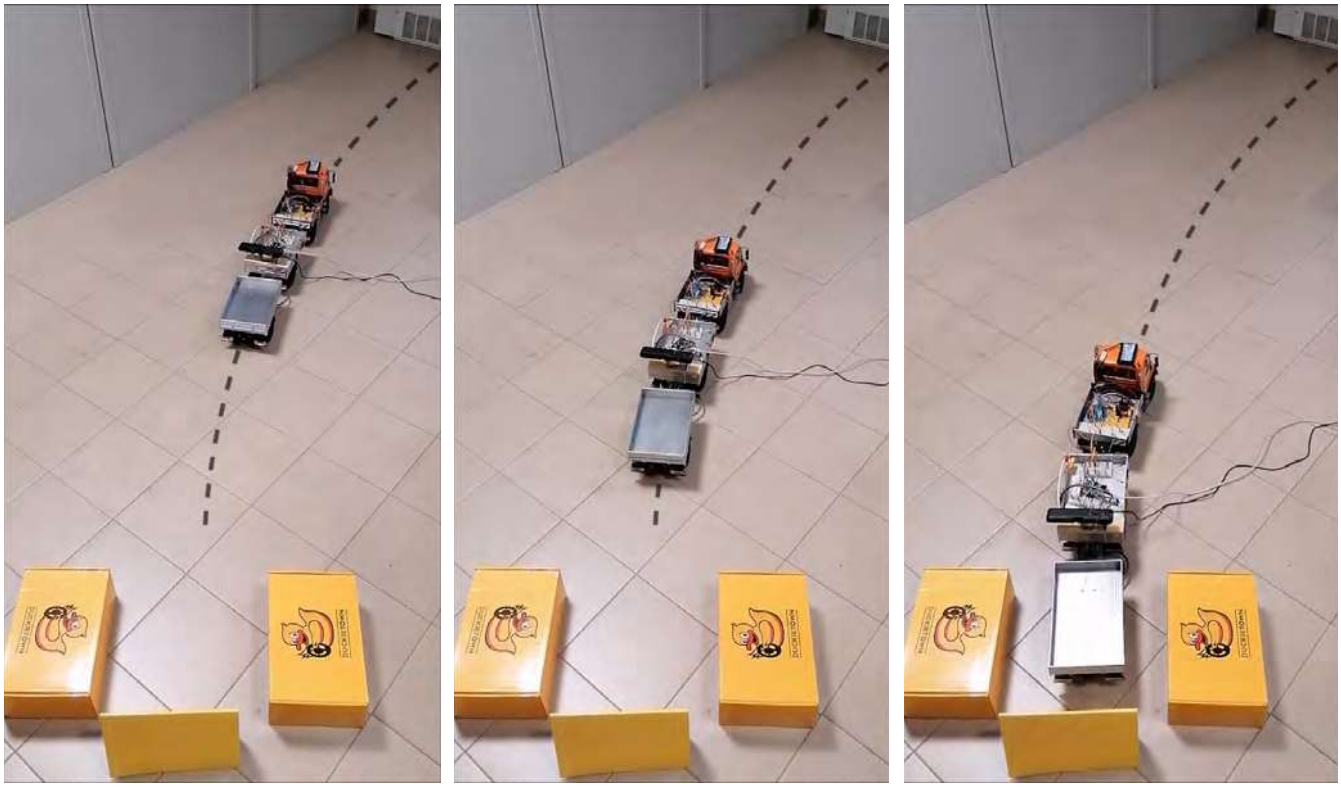

(d) $t = 20$s (e) $t = 28$s (f) $t = 37$s

Figure 31: shows experiment (**G**).

Die approbierte gedruckte Originalversion dieser Diplomarbeit ist an der TU Wien Bibliothek verfügbar
The approved original version of this thesis is available in print at TU Wien Bibliothek.
TU Bibliothek WIEN Your knowledge hub

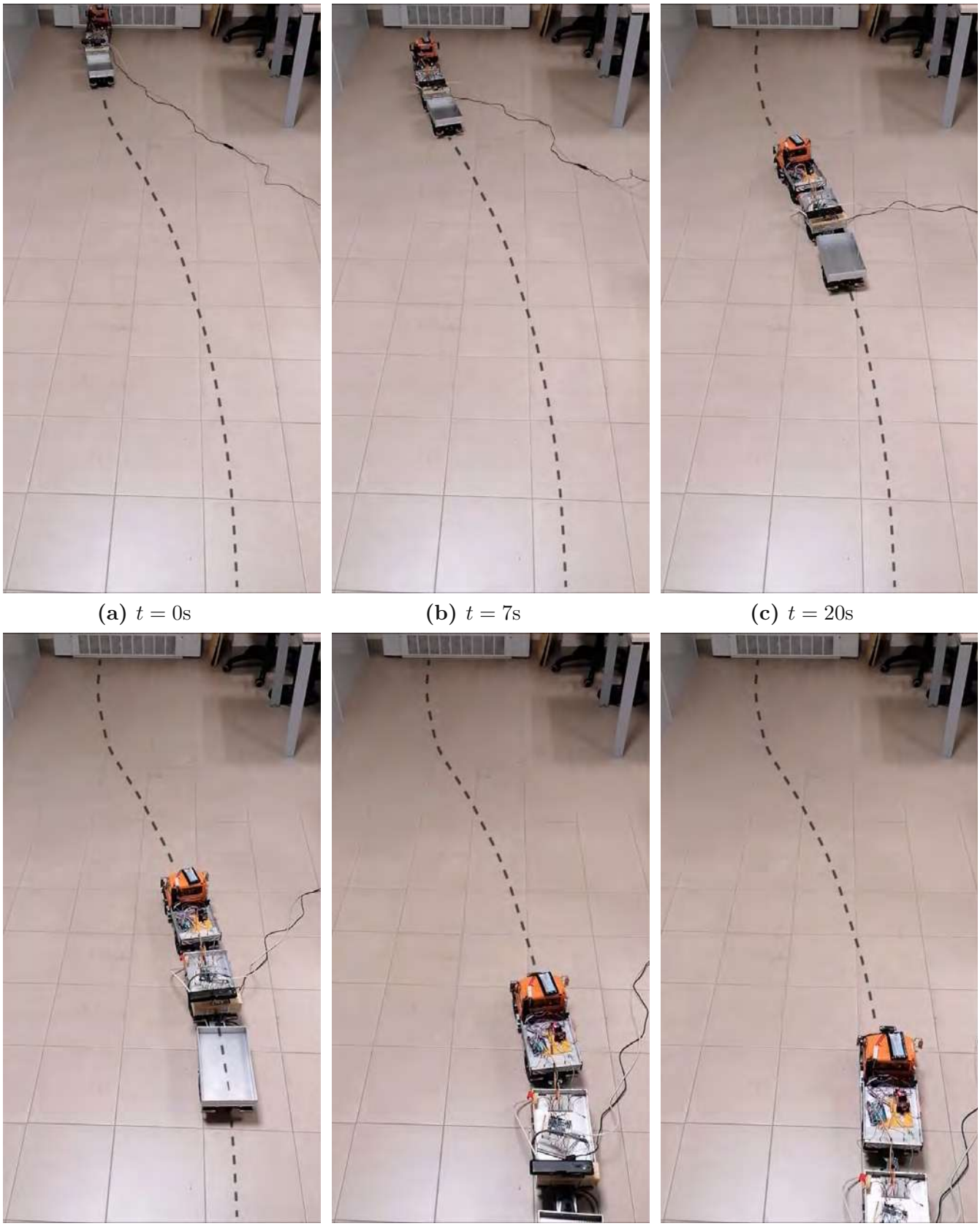

(a) $t = 0\text{s}$ **(b)** $t = 7\text{s}$ **(c)** $t = 20\text{s}$

(d) $t = 31\text{s}$ **(e)** $t = 37\text{s}$ **(f)** $t = 40\text{s}$

Figure 32: shows experiment (**H**).

Die approbierte gedruckte Originalversion dieser Diplomarbeit ist an der TU Wien Bibliothek verfügbar
The approved original version of this thesis is available in print at TU Wien Bibliothek.
TU Bibliothek Your knowledge hub WIEN

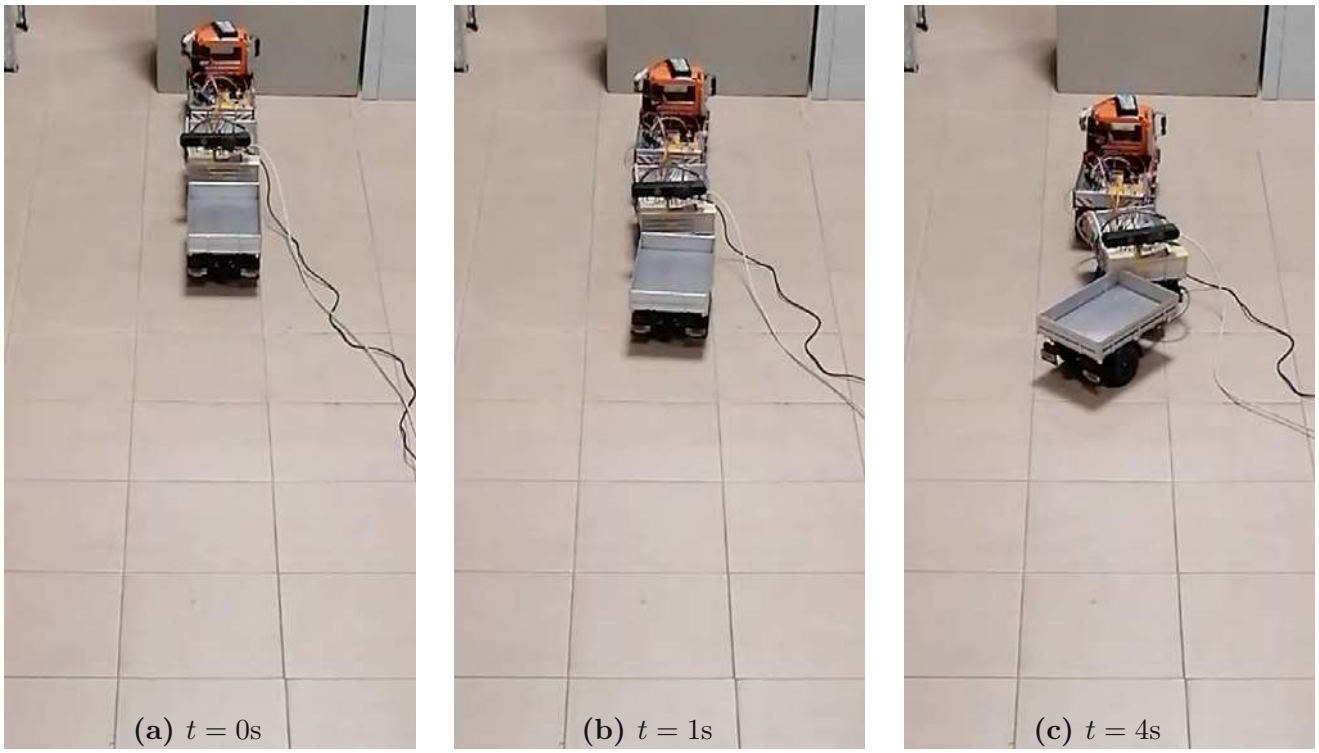

(a) $t = 0$s (b) $t = 1$s (c) $t = 4$s

Figure 33: shows the two-trailers system when the tracking controller, without the corrective input is used.

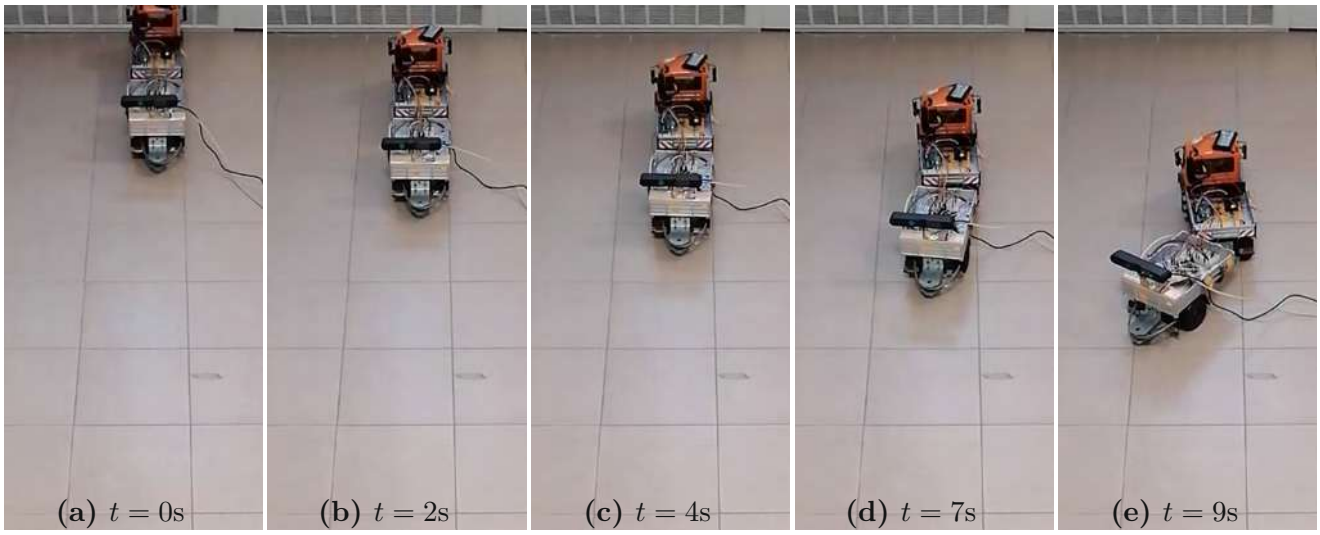

(a) $t = 0$s (b) $t = 2$s (c) $t = 4$s (d) $t = 7$s (e) $t = 9$s

Figure 34: shows the one-trailer system when the tracking controller, without the corrective input is used.

Die approbierte gedruckte Originalversion dieser Diplomarbeit ist an der TU Wien Bibliothek verfügbar
The approved original version of this thesis is available in print at TU Wien Bibliothek.
TU Bibliothek Your knowledge hub WIEN

6 Conclusions and Future Work

The preceding work has been extended in two ways. First, the backing up maneuver of the tractor with two trailers has been successfully addressed now as the experiments show. To that end several modifications were necessary as listed in the introduction. One of the modifications was the use of the faster HPIPM solver, for which the QP had to be re-formulated, including the transition of the stability constraint into a terminal constraint. Another part was the implementation of the Kalman filter where the state estimations using the prediction model on the one hand and the odometry on the other hand were merged. Since a depth camera is in use a possible future work could be a landmark-based localisation. The position (measured by the camera) of fixed and known landmarks w.r.t. the robot could be used to correct the odometry measurements. Furthermore, the ROS middleware, which was used in this work, also offers a package for simultaneous localisation and mapping (SLAM) through the ASUS depth camera. This method is particularly suitable if the environment is totally unknown, and therefore a map of it has to be created first in order to then localise the robot in it.

The second part of this work includes the online re-planning of the trajectory to avoid unexpected workspace obstacles. Unlike in other works, failures due to local minima do not appear and no assumption on the shape of workspace obstacles are necessary. However, as the environment gets gradually explored, the replanning might become infeasible because obstacles hidden behind other obstacles might get detected too late. Furthermore, the replanning requires that the whole control algorithm runs in real-time increasing the computational effort dramatically. This was also the reason why no experiments were performed with two trailers in which replanning was necessary. A possible solution could be the translation of the control algorithm into C programming language, where the computational time should be smaller. But also then the frequency cannot be significantly increased as it would be limited by the Arduino board. This could be exchanged with the more powerful Raspberry Pi. Another future work could be the consideration of the obstacle on two levels, once by replanning the trajectory and then explicitly as an MPC constraint, like already described in the introduction. Considering the obstacle as an MPC constraint only would probably fail as a linear approximation around the reference state trajectory is done. Therefore, bigger deviations from the reference (that are necessary to avoid obstacles) would violate the linearity of the MPC.

Die approbierte gedruckte Originalversion dieser Diplomarbeit ist an der TU Wien Bibliothek verfügbar
The approved original version of this thesis is available in print at TU Wien Bibliothek.
TU Bibliothek Your knowledge hub WIEN

References

[1] C. Altafini, *"Path following with reduced off-tracking for multibody wheeled vehicles"*, in IEEE Transactions on Control Systems Technology, 2003, pp. 598-605, DOI: 10.1109/TCST.2003.813374.

[2] A. Astolfi, P. Bolzern and A. Locatelli, *"Path-tracking of a tractor-trailer vehicle along rectilinear and circular paths: a Lyapunov-based approach"*, in IEEE Transactions on Robotics and Automation, 2004, pp. 154-160, DOI: 10.1109/TRA.2003.820928.

[3] A. González-Cantos, A. Ollero, *"Backing-Up Maneuvers of Autonomous Tractor-Trailer Vehicles using the Qualitative Theory of Nonlinear Dynamical Systems"*, The International Journal of Robotics Research, 2009, pp. 49–65. DOI: 10.1177/0278364908097588.

[4] C. Altafini, A. Speranzon, K.H. Johansson, *"Hybrid control of a truck and trailer vehicle"*, Lecture Notes in Computer Science, 2002 , DOI: DOI: 10.1007/3-540-45873-5_5.

[5] O. Ljungqvist, D. Axehill, A. Helmersson, *"Path following control for a reversing general 2-trailer system"*, in IEEE Conference on Decision and Control, 2016, p. 2455-2461. DOI: 10.1109/CDC.2016.7798630.

[6] O. Ljungqvist, D. Axehill, H. Pettersson, *"On sensing-aware model predictive path-following control for a reversing general 2-trailer with a car-like tractor"*, in IEEE Int. Conf. on Robotics and Automation, 2020, pp. 8813-8819, DOI: 10.1109/ICRA40945.2020.9197346.

[7] M. Beglini, L. Lanari, G. Oriolo, *"Anti-Jackknifing Control of Tractor-Trailer Vehicles via Intrinsically Stable MPC"*, in IEEE Int. Conf. on Robotics and Automation, 2020, pp.8806-8812. DOI: 10.1109/ICRA40945.2020.9197012.

[8] Alberto Isodori, *"Non Linear Control Systems"*, London: Springer Verlag, 1995.

[9] L. Lanari, S. Hutchinson, *"Inversion-based gait generationfor humanoid robots"*, in IEEE/RSJ Int. Conf. on Intelligent Robots and Systems, 2015, pp. 1592-1598, DOI: 10.1109/IROS.2015.7353580.

Die approbierte gedruckte Originalversion dieser Diplomarbeit ist an der TU Wien Bibliothek verfügbar
The approved original version of this thesis is available in print at TU Wien Bibliothek.
TU Bibliothek WIEN Your knowledge hub

[10] M. Beglini, *"Backing up a tractor-trailer vehicle via intrinsically stable Model Predictive Control"*, Rome: University of Sapienza, 2019.

[11] A. De Luca, G. Oriolo, C. Samson, *"Robot Motion Planning and Control"*, Berlin: Springer Verlag, 1998, pp. 171-253.

[12] N. Scianca, M. Cognetti, D. De Simone, L. Lanari, and G. Oriolo, *"Intrinsically stable MPC for humanoid gait generation"*, in 16th IEEE- RAS Int. Conf. on Humanoid Robots, 2016, pp. 101–108. DOI: 10.1109/HUMANOIDS.2016.7803336.

[13] O. Ljungqvist, N. Evestedt, D. Axehill, M. Cirillo, *"A path planning and path-following control framework for a general 2-trailer with a car-like tractor"*, New Jersey: Wiley, 2019. DOI: 10.1002/rob.21908.

[14] F. Lamiraux, D. Bonnafous, O. Lefebvre, *"Reactive Path Deformation for Nonholonomic Mobile Robots"*, in IEEE IEEE Transactions on Robotics, 2005, pp.967 - 977. DOI: 10.1109/TRO.2004.829459.

[15] M. Cognetti, D. De Simone, F. Patota, N. Scianca, L. Lanari, G. Oriolo, *"Real-Time Pursuit-Evasion with Humanoid Robots"*, in IEEE Int. Conf. on Robotics and Automation, 2017, pp. 4090-4095, DOI: 10.1109/ICRA.2017.7989470.

[16] D. De Simone, N. Scianca, P. Ferrari, L. Lanari, G. Oriolo, *"MPC-based Humanoid Pursuit-Evasion in the presence of Obstacles"*, in IEEE/RSJ Int. Conf. on Intelligent Robots and Systems, 2017,pp. 5245-5250. DOI: 10.1109/IROS.2017.8206415.

[17] G. Frison, M. Diehl, *"HPIPM: a high performance quadratic programming framework for model predictive control"*, in ArXiv vol. abs/2003.02547, 2020. n.pag.

[18] N. Scianca, D. De Simone, L. Lanari, G. Oriolo , and Fellow, *"MPC for Humanoid Gait Generation: Stability and Feasibility"*, in IEEE Transactions on Robotics, vol. 36, 2019, pp.1171-1188. DOI: 10.1109/TRO.2019.2958483

[19] M. J. Kurtz, M. A. Henson, *"Input-Ouput Linearizing Control of Constrained Nonlinear Process"*, in Journal of Process Control Vol. 7 Iss. 1, 1997, pp.3-17. DOI: 10.1016/S0959-1524(96)00006-6.

Die approbierte gedruckte Originalversion dieser Diplomarbeit ist an der TU Wien Bibliothek verfügbar
The approved original version of this thesis is available in print at TU Wien Bibliothek.
TU Bibliothek WIEN Your knowledge hub

[20] J. B. Rawlings, D. Q. Mayne, *"Model Predictive Control: Theory and Design"*, Madison: Nob Hill Publishing LLC, 2015.

[21] J.A. Rossiter, *"Model-Based Predictive Control: a Practical Approach"*, New York: CRC Press LLC, 2005.

Die approbierte gedruckte Originalversion dieser Diplomarbeit ist an der TU Wien Bibliothek verfügbar
The approved original version of this thesis is available in print at TU Wien Bibliothek.
TU Bibliothek Your knowledge hub WIEN

A System matrices after the linear approximation

$$A(t) = \begin{pmatrix} a_{11} & 0 & 0 & 0 & 0 & 0 \\ 0 & a_{22} & 0 & 0 & 0 & 0 \\ a_{31} & a_{32} & a_{33} & 0 & 0 & a_{36} \\ a_{41} & a_{42} & a_{43} & a_{44} & 0 & a_{46} \\ a_{51} & a_{52} & a_{53} & a_{54} & a_{55} & a_{56} \\ a_{61} & a_{62} & a_{63} & 0 & 0 & a_{66} \end{pmatrix}$$

the first row:

$$a_{11} = -K_1$$

the second row:

$$a_{22} = -K_2$$

the third row:

$$\begin{aligned} a_{31} &= -\frac{K_1}{L}\cos(\theta_r + \phi_r)\sin\phi_r, \qquad a_{32} = -\frac{K_2}{L}\sin(\theta_r + \phi_r)\sin\phi_r \\ a_{33} &= \frac{\sin\psi_r}{L}\left(-\sin(\theta_r + \phi_r)\,\dot{x}_r + \cos(\theta_r + \phi_r)\,\dot{y}_r\right) \\ a_{36} &= \frac{1}{L}\left(\cos(\theta_r + 2\phi_r)\,\dot{x}_r + \sin(\theta_r + 2\phi_r)\,\dot{y}_r\right) \end{aligned}$$

Die approbierte gedruckte Originalversion dieser Diplomarbeit ist an der TU Wien Bibliothek verfügbar
The approved original version of this thesis is available in print at TU Wien Bibliothek.
TU Bibliothek Your knowledge hub WIEN

the fourth row:

$$a_{41} = \frac{K_1}{L\,L_1}\left(h\sin\phi_r\cos\psi_{1,r} + L\cos\phi_r\sin\psi_{1,r} + L_1\sin\phi_r\right)\,\cos(\phi_r+\theta_r)$$

$$a_{42} = \frac{K_1}{L\,L_2}\left(h\sin\phi_r\cos\psi_{1,r} + L\cos\phi_r\sin\psi_{1,r} + L_1\sin\phi_r\right)\,\sin(\phi_r+\theta_r)$$

$$a_{43} = -\frac{1}{L\,L_1}\left(h\sin\phi_r\cos\psi_{1,r} + L\cos\phi_r\sin\psi_{1,r} + L_1\sin\phi_r\right)\left(-\sin(\theta_r+\phi_r)\,\dot{x}_r + \cos(\theta_r+\phi_r)\,\dot{y}_r\right)$$

$$a_{44} = -\frac{1}{L\,L_1}\left(-h\sin\phi_r\sin\psi_{1,r} + L\cos\phi_r\cos\psi_{1,r} + L_1\sin\phi_r\right)\left(\cos(\theta_r+\phi_r)\,\dot{x}_r + \sin(\theta_r+\phi_r)\,\dot{y}_r\right)$$

$$a_{46} = -\frac{1}{L\,L_1}\left(h\cos\phi_r\cos\psi_{1,r} + L\cos\phi_r\sin\psi_{1,r} + L_1\sin\phi_r\right)\left(\sin(\theta_r+\phi_r)\,\dot{x}_r - \cos(\theta_r+\phi_r)\,\dot{y}_r\right)$$

the fifth row:

$$C(\phi_r,\psi_{1,r},\psi_{2,r}) = \left[\frac{h\sin\phi_r}{LL_2}\left(\frac{L_2\cos\psi_{1,r}}{L_1} + \frac{(L_1+h_1)\cos\psi_{1,r}\cos\psi_{2,r}}{L_1}\cos(\psi_{1,r}+\psi_{2,r})\right) + \cdots \right.$$
$$\left. \cdots + \frac{\cos\phi_r\sin\psi_{1,r}}{L_1}\left(1 + \frac{(L_1+h_1)\cos\psi_{2,r}}{L_2}\right) - \frac{\cos\phi\sin(\psi_{1,r}+\psi_{2,r})}{L_2}\right]$$

Die approbierte gedruckte Originalversion dieser Diplomarbeit ist an der TU Wien Bibliothek verfügbar
The approved original version of this thesis is available in print at TU Wien Bibliothek.
TU Bibliothek Your knowledge hub WIEN

$$a_{51} = C(\phi_r, \psi_{1,r}, \psi_{2,r}) K_1 \cos(\theta_r + \phi_r)$$

$$a_{52} = -C(\phi_r, \psi_{1,r}, \psi_{2,r}) K_2 \sin(\theta_r + \phi_r)$$

$$a_{53} = C(\phi_r, \psi_{1,r}, \psi_{2,r}) \left(-\sin(\theta_r + \phi_r)\dot{x}_r + \cos(\theta_r + \phi_r)\dot{y}_r\right)$$

$$a_{54} = \left[\frac{h \sin\phi_r}{LL_2}\left(\frac{-L_2 \sin\psi_{1,r} - (L_1+h_1)\sin\psi_{1,r}\cos\psi_{2,r}}{L_1} + \sin(\psi_{1,r} + \psi_{2,r})\right) + \frac{\cos\psi_{1,r}\cos\phi_r}{1}\left(1 + \frac{L_1+h_1}{L_2}\cos\psi_{2,r}\right) + \cdots \right.$$
$$\left. \cdots - \frac{cos(\psi_{1,r}+\psi_{2,r})\cos\phi_r}{L_2}\right] \left[cos(\theta_r + \phi_r)\dot{x}_r + sin(\theta_r + \phi_r)\dot{y}_r\right]$$

$$a_{55} = \left[\frac{h \sin\phi_r}{LL_2}\left(\frac{L_2 \cos\psi_{1,r} - (L_1+h_1)\cos\psi_{1,r}\sin\psi_{2,r}}{L_1} + \sin(\psi_{1,r} + \psi_{2,r})\right) + \frac{\sin\psi_{1,r}\cos\phi_r}{L_1}\left(1 - \frac{L_1+h_1}{L_2}\sin\psi_{2,r}\right) + \cdots \right.$$
$$\left. \cdots - \frac{\cos(\psi_{1,r}+\psi_{2,r})\cos\phi_r}{L_2}\right] \left[cos(\theta_r + \phi_r)\dot{x}_r + sin(\theta_r + \phi_r)\dot{y}_r\right]$$

$$a_{56} = \left[\frac{h \cos\phi_r}{LL_2}\left(\frac{L_2 \cos\psi_{1,r} + (L_1+h_1)\cos\psi_{1,r}\cos\psi_{2,r}}{L_1} - \sin(\psi_{1,r} + \psi_{2,r})\right) + \frac{\sin\psi_{1,r}\sin\phi_r}{L_1}\left(1 + \frac{L_1+h_1}{L_2}\cos\psi_{2,r}\right) + \cdots \right.$$
$$\left. \cdots + \frac{\sin(\psi_{1,r}+\psi_{2,r})\sin\phi_r}{L_2}\right] \left[cos(\theta_r + \phi_r)\dot{x}_r + sin(\theta_r + \phi_r)\dot{y}_r\right] \cdots$$
$$\cdots + C(\phi_r, \psi_{1,r}, \psi_{2,r}) \left[-\sin(\theta_r + \phi_r)\dot{x}_r + \cos(\theta_r + \phi_r)\dot{y}_r\right]$$

the sixth row:

$$a_{61} = K_1 \left(\frac{\sin(\phi_r+\theta_r)}{b} + \frac{\cos(\theta_r+\phi_r)\sin\phi_r}{L}\right)$$

$$a_{62} = K_2 \left(\frac{\sin(\phi_r+\theta_r)\sin\phi_r}{L} - \frac{\cos(\theta_r+\phi_r)}{b}\right)$$

$$a_{63} = -\dot{x}_r \left(\frac{\cos(\theta_r+\phi_r)}{b} - \frac{\sin(\phi_r+\theta_r)\sin\phi_r}{L}\right) - \dot{y}_r \left(\frac{\cos(\theta_r+\phi_r)\sin\phi_r}{L} + \frac{\sin(\phi_r+\theta_r)}{b}\right)$$

$$a_{66} = -\dot{x}_r \left(\frac{\cos(\theta_r+\phi_r)}{b} + \frac{\cos(2\phi_r+\theta_r)}{L}\right) - \dot{y}_r \left(\frac{\sin(\phi_r+\phi_r)}{b} + \sin\cos(2\phi_r + \theta_r)L\right)$$

Die approbierte gedruckte Originalversion dieser Diplomarbeit ist an der TU Wien Bibliothek verfügbar
The approved original version of this thesis is available in print at TU Wien Bibliothek.
TU Bibliothek Your knowledge hub WIEN

$$B(t) = \begin{pmatrix} b_{11} & 0 \\ 0 & b_{22} \\ b_{31} & b_{32} \\ b_{41} & b_{42} \\ b_{51} & b_{52} \\ b_{61} & b_{62} \end{pmatrix}$$

with

$$\begin{aligned}
b_{11} &= 1, \\
b_{22} &= 1, \\
b_{31} &= \frac{\cos(\theta_r + \phi_r)\sin\phi_r}{L}, \quad b_{32} = \frac{\sin(\theta_r + \phi_r)\sin\phi_r}{L}, \\
b_{41} &= -\frac{1}{LL_1}\left(h\sin\phi_r\cos\psi_{1,r} + L\cos\phi_r\sin\psi_{1,r} + L_1\sin\phi_r\right)\cos(\theta_r + \phi_r), \\
b_{42} &= -\frac{1}{LL_1}\left(h\sin\phi_r\cos\psi_{1,r} + L\cos\phi_r\sin\psi_{1,r} + L_1\sin\phi_r\right)\sin(\theta_r + \phi_r), \\
b_{51} &= C(\phi_r, \psi_{1,r}, \psi_{2,r})\cos(\theta_r + \phi_r), \\
b_{52} &= C(\phi_r, \psi_{1,r}, \psi_{2,r})\sin(\theta_r + \phi_r), \\
b_{61} &= \left(\frac{\sin(\theta_r + \phi_r)}{b} + \frac{\cos(\theta_r + \phi_r)\sin\phi_r}{L}\right), \\
b_{62} &= \left(\frac{\cos(\theta_r + \phi_r)}{b} - \frac{\sin(\theta_r + \phi_r)\sin\phi_r}{L}\right).
\end{aligned}$$

Die approbierte gedruckte Originalversion dieser Diplomarbeit ist an der TU Wien Bibliothek verfügbar
The approved original version of this thesis is available in print at TU Wien Bibliothek.
TU Bibliothek WIEN Your knowledge hub

B Discrete stability condition

The stability constraint (24)

$$\varepsilon_u^\star(t_k) \quad = \quad -\int_{t_k}^{\infty} e^{-\Lambda_u(\tau)(\tau-t_k)} G_u(\tau) u^{corr}(\tau) d\tau$$

shall be applied to our LTV system and a discretisation is given. We start from the piecewise time invariant system (25) which will be devided into a stable and an unstable subsystem by a change of coordinates. This yields the following

$$\dot{\varepsilon}(t) = A_k \cdot \varepsilon(t) + B_k \cdot u_k^{corr} \qquad t_k \leq t \leq t_{k+1}$$

$$\begin{pmatrix} \dot{\varepsilon}_s(t) \\ \dot{\varepsilon}_u(t) \end{pmatrix} = \begin{pmatrix} \Lambda_{s,k} & 0 \\ 0 & \Lambda_{u,k} \end{pmatrix} \begin{pmatrix} \varepsilon_s(t) \\ \varepsilon_u(t) \end{pmatrix} + \begin{pmatrix} G_{s,k} \\ G_{u,k} \end{pmatrix} u_k^{corr}$$

$$\Lambda_k = T_k A_k T_k^{-1} \qquad \& \qquad G_k = T_k B_k \qquad \& \qquad T_k = U_k^{-1}.$$

In the above equations U_k contains the eigenvectors of the matrix A_k. The time t also runs through a discrete set of equidistant values $t_{j+1} = t_j + \delta$. The transformation matrix T depends on the eigenvalues of the system matrix A which is assumed to be constant during each sampling interval of duration δ. During the next sampling interval the sytsem matrix changes though

$$\Lambda_{u,j} = T_{u,j} A_{u,j} T_{u,j}^{-1} \qquad \& \qquad G_{u,j} = T_{u,j} B_{u,j} \qquad \& \qquad T_{u,j} = U_{u,j}^{-1} \qquad \forall \quad j = k, k+1, \cdots \infty.$$

A naive approximation used, that works fine for the tractor-trailers system though, is the following

$$T_{u,j} = T_{u,k} \qquad \forall \quad j = k, k+1, k+2, \cdots \infty.$$

In general $T_{u,j}$ is different for each j, but it is held constant to yield the simple change of coordinates shown above and to save computation time. The discretisation is applied now on

Die approbierte gedruckte Originalversion dieser Diplomarbeit ist an der TU Wien Bibliothek verfügbar
The approved original version of this thesis is available in print at TU Wien Bibliothek.
TU Bibliothek WIEN Your knowledge hub

the stability constraint, yielding

$$\begin{aligned}
\varepsilon_u^\star(t_k) &\cong -\sum_{j=k}^{\infty}\left[\int_{t_j}^{t_{j+1}} e^{-\Lambda_{u,j}(\tau-t_k)}d\tau\right] G_{u,j}u^{corr} \\
&= \sum_{j=k}^{\infty}\left[\Lambda_{u,j}^{-1}e^{-\Lambda_{u,j}(\tau-t_k)}\right]_{t_j}^{t_{j+1}} G_{u,j}u_j^{corr} = \\
&= \sum_{j=k}^{\infty}\Lambda_{u,j}^{-1}\left[e^{-\Lambda_{u,j}(-t_k+t_j+\delta)} - e^{-\Lambda_{u,j}(-t_k+t_j)}\right] G_{u,j}u_j^{corr},
\end{aligned}$$

and thus the stability constraint that can be used by a dense QP solver (e.g. quadprog in Matlab) becomes

$$\varepsilon_u^*(t_k) = \sum_{j=k}^{\infty}\Lambda_{u,j}^{-1}e^{-\Lambda_{u,j}(t_j-t_k)}\left[e^{-\Lambda_{u,j}\delta} - I\right] G_{u,j}u_j^{corr}.$$

The control horizon is defined as $T_C = C \cdot \delta$, where C is the number of time steps to reach $t_{k+C} = t_k + T_C$ from the current time instant t_k. The just obtained discrete stability condition can be split into two sums

$$\begin{aligned}
\varepsilon_u^*(t_k) &= \sum_{j=k}^{k+C-1}\Lambda_{u,j}^{-1}e^{-\Lambda_{u,j}(t_j-t_k)}\left[e^{-\Lambda_{u,j}\delta} - I\right] G_{u,j}u_j^{corr} + \sum_{j=k+C}^{\infty}\Lambda_{u,j}^{-1}e^{-\Lambda_{u,j}(t_j-t_k)}\left[e^{-\Lambda_{u,j}\delta} - I\right] G_{u,j}u_j^{corr} \\
&= \sum_{j=k}^{k+C-1}\cdots + \sum_{j=k+C}^{\infty}\cdots .
\end{aligned}$$

The second sum represents the tail. There are two strategies how to deal with the infinite sum (the tail).

1. The truncated tail: $\sum_{j=k+C}^{\infty}\cdots = 0$, which consists of the idea that the integral of the stability constraint depends stronger on the first time instants, thus later times can be neglected.

2. The periodic tail: $\sum_{j=k+C}^{\infty}\cdots$ is a finite repetitive replication of $\sum_{j=k}^{k+C-1}\cdots$. Finite in the sense that the infinite sum gets truncated at after some replications as well. The idea is that the corrective maneuvers for reversing a tractor-trailer system are repetitive.

Die approbierte gedruckte Originalversion dieser Diplomarbeit ist an der TU Wien Bibliothek verfügbar
The approved original version of this thesis is available in print at TU Wien Bibliothek.
TU Bibliothek WIEN Your knowledge hub